# PRESSURE DROPS ALONG THE BORES OF HOLLOW FIBRE MEMBRANES - THEIR MEASUREMENT, PREDICTION AND EFFECT ON FIBRE BUNDLE PERFORMANCE

By

AHMET YÜCEER, B.Sc., M.Sc.

Thesis submitted to the University of Glasgow for the Degree of Ph.D.

AUGUST, 1985

Department of Mechanical Engineering,
University of Glasgow,
Glasgow,
United Kingdom.

# C O N T E N T S

I

# ACKNOWLEDGEMENTS

The research work was carried out in the Desalination Laboratory of the Department of Mechanical Engineering at the University of Glasgow.

I would like to thank Professor B.F. Scott, head of the Mechanical Engineering Department, for providing the research facilities in the department.

The author wishes to thank Dr. W.T. Hanbury, Senior Lecturer in Mechanical Engineering, for the supervision of this research work, his guidance and helpful suggestions throughout the course of this project.

Thanks to Mr. A. Ritchie for his technical assistance on the experimental rig and the other technicians are also acknowledged for their help.

Gratitude is extended to Mrs. K.A. Byrne for typing this thesis.

The author also wishes to express his thanks to the Ministry of Education, Youth and Sports in Turkey who funded this project.

# SUMMARY

This thesis investigates the pressure drops along the bores of B-9 and B-10 hollow fibre membranes, their measurements, prediction and effect on fibre bundle performance.

The theory of osmosis and reverse osmosis, the transport models, membrane configurations and productions were reviewed. Laminar flow in circular impermeable and porous pipes and the flow through a bundle of hollow fibres were also reviewed for the better understanding of the theoretical analysis.

A theoretical model of the fibre behaviour is studied and analysed. An analytical solution is obtained for the case of a fibre in a uniform crossflow of brine of uniform concentration and uniform pressure. A numerical procedure, making use of this analytical solution, is developed to solve the more general problem of detailed bundle behaviour. The experimental data are analysed using a computer program based on the numerical procedure presented in Chapter 5.

Experiments were carried out on small B-9 and B-10 hollow fibre membranes. The performances of the fibre bundles, including the measurements of the closed end bore pressures were investigated for two feeds, pure water and sodium chloride solution, under various ranges of operating conditions. From the resulting membrane performances, in both modules, it was seen that:

1. The water permeability constant, $k_1$, increased with increasing temperature. The $k_1$ was pratically independent of applied pressure at feed temperature of $20^{o}C$ and $25^{o}C$. However, the $k_1$ tended to decrease with increasing pressure at $30^{o}C$.

2. The salt permeability constant, $k_2$, increased with increasing temperature and pressure in the experiments with B-9 module. The salt permeability constant, $k_2$ of the B-10 modules was found to be highly dependent upon the PT-B post-treatment history.

A computer program (FD), assuming a fixed fibre geometery was used to determine the values of $k_1$, $k_2$ and the closed end fibre bore pressure. However, these theoretically precited values of fibre bore pressures were found to be significantly lower than the experimentally measured values of fibre bore pressures. A second program (VID) used the overall bundle performances together with the measured values of bore pressures to predict the effective bore diameters, Dia, and modified membrane constants $k_{1eff}$ and $k_{2eff}$. As a result of these calculations, the effective bore diameters were found to be smaller than the nominal bore diameters. This suggests that the hollow fibres are compressed, by as much as 25%, under the effect of external pressure. Furthermore, the constriction of fibre bore diameters increased with increasing temperature. The experiments with B-10 modules indicated that the compaction of the fibres may also be non-linear and limited, and the apparent fibre bore shrinkage decreases radially outward through the bundle.

As a result, the modified values of $k_{1eff}$ were found to be higher than the values neglecting the fibre bore shrinkage effect. The salt permeability constant appears to be independent of allowance for bore shrinkage.

The analysis of the whole bundle behaviour, allowing for the fibre bore shrinkage, showed that the axial distribution of brine concentration varies significantly due to the variation of the net driving pressure along the fibre. The fibres towards the open end tube plate are exposed to the highest net driving pressure and hence, increase in productivity and local brine concentration which may lead to a polarisation type effect.

New modified water and salt permeability constants, $k_{1A}$ and $k_{2A}$ were determined assuming the fibre outside diameter shrank by the same amount as the internal diameter. The new modified values of $k_{1A}$ and $k_{2A}$ were found to be higher than the values of $k_{1eff}$ and $k_2$. This is obviously due to the resulting reduction in the membrane surface area used in the calculations with the same bundle performance.

# CHAPTER 1. INTRODUCTION

# INTRODUCTION

It is very well known that life on earth is dependent on water in its many forms. Without water this planet would have been different and a lifeless one. 75% of the earth is covered by water but however only less than 1% is distributed as fresh water in streams, lakes and ground water. In the past people settled near water resources or moved from one water resource to another to provide water for their needs. Increasing population and industrialisation have increased the water demand. In many parts of the world the quality of water is not always suitable or suitable water resources are not enough for our consumption. The water scarcity has pushed people into finding new fresh water resources. Rain water was collected and wells were dug for water. They did not meet the increasing demand for fresh water in many places.

The seawater and brackish waters which are unsuitable for consumption, due to the salinity, are often readily available. The mineral salts had to be removed from the saline water to obtain fresh water. Saline waters may be desalted by several different methods. Reverse osmosis, distillation, ion exchange and electrodialysis are the major desalination processes currently in use. Desalination may be defined as: the art of producing fresh palatable water from a saline supply at a reasonable cost with reasonable reliability.

The process reverse osmosis is generally the most economical for desalting either brackish or dilute sea water. Reverse osmosis is a membrane permeation process for separating relatively pure water from a less pure solution. The solution is passed over the surface of an appropriate semipermeable membrane at a pressure in excess of the effective osmotic pressure of the feed solution. The permeating water is collected as the product (fresh water). It is obvious that the membrane must be highly permeable to water, highly impermeable to solutes (salts), and capable of withstanding the applied pressure without failure.

Within the last twenty years considerable improvements have been achieved in membrane materials, production techniques and module designs. One of them is a hollow fine fibre membrane module. Very large surface to volume ratios, negligible concentration polarisation and self supporting strength have made them very attractive for desalination of saline waters.

In the design of hollow fibre membrane systems, the physical fibre parameters should be chosen to obtain an optimum bundle performance. A number of hollow fibre analysis can be found in the literature (14, 15, 20, 23, 24). These concern mainly mass transport, the fibre diameter, length, wall thickness, packing density and fluid flow inside and outside of the fibre. The assumptions upon which these analyses are based vary. However, all the analyses (14, 15, 20, 24, 46) assumed the fibre cross section, where there is a very dense skin outside and a porous wall underneath, to remain undistorted under working conditions.

In the experimental literature (12, 15, 27, 36, 38, 46) there is ample evidence that the water and salt permeabilities (based on constant fibre geometry) vary considerably with both temperature and pressure. The purpose of this work was to attempt to find out how much of this variation can be attributed to changes in the fibre geometry under the influence of external pressure. Since the theoretical solution to the performance of a fibre is particularly sensitive to changes in the bore diameter, it was thought that measurements of the pressure drops along the fibre bores, under working conditions might provide some evidence of changes in the bore diamter. To this end a small 4" B-9 and B-10 hollow fibre modules were disassembled and pressure tapping holes drilled into the resin blocks supporting the looped 'closed' ends of the fibres.

Fibre bore pressure measurements have been made under various ranges of operating conditions. The results were analysed using a computer program. Evidence from the fibre bore pressure measurements tends to show that the fibre bore diameters shrink under pressure and this effect increases with increasing temperature. As mentioned before that the theoretical solution to the performance of a fibre is particularly sensitive to changes in the bore diameter. The membrane constants $k_1$ and $k_2$ were recalculated (as $k_{1eff}$ and $k_{2eff}$), allowing for the fibre bore shrinkage. The modified effective water permeability constants ($k_{1eff}$ were found to be higher than the values neglecting the bore shrinkage effect. The salt permeability constant, $k_2$, appears to be independent of allowance for bore shrinkage.

The hollow fibre analyses in the literature (14, 15, 20, 24, 46) also neglected the axial variation of brine concentration in the fibre bundle. If the fibre bore shrinkage is taken into account, because of the axial variation of the net driving pressure, the axial variation of brine concentration may become significant, producing a concentration polarisation type effect.

# CHAPTER 2: OSMOSIS AND REVERSE OSMOSIS

## 2.1 Introduction

The purpose of this chapter is to give some information about the natural osmosis and reverse osmosis which is one of the process used in desalination of saline waters. The thermodynamics of the process is reviewed for the better understanding of the process.

## 2.2 Osmosis and Reverse Osmosis

Natural osmosis occurs in a closed system containing pure water separated from an aqueous salt solution by a semi-permeable membrane. The characteristics of an ideal membrane are such that water molecules can pass through the membrane but the salt molecules may not.

The pure water will flow through the membrane to dilute the salt solution (Fig. 2.1.A). This spontaneous flow of pure water is termed "osmosis". Due to the permeation, the volume of salt solution will increase and create a build up of pressure on the solution side. The flow of pure water will stop when it reaches the osmotic pressure of the solution, (Fig. 2.1.B). On the other hand, if a pressure is applied on the salt solution side, the rate of pure water flow will be decreased. As the pressure is increased a point will be found where there is no flow on either side, (Fig. 2.1.C). Then the system is said to be in "Osmotic Equilibrium" and the applied pressure is equal to the osmotic pressure of the solution. Under isothermal condition, osmotic pressure of a solution is directly proportional to the concentration and it can be written in a simple form as $\pi = \phi RTC$ where $\phi$, osmotic coefficient, R, universal gas constant, T, absolute temperature and C is the concentration. The osmotic pressure of standard seawater (35000 ppm which is equivalent to 3.2% NaCl solution) is of the order of 25 atmospheres. At the point where osmotic equilibrium is reached, as the pressure is increased the direction of pure water flow is reversed, Fig. 2.1.D. Thus, the pure water molecules in the salt solution will pass through the membrane leaving the salt molecules behind. This last phenomenon is the basis of the reverse osmosis method of desalination. A simplified flow diagram of a typical reverse osmosis system is shown on Fig. 2.2.

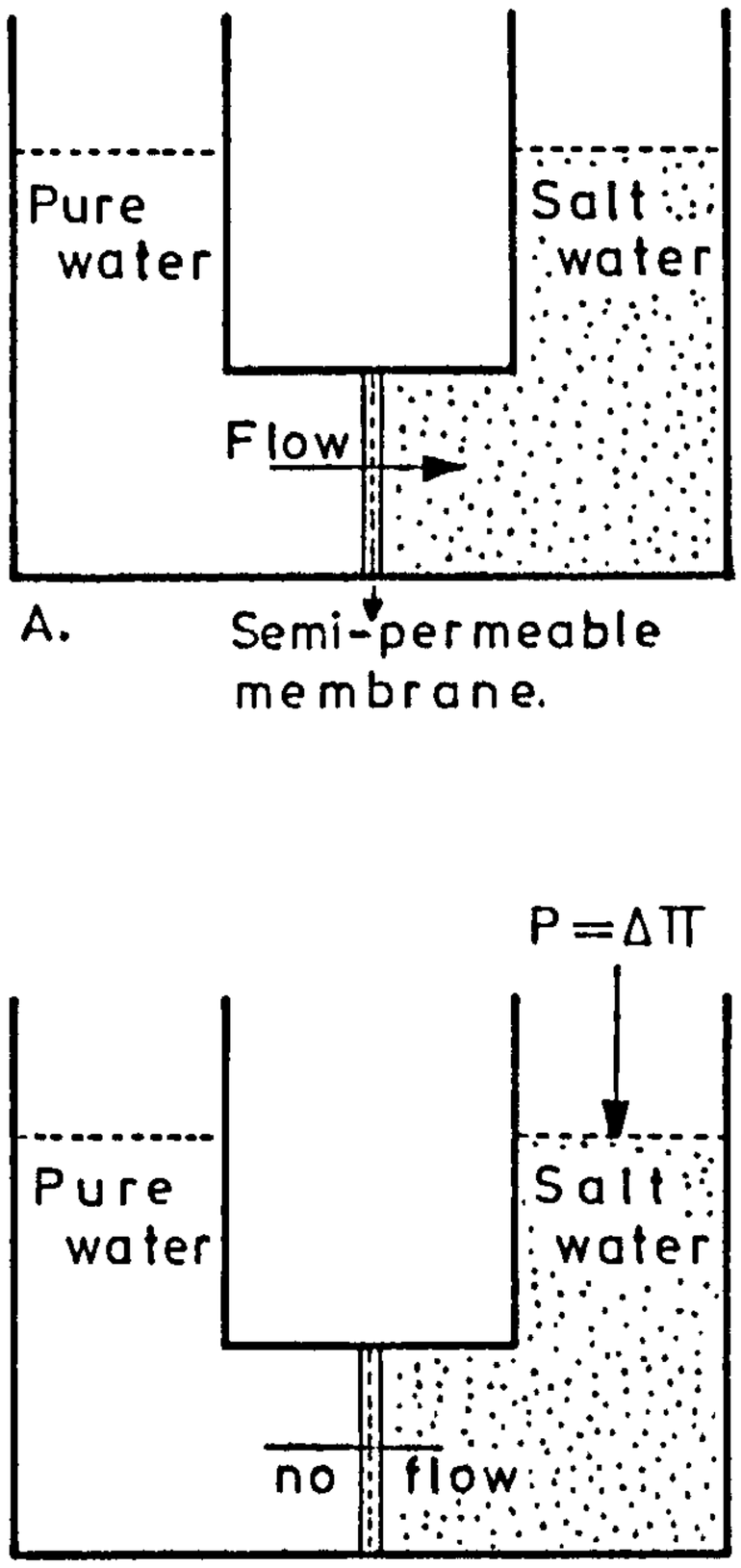


Figure 2.1 Osmosis and Reverse Osmosis.

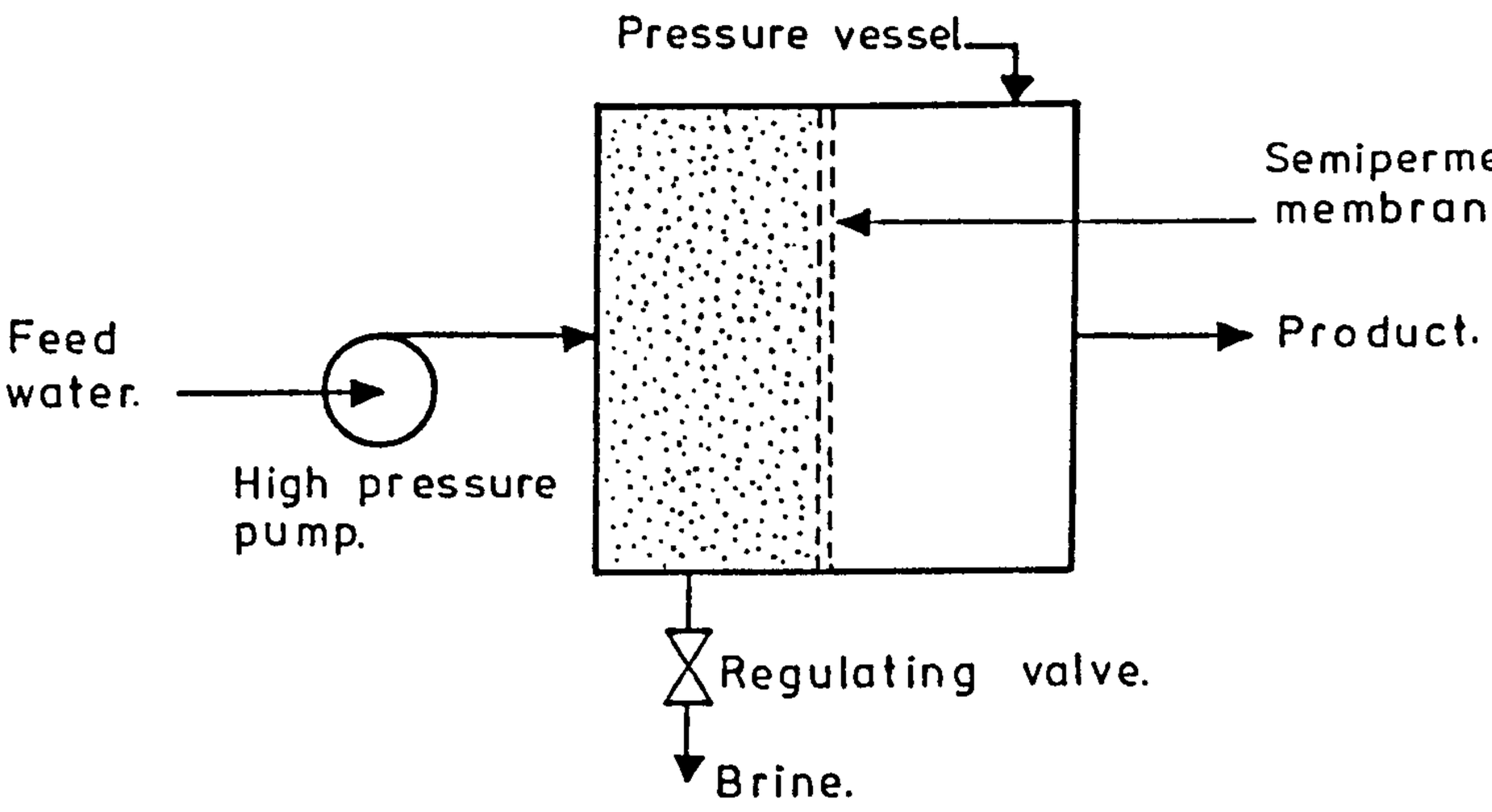


Figure 2.2 Simplified reverse osmosis flow diagram.

## 2.3 Some thermodynamic considerations

Flow of matter from one region to another is determined by a property called the "chemical potential". Any kind of matter, such as water, flows in the direction of in which its chemical potential decreases. The pure water molecules pass through the membrane, under the pressure which is higher than the osmotic pressure of the solution, and cause a solute separation in reverse osmosis systems. Consequently the chemical potential of pure water in aqueous solutions and the osmotic pressure of solutions are of interest. Hence some of the basic thermodynamic relations involving chemical potentials and osmotic pressure are summarised below, (34, 44, 48, 52).

The chemical potential ($\mu_i$) of a component i in a solution is defined in terms of the Gibbs free energy (G) by the relation

$$dG = -Sdt + VdP + \sum_i \mu_i \, d\,Ni \qquad (1)$$

where S is the entropy, T the absolute temperature, V the volume, P the pressure, and Ni the number of moles of component i.

From equation 1, the chemical potential, $\mu_i$ (or partial molar Gibbs free energy) may be written as

$$\mu_i = (\partial G/\partial Ni)_{T,P,N_J} \qquad (2)$$

and

$$V = (\partial G/\partial P)_{T,N} \qquad (3)$$

where N represent the entire set of N's and $N_J$ represents all N's except Ni.

Differentiating equation 3 with respect to Ni

$$\left[\frac{\partial^2 G}{\partial Ni\ \partial P}\right]_{T,N_J} = \left[\frac{\partial \mu_i}{\partial P}\right]_{T,N} = \left[\frac{\partial V}{\partial Ni}\right]_{T,P,N_J} = \bar{V}i \qquad (4)$$

where $\bar{V}i$ is the partial volume of component i.

In actual calculations it is customary to use not the chemical potential itself but a quantity called the activity ai and related to the chemical potential by:

$$\mu_i = \mu^{\circ}_i + RT \ln ai \qquad (5)$$

where R is the gas constant, and $\mu^{\circ}_i$ is the standard chemical potential of i which at a given pressure, is dependent on temperature only not on concentration. Various conventions are available for defining $\mu^{\circ}_i$, but for the solvent, $\mu_i$ in the treatment of solutions it is always taken to be the chemical potential of pure solvent; this means that the activity of pure solvent is unity.

The thermodynamic requirement for osmotic equilibrium is that the chemical potential of the solvent should be the same on both sides of the membrane; no such condition is imposed on the solute since the membrane prevents its passage.

If there is just pure water at pressure P1 on both sides of the membrane, the two phases will be in equilibrium (the chemical potential of water in both phases being $\mu^*_w$), and there will be no net transfer of water through the membrane. If pure water on one side of the membrane is replaced by an aqueous solution (both sides still being at pressure P1), the chemical potential of water in the solution is less than that of pure water, and the former is given by

$$\mu_w = \mu^*_w + RT \ln a_w \qquad (6)$$

where $\mu_w$ is the chemical potential of water in solution at pressure P1. The equilibrium can be restored by increasing the pressure on the solution side to P2 such that the chemical potential of water in the solution is raised to that of pure water. The increase in chemical potential of water in the solution as the pressure is increased from P1 to P2 is obtained from equation 4, as;

$$\int_{P_1}^{P_2} (\partial \mu w / \partial P)_{T,N} \, dP = \int_{P_1}^{P_2} \bar{V}_w dP \qquad (7)$$

Since this increase, added to $\mu_w$ given by equation 6, must restore the chemical potential of water in solution to that of pure water,

$$\mu_w + \int_{P_1}^{P_2} \bar{V}_w dP = \mu_w^* \tag{8}$$

Therefore

$$\int_{P_1}^{P_2} \bar{V}_w dP = \mu_w^* - \mu_w \tag{9}$$

$$= -RT \ln a_w \tag{10}$$

From equation 6, if $\bar{V}w$ is assumed constant

$$\bar{V}w\ (P2 - P1) = -\ RT \ln a_w \tag{11}$$

The pressure difference (P2 - P1) is by definition the osmotic pressure of the solution, usually represented by $\pi$, thus

$$\bar{V}w\ \pi = -\ RT \ln a_w \tag{12}$$

or

$$\pi\ = -\ RT/\bar{V}w \ln a_w \tag{13}$$

for calculating the activity of water in solution, $a_w$, vapour pressure data are needed, often, $a_w$ is calculated from the relation

$$a_w = Pw/Pw^* \tag{14}$$

where Pw is the vapour pressure of water in equilibrium with the solution, and $Pw^*$ is that of pure water at a given temperature.

## 2.4 Electrolyte solutions

Aqueous solutions of salts are mainly concerned in desalination. For this reason a great many physical-chemical measurements have been made on ions in solutions and theories of their behaviour have been developed. For example, an electrolyte of the form $C_{\nu+}\ A_{\nu-}$, which in solution ionise completely according to the chemical equation:

$$C_{\nu+}A_{\nu-} = {}_{\nu+}C^{+Z} + {}_{\nu-}A^{-Z} \qquad (15)$$

$$(\text{i.e. } Na\ Cl = {}_{1+}Na^{+1} + {}_{1-}Cl^{-1})$$

Considering, each of the ions has its own chemical potential and its own activity, equation 5 can be written in the form:

$$\mu_+ = \mu_+^{\circ} + RT \ln a_+$$

$$\mu_- = \mu_-^{\circ} + RT \ln a_-$$

The partial molar free energy (chemical potential $\mu_i$) of the overall electrolyte will be the sum of the ionic chemical potentials, each multiplied by the appropriate number of ions derived from the undissociated molecule. Therefore, equation 15 can be written for the electrolyte;

$$\mu_i = \mu_i^{\circ} + RT \ln a_i \qquad (16)$$

$$= \nu_+ \mu_+^{\circ} + \nu_- \mu_-^{\circ} + \nu_+ RT \ln a_+ + \nu_- RT \ln a_-$$

It now becomes convenient to define what will be known as the mean ion activity, $a_{\pm}$, which is a quantity that will satisfy the following equation:

$$a_{\pm}^{\nu} = a_{+}^{\nu+} a_{-}^{\nu-} \qquad (17)$$

In this equation, $\nu = \nu_+ + \nu_-$, the total numbers of ions formed from the salt. Thus the chemical potential of the salt may be written in the simple form

$$\mu_i = \mu_i^{o} + \nu \, RT \ln a_{\pm} \qquad (18)$$

When defining the activity of a particular ion, it may be convenient to use m, the molal concentration, or c, the molar concentration, as the reference function. Thus the activity coefficients for the ions may be written as

$$a_+ = \gamma_+ \nu_+ m \qquad (19)$$

$$a_- = \gamma_- \nu_- m$$

In these equations, $\nu_+ m$ and $\nu_- m$ equal to the concentrations of the two kinds of ions. Hence the mean activity coefficient, $\gamma_{\pm}$, may be defined by the expression

$$\gamma_{\pm}^{\nu} = \gamma_{+}^{\nu+} \gamma_{-}^{\nu-} \qquad (20)$$

The mean activity of a simple uni-univalent salt like sodium chloride is simply the square root of the product of the separate activities, and the mean activity coefficient is likewise the square root of the product of the separate activity coefficients. In general, the activity of the electrolyte will be;

$$a_i = a_{\pm}^{\nu} = \gamma_{\pm}^{\nu} \nu_{+}^{\nu+} \nu_{-}^{\nu-} m^{\nu} \tag{21}$$

In equation 19, if the reference function is taken as the mole fraction of the component i, $x_i$, the activity may be written as

$$a_i = \gamma_i x_i \tag{22}$$

or the activity coefficient $\gamma_i$ is;

$$\gamma_i = a_i / x_i$$

For an ideal solution the activity coefficient will be unity. In the case of dilute electrolyte solutions, the activity coefficients of water may differ from the unity by less than one in $10^4$ (e.g., the activity of water in a 5% sodium chloride solution at room temperature is 0.97 times the activity of pure water, Merten (32).

Therefore equation 13 can be written for an ideal solution as

$$\pi = - RT/\bar{V}_w \ln x_w \tag{23}$$

where $x_w$ is the mole fraction of pure water. In an electrolyte solution, the mole fraction of pure water will be

$$x_w = 1 - \nu x_s \tag{24}$$

where $x_s$ is the mole fraction of salt. Hence, equation 23 may also be written as;

$$\pi = - RT/\bar{V}_w \ln (1 - \nu x_s) \tag{25}$$

Equation 25 can be written by evaluating the second part as:

$$\pi = \nu RT/\bar{V}_w \, x_s \qquad (26)$$

Hence, the osmotic pressure of an electrolyte solution can be calculated by using equation 26.

## 2.5 Transport mechanism

Under isothermal conditions, in both osmosis and reverse osmosis, the transport of material through the membrane is always in the direction of lower chemical potential. This is a thermodynamic requirement which says nothing about the mechanism of the separation process.

The osmosis process is associated with aqueous solutions and semipermeable membranes. The term 'semipermeable' describes the membrane but does not explain why the membrane is permeable to the solvent but not the solute.

Several mechanisms of water and solute transport through the reverse osmosis membranes are discussed in the literature, Merten (32), Kedem (26), Sourirajan (48), Sourirajan and Matsuura (47), Lonsdale et al (31), and Banks and Sharples (4). However, the fundamental transport mechanism is not fully understood. Some useful models are shown diagrammatically in Fig. 2.3 A,B,C, Blais (10). These are (a) - solution diffusion, (b) - sieve model and (c) - preferential sorption.

A - Solution diffusion model. Reverse osmosis separation is governed by a solution diffusion mechanism which requires that the solute and solvent dissolve in the membrane material and permeate through the membrane by diffusion through the homogenous non-porous surface layer. The water (solvent) is readily soluble in the membrane material but the salt (solute) is only slightly soluble. The water, being more soluble, can maintain higher concentrations and therefore higher concentration gradient and rates of diffusion. The salt is only slightly soluble in the membrane limiting the possible diffusion flow rates and thus leading to relatively small salt fluxes.

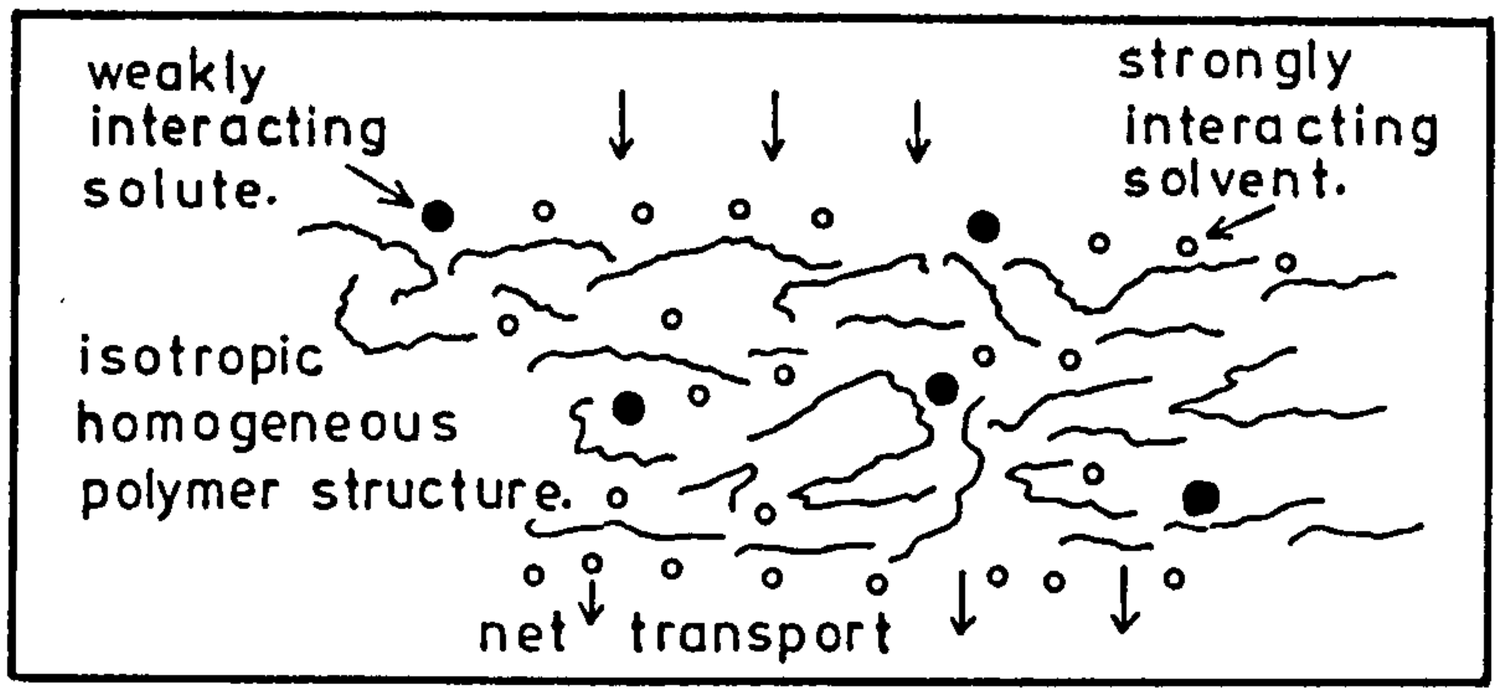


A- Solution Diffusion model.

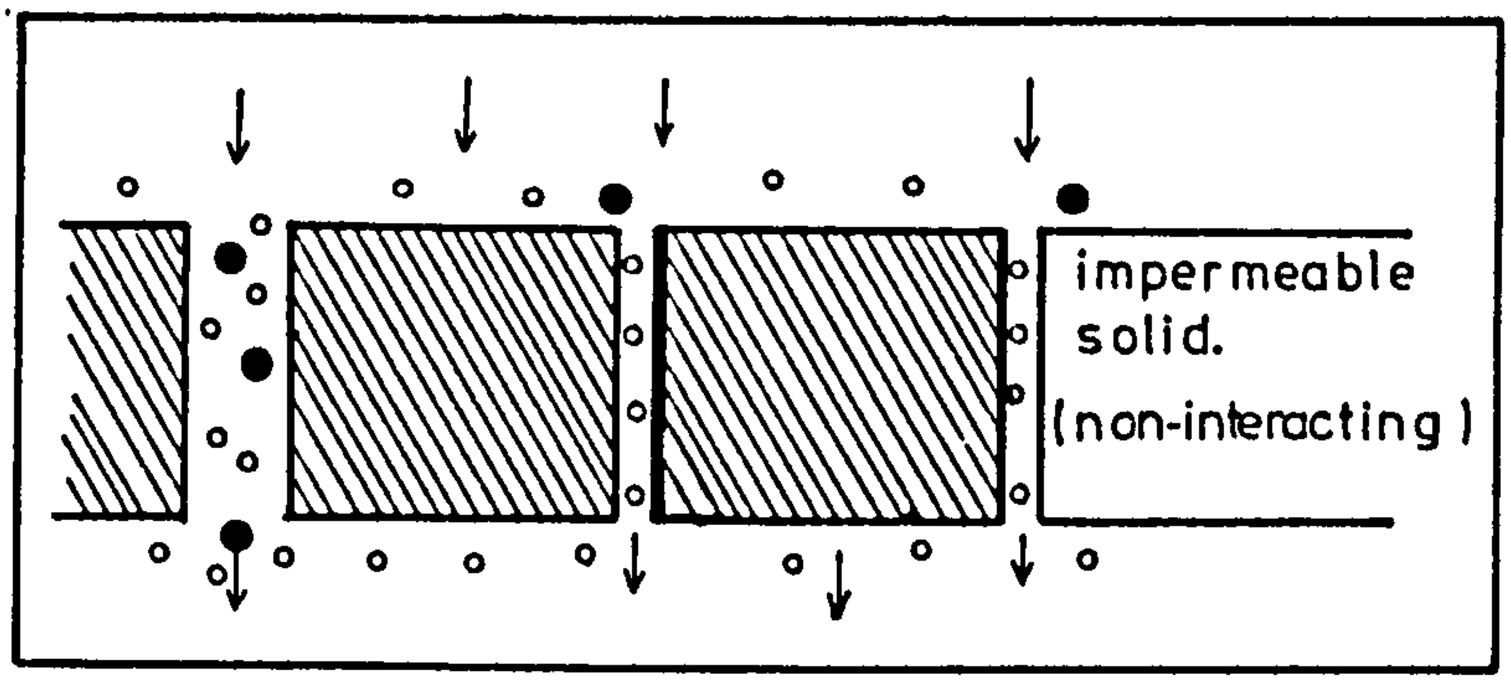


B- Sieve Transport model.

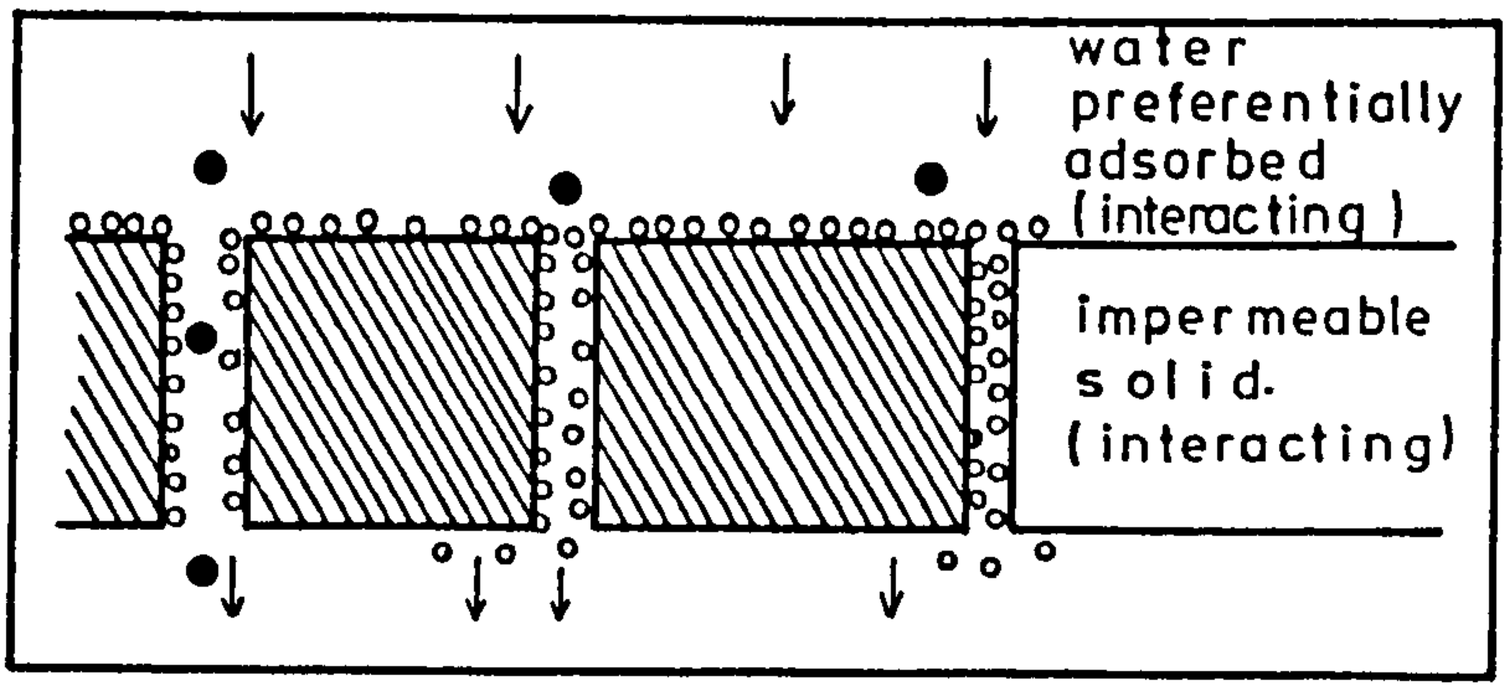


C- Preferential Sorption model.

Figure 2.3 Reverse osmosis transport models.

The active layer of membrane is envisaged as a molecular lattice into which water molecules can penetrate and through which they can pass by diffusion. In certain areas the lattice is open enough to permit the entry of salt molecules. The variation in properties from membrane to membrane was explained to be a variation in lattice tightness by Hodgson (25). It is also known that the water sorption properties of cellulose and its derivates may depend on such factors as their degree of crystallinity, Lonsdale et al (31).

The overall solubility of water and salt are considered to be independent so that the water flux will not necessarily change in proportion to the salt flux, so that for a given salt rejection there can be a range of water flow rates.

The water flux through the membrane is essentially pressure dependent and is proportional to the net driving force. It can be written as: Lonsdale et al (31).

$$J_1 = - D_1 C_1 \bar{V}_1 (\Delta P - \Delta \pi)/RT \Delta X \equiv K_1 (\Delta P - \Delta \pi) \qquad (27)$$

In arriving at this result, it is assumed that $D_1$, $C_1$ and $\bar{V}_1$ are independent of pressure P, where $\bar{V}_1$ partial molar volume of water, $D_1$ diffusion coefficient and $C_1$ concentration of water dissolved in the membrane, and $\Delta X$ is the membrane thickness. The water permeability constant, $K_1$ ($g/cm^2$.sec.atm.), can be calculated simply as; Lonsdale (29)

$$K_1 = J_1/(\Delta P - \Delta \pi) \qquad (28)$$

On the other hand, the salt flux is pressure independent, the driving force is almost entirely due to the salt concentration difference. The salt flux can be written as

$$J_2 = - D_2 K \Delta C_s/\Delta X = K_2 \Delta C_s \qquad (29)$$

The distribution coefficient, K, for salt between the membrane and water, and the diffusion coefficient $D_2$ are independent of salt concentration $C_s$. The salt permeability, $D_2K$, of the membrane is variable in real membranes (not-perfect) due to the salt leakage through defects in the membranes.

B - Sieve transport model According to this model, the transport mechanism in reverse osmosis is one of diffusive flow through the membrane without specific interation between the barrier surface, the solute and the solvent.

Membrane structure is porous and the pores are too small for solute molecules or hydrated ions to pass through but large enough for water molecules to pass. The membrane acts as a micro sieve. In such a structure there is bound to be some variation in the pore sizes and some will inevitably be large enough to pass the solute molecules or ions (imperfect membrane) thus accounting for slight permeability to salt.

Solvent flow through the rejecting pores is given by $K_1$ $(P-\Delta\pi)$ but solution flow through the non-rejecting pores is determined only by the applied pressure $K_2P$, Banks and Sharples (4).
Therefore water flux through the membrane;

$$J_1 = K_1 (P-\Delta\pi) + K_2P \qquad (30)$$

and the solute flux is given by;

$$J_2 = K_2 P C_b \qquad (31)$$

where $K_1$ and $K_2$ are solvent and solution flow constants respectively.

C - Preferential sorption model According to this model, the reverse osmosis separation mechanism is governed, in part, by a surface (interfacial) phenomenon. The characteristic of the membrane is that it attracts water more than the solute. When the surface of a porous membrane is in contact with the solution a multimolecular layer of preferentially sorbed pure water forms on the membrane surface. A continuous removal of this interfacial layer (water) by flow under pressure through the membrane capillaries results in a product solution.

If the pore diameter is bigger, permeability will be higher but solute separation will be lower since the effective feed solution (concentrated boundary solution) will also flow through the pores. When the size of the pores on the membrane surface is only a few times bigger than the size of the permeating molecules, and the interfacial forces are important enough to cause solute separation.

In this mechanism, the transport equations are based on Kimura-Sourirajan Analysis which based on a generalised capillary flow model involving viscous flow for water transport, pore diffusion for solute transport, and "film" theory for calculating an effective mass transfer coefficient applicable to the concentration polarisation situation, Sourirajan and Matsuura (47).

The basic equations relating to the pure water permeability (PWP, g/hr) constant A ($g.mol/cm^2.sec.atm$)

$$A = PWP/M_B \times S \times 3600 \times P \qquad (32)$$

where $M_B$ is molecular weight of water and S is the membrane surface area as $cm^2$.

The transport of solvent water $N_B$ is given by

$$N_B = A\ (P-\pi(X_{A2}) + \pi(X_{A3})) = A\ (\Delta P-\Delta\pi) \qquad (33)$$

where $\pi(X_{A2})$ and $\pi(X_{A3})$ represent the osmotic pressure $\pi$ corresponding to mole fractions of solute $X_{A2}$ and $X_{A3}$ in the boundary layer and in the product respectively.

The transport of solute through the membrane phase is treated as being due to pore diffusion. Consequently, the solute flux, $N_A$, through the membrane is proportional to the concentration difference across the membrane and is given simply by:

$$N_A = X_{A3}/(1-X_{A3})\ N_B \qquad (34)$$

It seems likely that all of these situation exist to some degree in practical reverse osmosis membranes. However, the preferential sorption depends on the chemical nature of solution relative to the chemical nature of the membrane surface. Therefore the chemical nature of the barrier must have some influence on the reverse osmosis properties of membranes. Hence, if the appropriate chemical relationships exist between the barrier, the solute and the solvent, the preferential sorption mechanism may superpose on the other two mechanisms.

However, for engineering purposes, real membrane behaviour can be closely approximated by using solution-diffusion model which has widely been used in determining the membrane characteristics. Thus, the transport equations in solution-diffusion model will be used to explain the experimental data in the next chapter.

## 2.6 Reverse osmosis membranes

A membrane may be defined as a thin sheet-like piece of material forming a barrier between two phases. The characteristics of the membrane is that certain constituents in the phases separated by a membrane will pass through the membrane more easily than others under the actions of particular driving forces.

An ideal or perfect membrane is described to be completely impermeable to certain species. However, in reality membranes are not often completely impermeable to any component. It is merely a question of being much more permeable to some components than others.

Several characteristics of membranes are important for desalination. An effective membrane should have:

a - wide operating range (pressure, temperature and concentration)

b - high water and low salt permeabilities

c - physical, chemical and biological stability

d - easily repreducible characteristics

e - long service life and low cost

f - high surface to volume ratio

There is no perfect membrane, and the ones in use today vary in quality with regard to these characteristics.

One of the most important characteristics of a R.O. membrane is the quantity of water which can flow through the membrane. This is described by the following simplified equation:

$$J_1 = K (\Delta P - \Delta \pi) \qquad (35)$$

where $J_1$ = water flux, $cm^3/cm^2$ sec. (m/d)

Therefore membrane surface area of a unit becomes very important in overall productivity.

### 2.6.1 Membrane materials

Membranes are made from a variety of materials. Cellulose Acetate (C.A.) was used in much of the original development work by Loeb, Reid and Sourirajan in the 1950's. The C.A. membrane was about 25 micron thick film, symmetric in structure, given a flux of 0.01 m/day with a 50-fold reduction in salt concentration.

Loeb and Sourirajan, in 1960, developed membranes which effectively separated salts from water and led into commercial development of the process. The membranes were made of cellulose diacetate which had an acetyl content of 38 to 40%. The active layer of membrane was about 1 micron thick given water flux up to 100 times that previously available.

The original C.A. material has been largely displaced by various derivatives of other cellulose acetates, polyamides and other polymers, (3, 5, 6, 16, 48). The following list gives some idea of the materials that have been investigated and used in membrane production.

a - Cellulose based polymers (C.A., cellulose triacetate, C.A. butyrate)

b - Commercial polymers (66 Nylon, Polyethylene terephthalate, Polyvinyl alcohol)

c - Polymer blends (Polyvinyl alcohol-polyvinyl pyrrolidone, Polyacrylonitrile - Polyvinyl tetrazole)

d - Miscellaneous experiemental polymers. (Acrylonitrile - N - (2 - hydroxyethyl) acrylamide, Polyaminopivalic acid)

e - Nitrogen linked polymers (Aliphatic polyamides, aromatic polyamides, aliphatic-aromatic polyamides, polybenzimidazoles, aromatic polyhydrazides, polysemicarbizides, polyimides).

Out of hundreds of candidate polymers, three classes proved to be most promising for development of commercial R.O. membranes (a) cellulose acetate (b) aromictic polyhydrazides and (c) aromatic polyamides. All of these could be made into the required asymmetric membrane structures. However, aramid polymers have been replacing C.A. polymers in membrane manufacture, because of their better resistance to mechanical change, as well as chemical and biological attack. One of the reasons is that aramid polymers do not exist in nature and there is no known case of micro-organisms attacking them. Secondly C.A. membranes must be used within a narrow pH range (4 to 9) to prevent hydrolysis. However, C.A. membranes are cheaper to produce than aramid polymer membranes.

### 2.6.2 Membrane fabrication methods

Understanding of the structure of desalination membranes is important for understanding the mechanism of desalination by reverse osmosis.

The most important characteristics of an R.O. membrane is high salt rejection and water flux. Studies in membrane technology show that membrane structure is important as well as membrane materials. Usually thinner membranes give better permeation. Hence, membrane must be as thin as possible and the supporting porous structure must be able to transport the permeate easily.

The factors governing membrane structure and its characteristics depend on membrane fabrication technique. There are several techniques of membrane fabrication using different membrane materials. However, the two most common membrane fabrication methods will be reviewed for understanding of the membrane formation mechanism. These are asymmetric cellulose acetate flat-sheet and aromatic polyamide hollow fine fibre membranes.

A - The asymmetric cellulose acetate (C.A.) flat sheet membranes

These asymmetric membranes are formed by precipitation from a solution of the polymer in good solvent such as acetone. The procedure is as follows: (32).

a. Solution. The polymer is made up into a viscous solution in the solvent (acetone) together with a number of modifying additivities (e.g. C.A. - magnesium perchlorate - water - acetone in the proportions 22.2 - 1.1 - 10.0 - 66.7 wt%). The inclusion of the modifyers in the solution produces the porous structure in the cast membrane.

b. Casting. A thin (150 ~ 250 micron) layer of the solution is spread out on a glass plate (if it is desired to separate the membrane from the surface later) or porous substate (if membrane is being cast directly onto its support which may be in the form of a sheet or tube). In this phase, the thickness of the film is determined.

c. - Evaporation. The film is then exposed to the air (e.g. 3 minutes). The solvent evaporates from the surface of the film (concentrating the surface layer) resulting a think active layer. The long evaporation time causes a thin active layer with a low water flux and high salt rejection. If the evaporation time is too short the active layer becomes very thin and probably the membrane is not complete leading to poor rejection.

d. - Gelation. The membrane is solidified by immersion in water (e.g. 0-2$^{o}$C) for about one hour. The main effect is to produce inhomogenous precipitation in the bulk of the membrane thus producing the porous structure. The temperature of, and additivities in, the gelation bath are used to alter the membrane properties. In general a higher gestation temperature produces a more brittle membrane.

e. - Annealing. The membrane is transferred to a warm water bath at a temperature between 60 and 85$^{o}$C for a few minutes to improve salt rejection. Increasing annealing temperature increases the salt rejection but decreases the water flux. Treatment at temperatures below 60$^{o}$C has no effect whereas temperature above 85$^{o}$C tend to destroy the porosity of the membrane bulk.

The membrane produced by this process is relatively robust, slightly thinner than the cast layer, and can range from being almost transparent to being opaque.

B. Hollow fibre membranes

There are several techniques for spinning hollow fibres. However, the fabrication of aromatic polyamide asymmetric hollow fibre membrane will be reviewed here, Caracciolo et al (12). The procedure is as follows:

a. Fibre spinning. The asymmetric hollow fibre membrane is spun from a solution of the aromatic polyamide polymer and inorganic salts in dimethylacetamide through a shaped orifice. The extrusion orifice, or spinnerette, used for preparation of hollow fibre may be of several designs. For example, in the dry-jet wet process, the tube-in-orifice design is used with nitrogen gas injection. The spin dope is extruded through a sealed, vented insert spinnerette, which admits nitrogen to the centre of the filament to maintain bore integrity while the final structure is setting in the subsequent drying and extraction steps. Techniques utilising the wet or dry-jet wet spinning approach often are favoured for hollow fibre membrane applications, Orofino (39).

b. - Stabilisation. In a continuous fibre spinning process, the threadline emerging from the spinnerette must be quickly stabilised and thus given sufficient mechanical integrity to permit subsequent passage over guides and rolls under moderate tension. First, the major fraction of the solvent is removed from the fibre exterior with heated nitrogen gas. The balance between the rate of surface evaporation and of solvent migration to the outer fibre wall has a determining effect on the skin properties of the hollow fibre membrane. The remaining solvent and salts are extracted with water and the porous body which support the skin is set up as water displaced the solvent. To retain its asymmetric properties, the fibre is kept wet. Thermal annealing increases the resistance of the hollow fibre to deformation and improves its salt rejection properties.

c. - Post-treatment. When the permeator assembly is completed all the ingredients from the various manufacturing steps are flushed out and post treatments to tailor the salt passage are applied. For example, B-9 permeators are post-treated with PT-A (polyvinyl methyl ether) during the manufacturing process to increase salt rejection. On occasion, PT-B (tannic acid) has been used to increase the salt rejection.

B-10 permeators are post-treated with PT-B to reduce the salt passage by about 30-50%. However, this treatment may also cause loss in product flow of 5-10%.

d. - Bundle formation and permeator assembly

The hollow fibre yarns are wound around a flat porous web. (All fibres are arranged in a parallel configuration. Cross overs or other misalignments have a significant effect on bundle packing density and flow distribution). The web with the layers of fibre on both of its sides is rolled around the rotating central distributor tube which forms the axis of the fibre bundle. As the web moves forward and is rolled spirally around the distributor, an epoxy adhesive is applied to one of the two edges, which later forms the tube sheet (open end). The distributor opening in the tube sheet is sealed after the epoxy has cured. A plastic tube to connect the distributor tube with a feed inlet is attached at the other end (closed end), which is thereafter completely sealed to prevent short circuiting of the feed stream to the concentrate outlet.

The flow screen is attached on the outside of the bundle and the tube sheet face is cut to open the fibre ends and to provide the groove for the O-ring seal. The bundle with the porous back-up disc is then assembled in the pressure vessel.

### 2.6.3 Membrane structures

There are two basic types of membranes used in R.O., the fixed membranes and dynamic membranes. The overwhelming majority of the membranes are now being utilised in R.O. have a fixed membrane structure. All membrane structures have two sequential components. The first is about 1 micron thick skin surface layer which determines the salt and water flux characteristics. The other one is the porous body which supports the surface layer and transfers the permeate.

a. - Fixed membranes. The active surface and the porous support layers are joined together permanently which makes them asymmetric in structure. In some instances, the surface layer can be made from the same material as the porous base, in which case the surface is usually altered during or after the forming process. Most of the polyamide and cellulose based hollow fibre and flat membranes are made in this fashion.

Thin film composit membranes (such as PA-300 spiral membrane) are made by incorporating the separate active layer on the porous base by polymerisation or other means. These membranes can be more complex to produce commercially.

b. - Dynamic membranes. The two components are produced separately and joined as part of the operating process. The membrane structure is produced by adding certain chemicals to the feed water as it flows through porous structure. Deposits from these solutions collecting on the surface of the porous medium form an active layer. These types of membranes do not have a good combination of water flux and salt rejection comparing to the fixed membranes.

### 2.6.4 Reverse osmosis membrane configurations

Several types of R.O. membrane configurations have been explored over the past 20 years. Only four membrane configurations have been advanced to commercial applications. These are plate and frame, tubular, spiral wound and hollow fine fibre systems. These membranes have been manufactured by different companies using different techniques and membrane materials. Manufacturers and their representaties generally distribute specification sheets describing the nominal performance of their units under certain operating conditions.

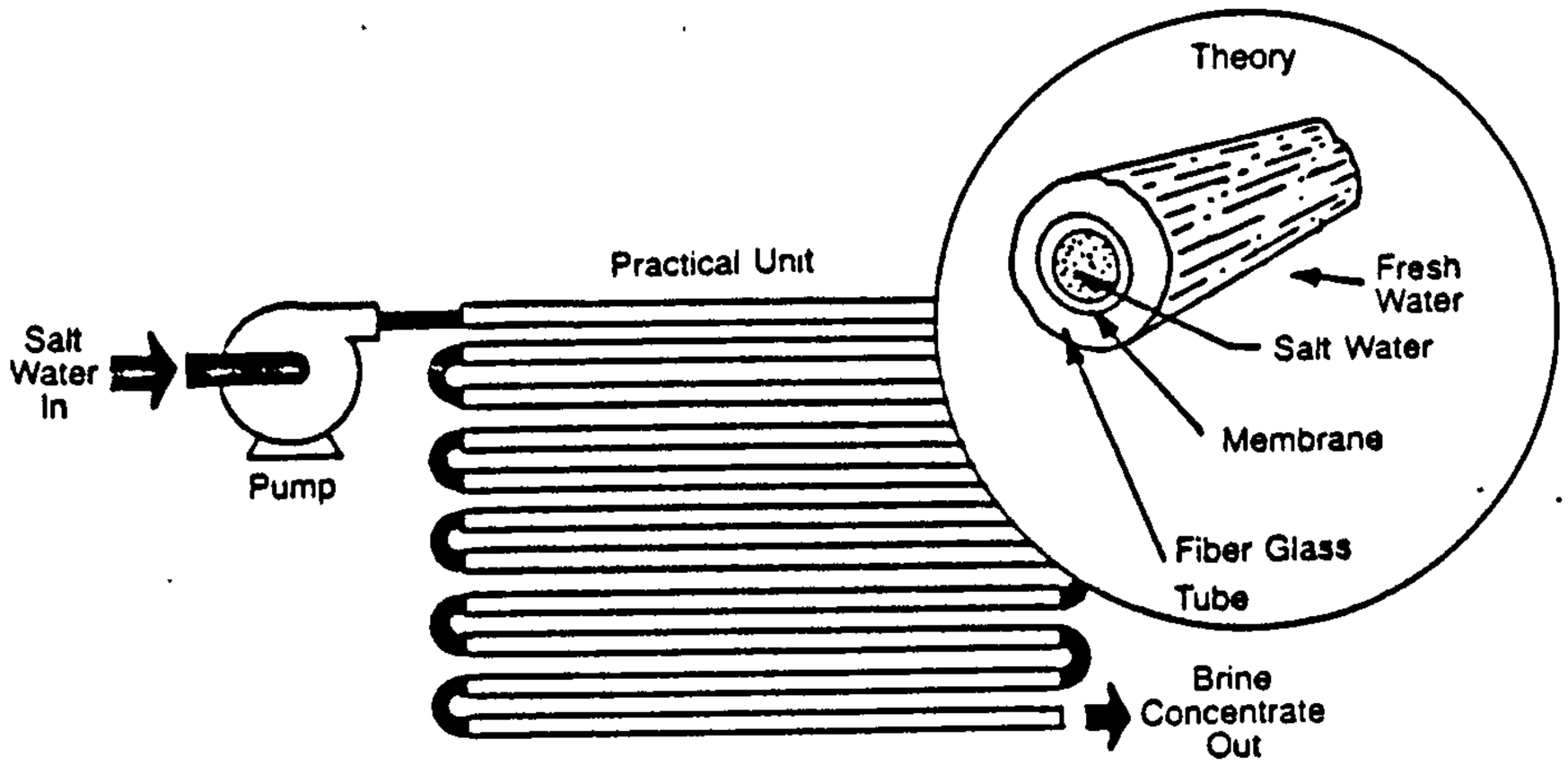


Fig. 2.4 Tubular Reverse Osmosis Membrane

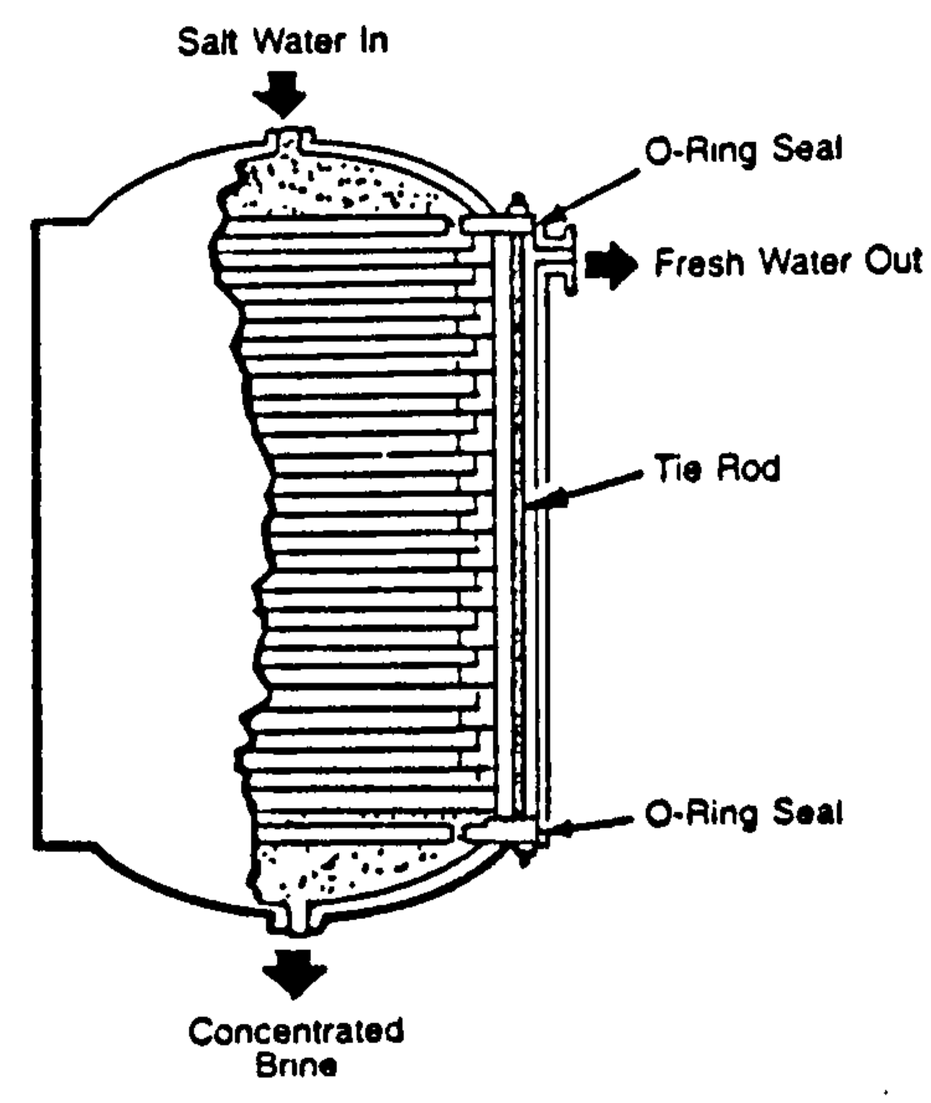


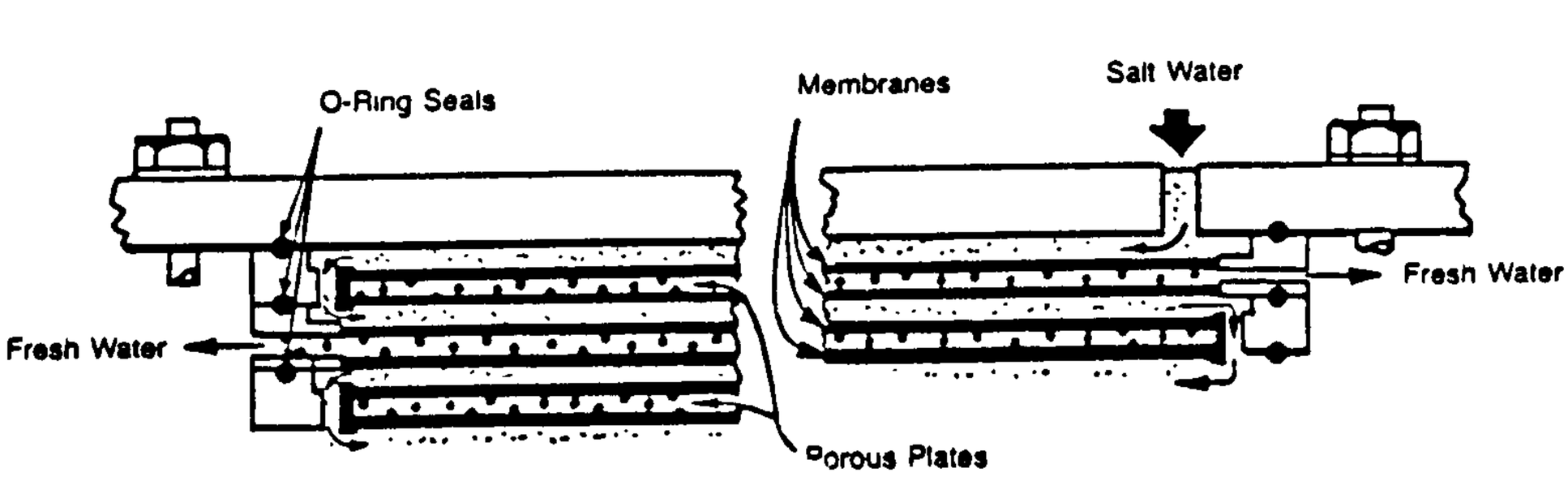


Fig. 2.5 Plate and Frame Reverse Osmosis Membrane

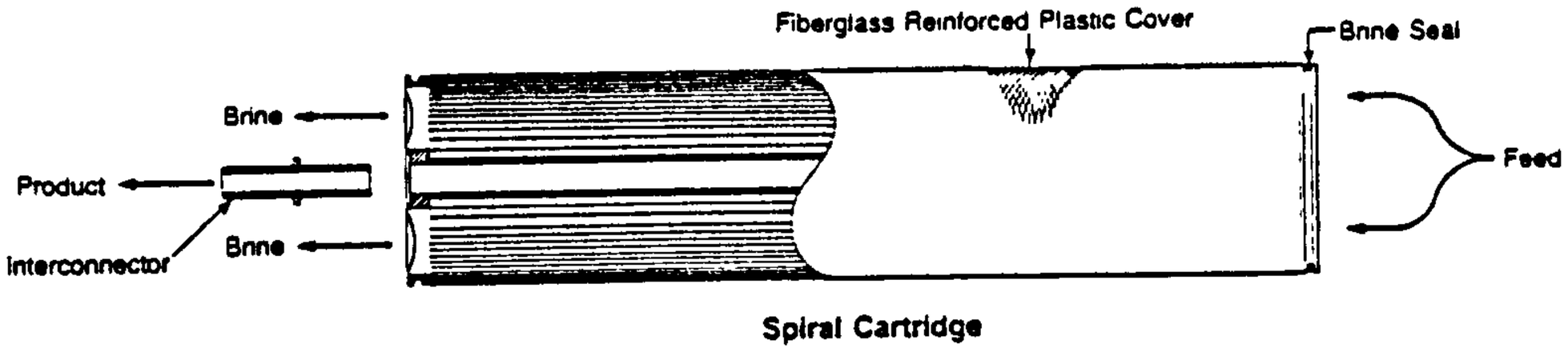


Spiral Cartridge

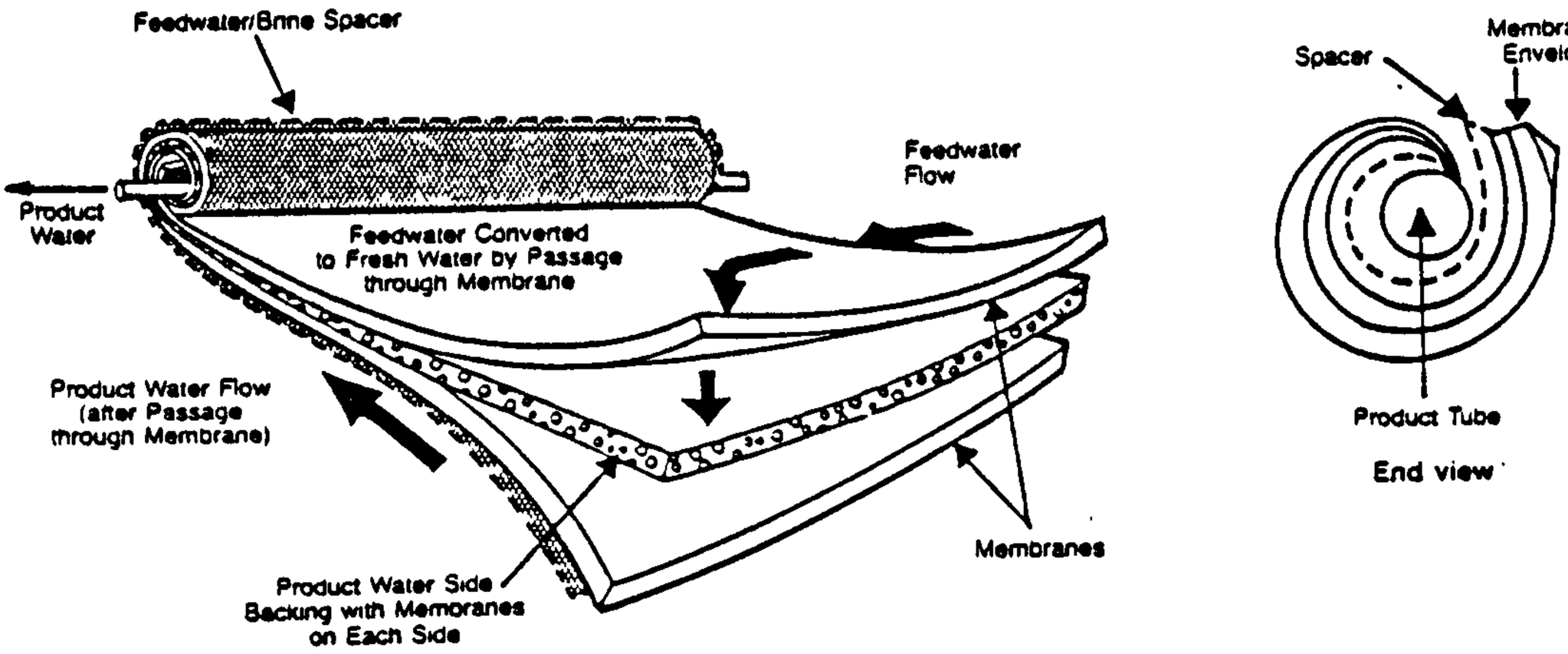


Fig. 2.6 Spiral-wound R.O. membrane and the cartridge

(Fig. 2.4, 5 and 6, U.S. Dept. of the Interior, Office of Saline Water)

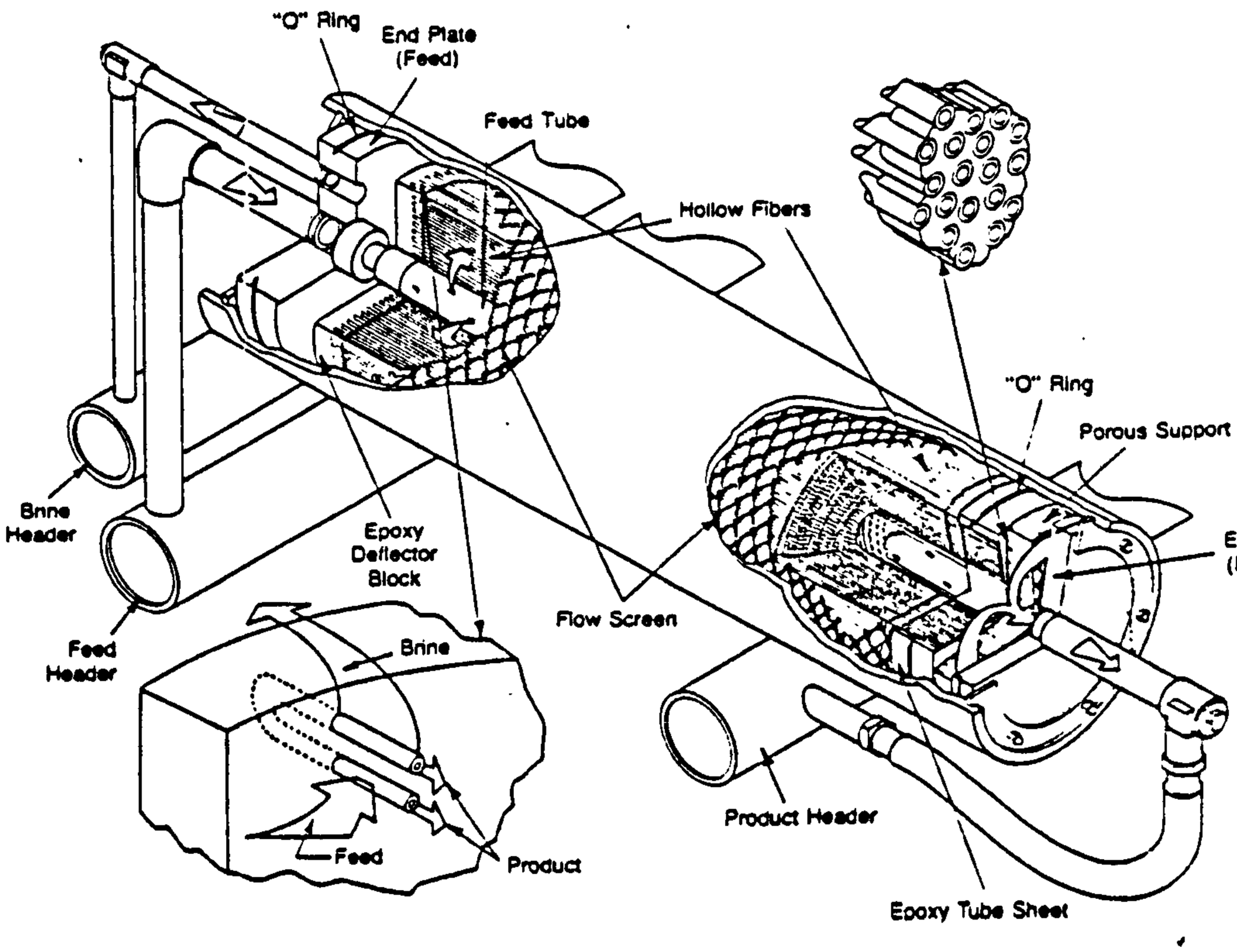


Fig. 2.7 "Permasep" Hollow Fibre Membrane (PEM, 42)

A comparison of the modules characteristics is given in Table 2.1.

A brief description of these systems is given below.

a. - Tubular membranes. The membrane is placed or coated on inner wall of the porous tubes with a diameter of about 0.7 to 2.5 cm. Bundles of these tubes are joined to a header in parallel or in series like a shell and tube heat exchanger. The feed water flows inside the tube and the brine exists from the far end of the tube. The product water passes through the membrane to the porous tube wall and is collected inside the shell, Fig. 2.4. The system is not efficient for large scale water treatment applications because they contain a small membrane area per unit volume. Packing densities for tubular membrane systems are within the range from 32 to 320 $m^2/m^3$. Water flux may be around 0.5m/day. However, the system is used in special applications where the particulate count is very high. They can be cleaned easily and frequently.

b. - Plate and frame membranes. In this device, the membranes are mounted on opposite sides of a rigid porous plate and sealed to the plate. The feed water is applied on the outer side of the plate and product water is collected at the interior of the supporting plate, Fig. 2.5. Comparing with other devices, plate and frame R.O. systems contain a relatively small membrane surface area for the volume of the pressure vessel required. The membrane packing density in current designs ranges from 150 to 500 $m^2$ per $m^3$ unit volume. The water flux may be given around 0.4 m/day.

Plate and frame equipment, however, does offer flexibility of selecting different membranes for different applications.

c. - Spiral wound membranes. The spiral wound membrane configuration uses flat sheet membranes. The membrane is cast on a fabric support and then two of these fabric supported membranes are glued together with a porous material. This porous material provides a route for the product weater, which passes through the membrane. The membrane leaf is glued together on three of its four edges forming an envelope. The fourth edge is joined to a tube which acts as a collector for product water. These envelopes together with brine side spacer screens are wound around the

collector tube and the module is housed in a pressure vessel. Usually 2 to 26 membrane envelopes are attached to the central tube. The feed flows axially along the side spacer screen and the permeate flow through the membrane into porous backing material and then to the central collector, Fig. 2.6.

Two to six modules are usually placed in series in a long tubular pressure vessel to make up a single production unit. The diameters of the modules range from 5 to 30 cm. The spiral wound design is compact, with membrane area ranging from 650 to 1650 $m^2$ per $m^3$ unit volume of module. Initial capital costs of larger modules are less than the smaller modules.

d. - Hollow fibre membranes. Modern technology has made possible the preparation of R.O. membranes in the form of hollow fine fibres. They are asymmetric in structure with a very dense skin on the outside, supported by a porous structure, usually, of the same chemical composition. The feed solution flows on the outside of the fibres and the product water flows inside the fibres.

The main advantage of hollow fibre membranes is that very large surface area can be packed in a shell volume, i.e. ranging from 2900 to 60000 $m^2$ per $m^3$. The ratio of outside to inside diameter (O.D. = 95 micron, I.D. = 45 micron) is at least 2 to 1, so these fibres can be viewed as thick-walled cylinders. They have the strength to withstand high operating pressure (68 atm.) without additional physical support.

A bundle of hollow fibres are sealed on both ends and one end is cut open to remove the permete. The feed tube (at the centre of the bundle) is sealed at one end and is porous along its length within the fibre bundle. The bundle of fibres is placed in a pressure vessel. Fig. 2.7 is a cross section of a permeator. The construction resembles a shell and tube heat exchanger. Feed water under pressure enters the pressure vessel through the feed tube and is forced from the centre of the fibre bundle radially outward around the many fibres within the bundle. The high pressure concentrated solution leaves the shell while the product water is collected and carried away on the other side.

The permeate flux rate through these fibres is low (0.02 · 0.4 m/day). However, the enormous surface area of such fibres packed into a unit volume, tends to compensate, for the low flux rate.

TABLE 2.1

Reverse Osmosis Module Characteristics

| Module | Pressure (atm.) | Flux (1) | Packing density (2) | Flux density (3) |
|---|---|---|---|---|
| Tubular | 40 | 0.40 | 32-330 | 13-132 |
| Plate and Frame | 40 | 0.40 | 150-500 | 60-200 |
| Spiral Wound | 40 | 0.40 | 650-1650 | 260-660 |
| Hollow Fibre | 27 | 0.013 | 29000-60000 | 377-780 |

(1) Flux (cubic meter product water/sq. meter day (m/day))

(2) Packing density (sq.m. membrane area/cu.m. module volume ($m^2/m^3$))

(3) Flux density (cu.m.water/cu.m. module volume per day ($m^3/m^3$))

NOTE: The data in Table 2.1 are only informative, they depend on the type of membrane used. Membranes with a wide range of flux rates are commercially available, (9, 13, 21).

# CHAPTER 3: SOME ASPECTS ON BRINE, FEED AND PRODUCT WATER IN DESALINATION

## 3.1 Introduction

The purpose of this chapter is to give some idea about the physical and chemical characteristics of water used in desalination by reverse osmosis.

The water enters the system, called "feedwater", is separated by reverse osmosis membrane into two streams. The highly concentrated reject solution is called "brine" (or concentrate) and the other one is called "product water" (permeate or fresh water). The characteristics of brine, product and feed water are very important factors in designing a desalination plant. Normally reverse osmosis systems are designed, constructed, and installed by the original equipment manufacturers or their representatives. Regardless of who is involved with the design, it is important to know about the solution processed in a desalination plant.

## 3.2 Feed water

The main raw water supplies are surface and underground waters. Defining the characteristics of raw water supply is an important item in the design of a reverse osmosis system. The chemical and physical characteristics and their variability should be thoroughly investigated.

One of the major problems in operation of a plant is fouling. It is the deposition of materials within the plant which result in reduced performance of the system. The membrane surface especially is very sensitive to fouling, both biological or non-biological, which can reduce the water flux to a major degree. In bad cases the membrane replacement may become necessary.

The proper pretreatment of the water before it reaches the membrane is the key to successful operation of a reverse osmosis plant. Brackish well water and sea water from shore wells generally require only basic treatment since the water has already filtered through the earth. Surface waters, both brackish and sea water, usually require more extensive pretreatment to make the water suitable for the reverse osmosis process.

Different membrane modules may require different feed water treatment. In the case of Du Pont hollow fibre membrane systems, the feed pretreatment techniques for the removal of different substances may be found in Permasep Engineering Manual (PEM) (42).

## 3.3 Brine

The brine stream has a concentrated salt solution and often some levels of chemical additivities which must be disposed safely. The brine in a brackish water reverse osmosis plant can amount to 10 to 50% of the water produced and that of about 70% in a sea water reverse osmosis plant.

In coastal locations the brine stream can usually be discharged into the sea or ocean without problems. However, the concentrated brine with chemical additivities may cause some problems to aquatic life if discharged into estuarian areas.

Inland brine discharges can be an important problem, since the brine can adversely affect the quality of the existing ground water if the brine is allowed to enter the aquifer. One of the first items that should be considered in an inland desalting project is the disposal of the brine. The necessity for a special disposal technique could make the system very costly.

## 3.4 Product water

Product water is the most important item because it is the one being consumed as drinking or industrial water. In designing a reverse osmosis plant, information on the desired quantity and quality of the finished water is needed. The quality of the product water is referred to its total dissolved solids (TDS) content. The desired quality of the product water will determine the salt rejection required.

If the product water is for human consumption then it should be within W.H.O. limits which is less than 500 mg/L as TDS. For specialised uses, (electronic industry, boiler feed water) much higher degrees of purity may be required.

The product water emerging from the membrane assembly needs some type of post-treatment before being distributed as potable water, (pH adjustment, removal of dissolved gases such as $H_2S$ and $CO_2$).

However, the palatability and health aspects of product water should be considered. The effect of mineral content of product water when comparing to WHO standards on the palatability and health have been discussed in the literature (7, 8, 18).

## 3.5 Osmotic pressures of solutions

Knowledge of the properties of saline waters and their concentrates is important in the development, design and operation of desalination processes.

The total dissolved solids (TDS) content of a saline solution is the most important one in desalination by reverse osmosis. Because the osmotic pressure of a solution is directly related to its TDS content, increasing the TDS level of a solution increases the osmotic pressure in direct proportion. A solution with a higher osmotic pressure requires higher applied pressure, hence increases the size of plant and energy consumption.

Saline waters having a TDS content below 10000 mg/L (ppm) is generally described as "brackish water". At higher TDS levels, it becomes "high brackish" or "sea water".

In the literature the properties of electrolyte solutions and sea water are well documented, (17, 48). Concentration of seawater may be found different in different locations but sodium chloride is the predominant salt component with a proportion of about 78% with 10.5% Mg $Cl_2$.

When brackish waters are considered, there is no specific predominant salt component in common. However, Calcium, Magnesium and Sodium cations with Sulphate and Chloride anions are generally found in different proportions. One of the cations with an anion may become the predominant salt content in a specific brackish water. Mineral content analyses of some brackish waters can be found in the literature (1, 2, 19, 28, 41).

Different salt component of solutions may give different osmotic pressures due to their physical and chemical properties, such as approximately, one weight percent of NaCl gives 116 psi, Ca $Cl_2$ 92 psi, $Na_2SO_4$ 60 psi and Mg $SO_4$ 36 psi. Osmotic pressure determination of solutions is given in Chapter 2 and related references.

In desalination practice, concentration of solutions are determined by measuring the electrolyte conductivity as mhos/cm (or Siemen (S)/cm). The tables of conductivity vs. concentration used in these experiments are given in Appendix 3.

# CHAPTER 4 FLUID FLOW

## 4.1 Introduction

In the experimental work, the analyses of pressure drops along the bores of hollow fibre membrane were made. The hollow fibres are actually pipes (or tubes with Do/Di = 95/45 microns) with permeable walls. The fluid flow inside the tubes were assumed to be laminar due to the small Reynold number. The analyses here and in the literature are based on Hagen-Poiseuille equation for laminar flow in pipes. Because of this reason it was thought to be useful to review the laminar flow characteristics in pipes. Fluid flow through a bundle of hollow fibres were also reviewed.

## 4.2 Laminar flow in a circular pipe.

Laminar flow may occur in many situations. Its distinguishing features however, are always the same; individual particles of fluid flow paths which do not cross the neighbouring particles, (33, 35).

The steady flow of an incompressible fluid through a circular pipe of radius R and length L, is illustrated on Figure 4.1.

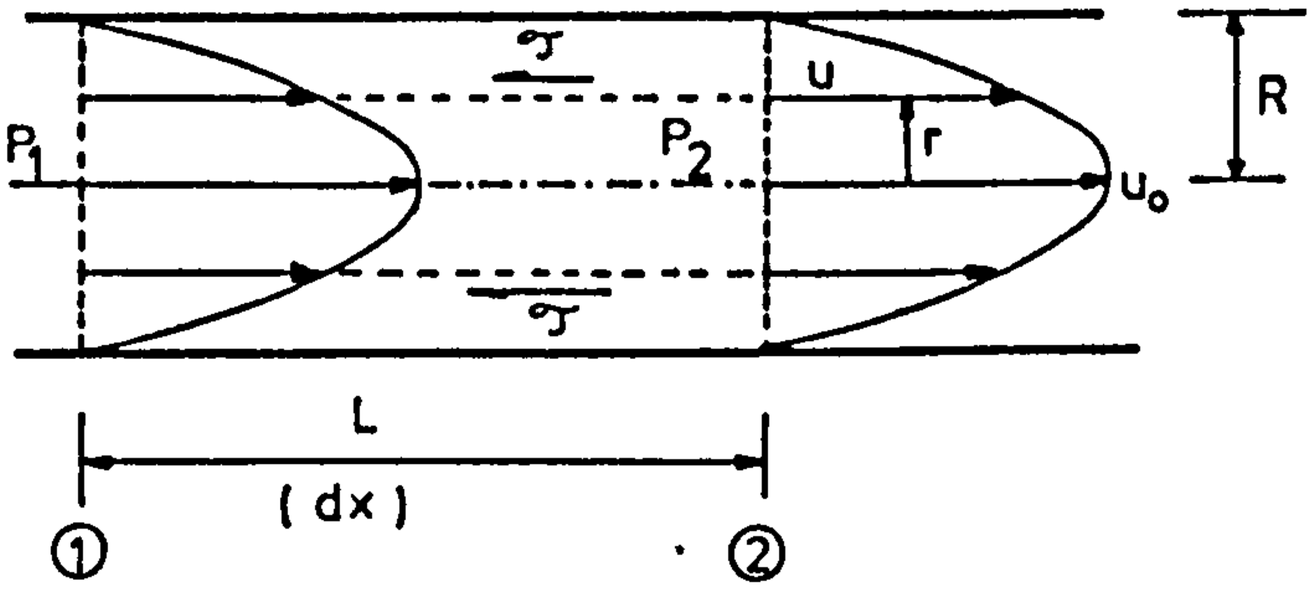


Figure 4.1 Laminar flow in a circular pipe.

The pressure at the upstream and downstream reference sections are denoted by P1 and P2 respectively.

The flow of fluid within the cylindrical core of radius ($r \leq R$) is in equilibrium under the action of a viscous resisting force and a net pressure force. The tangential (or shear) stress experienced by the fluid at radius r is,

$$\tau = \mu \, dU/dy$$

where dU/dy is the value of the velocity gradient at radius r, y is the distance from the wall of the pipe, and $\mu$ is the viscosity. Since the distance y is measured in the opposite to the radius it follows that

$$\tau = -\mu \, dU/dr$$

The viscous resistance force is then obtained by multiplying this stress by the area subjected to that stress, i.e., $2\pi rL$.

The net pressure force on this core of fluid is $(P1 - P2)\,\pi r^2$. Hence, for equilibrium in steady motion,

$$(P1 - P2)\,\pi r^2 = -\mu \, dU/dr \, 2\pi rL$$

and the velocity gradient is given by

$$dU/dr = -(P1 - P2)\, r/2\mu L \qquad (1)$$

The velocity distribution in the pipe is now obtained by integrating equation 1

$$U = -(P1 - P2)\, r^2/4\mu L + A \qquad (2)$$

where A is a constant of integration which may be evaluated with reference to a suitable boundary condition, the appropriate boundary condition in this case is the no-slip condition at the pipe: u = 0 when r = R. Inserting these boundary values into equation 2;

$$A = (P1 - P2)R^2/4\mu L$$

and, on substituting for the constant A, it becomes

$$U = (P1 - P2)/4\mu L \; (R^2 - r^2) \qquad (3)$$

From equation 3 it is clear that the maximum velocity, Uo, occurs at the centre of the pipe, where r = 0.

$$Uo = R^2/4\mu L \quad (P1 - P2) \qquad (4)$$

The distribution of velocity over the cross-section may be represented graphically by plotting U against r as in Figure 4.1 and seen that it is parabolic in form.

The volume flow rate may be evaluated by an integration of the velocity distribution given by equation 3.

$$\text{Hence,} \quad Q = \int_0^R U\, 2\pi r\, dr = \pi R^4/8\mu L \quad (P1 - P2) \qquad (5)$$

It may be written over an elemental length (dx) and pressure drop, (P1 - P2) = $\Delta P$.

$$Q = -\pi R^4/8\mu \quad d\Delta P/dx$$

The mean velocity $\bar{U}$ is given by

$$\bar{U} = Q/\pi R^2$$

and it becomes;

$$\bar{U} = R^2/8\mu L \quad (P1 - P2) \qquad (6)$$

Thus, a comparison of equation 4 and equation 6 shows that

$$\bar{U} = Uo/2$$

The usual problem associated with this type of flow is the determination of the pressure drop resulting from a given rate of flow. Therefore, re-arranging equation 5;

$$\Delta P = 8\mu LQ \;/\; \pi R^4$$

in terms of the diameter Di of the pipe,

$$\Delta P = 128\ \mu LQ \;/\; \pi Di^4 \qquad (7)$$

or, the pressure gradient may be written over an elemental length (dx) in different forms, such as;

$$- dP/dx = 128_{\mu}Q/\pi Di^4 = 32_{\mu}\bar{U}/Di^2 \qquad (8)$$

This equation is known as Hagen-Poiseuille's equation and it enables the pressure drop in laminar flow of a fluid of known viscosity in a circular pipe to be calculated.

## 4.3 Laminar flow in porous pipes

Some interesting properties of liquid flow in tubes with permeable walls have been disussed by Weissberg (59) and, Terril and Thomas (51) on the basis of the complete Navier-Stokes equations. However, their analysis and solutions were rigorous and may be used for special cases.

In the case of a fluid flow in a fibre with permeable wall is considered, it may be an excellent approximation to ignore the radial component and to treat the axial flow on the bore side as Hagen-Poiseuille flow;

$$-d\ P(x)/dx = 8\mu/\pi R^4 \int_0^R 2\pi r\ U(x,r)dr \qquad (9)$$

The integration gives the total volume flux (Q) through the cross- section at the level x. It is assumed that steady state conditions prevail and that Reynolds' number for the axial flow: $\rho\ UD_1/\mu$ is sufficiently small to neglect the inertia effects, (15, 24, 49). The radial velocity as a result of permeation is always small that its contribution to the Reynolds number is quite negligible.

If above equation is used for a tube with permeable walls, the flux Q is a function of x, because liquid is fed into the tube along the entire length. If J1(x) is the volume of liquid that enters per unit time per unit area of outside tube wall, continuity requires that $dQ/dx = 2\pi RJ1$. Hagen- Poiseuille law may not be rigorously valid when the wall is permeable, but the relative error in the equation in all cases of practical interest is very small.

Detailed analysis and an analytical solution of a laminar flow in a fibre with permeable wall is given in Chapter 5, which is based on Hanbury et al's work (23).

## 4.4 Flow through a bundle of hollow fibres

The flow of fluids through porous media was investigated by Carman as a method for the determination of the specific surface of the media and related studies by Sullivan and Hertel (49) recommended an equation for calculating pressure drop in cross flow systems using solid fibres. Dandavati et al (15) adopted their equation into the pressure drop determination in hollow fibre bundles and shown as;

$$\frac{dP1}{dr} = - ko\,\mu \left[ S_o^2 \frac{(1-E)^2}{E^2} \right] \frac{\bar{V}_1}{E} \qquad (10)$$

where P1 is the radial pressure distribution on the shell side; r is the radial distance from the centre line of the shell, So is the surface area per unit solid volume given by 2/ro, ro fibre outside radius; E is the void fraction of the fibre bundle, $\bar{V}_1$ is the radial superficial flow velocity and ko is a constant which depends on the fibre orientation with respect to the flow. The calculated and experimental values, obtained from a standard B-9 hollow fibre bundle, showed less than 5% difference in their experiments.

Orofino (39) and Hermans (24), separately, discussed the radial pressure gradient in hollow fibre bundles on the basis of Darcy's Law where the radial pressure gradient is proportional to the average radial velocity $\bar{V}$ on the shell side.

A different approach to the problem was made by Hanbury et al (23) giving the radial pressure gradient in hollow fibre bundles to be of the form

$$Pbi - Pb = (Pbi - Pbo)\ \ln (r/ri)/\ln (ro/ri) \qquad (11)$$

neglecting the recovery ratio or the permeation rate which is assumed to be small. The discussion of brine flow is given in Chapter 5.

# CHAPTER 5 - ANALYSIS OF HOLLOW FIBRE SYSTEMS

## 5.1 Introduction

In this chapter, theoretical and numerical analyses were made to describe the hollow fibre reverse osmosis systems. First, the performance of a single fibre was analysed then secondly the behaviour of the bundle of fibres as a whole.

The numerical solution to the fibre bundle performance problem will be used to analyse the experimental results in the next chapter.

## 5.2 Description of the system

The system consists of a shell which houses the hollow fibre bundle. The fibres are grouped together in a parallel array with one end sealed and the other open. The feed solution is fed into the bundle from a central distributor tube and moves radially outward through the bundle flowing around the outside of the fibres, Figure 5.2. Water permeates through the fibre membrane and emerges from the open end while concentrated brine leaves the shell side. The feed flows outside the fibres is radial and the permeate flow inside the fibre bores is axial.

## 5.3 Theoretical analysis

In the hollow fibre systems two analyses are considered: the performance of a single fibre and the bundle as a whole. The analysis presented here was based on that of Hanbury et al (23).

The analysis is based on the premisis that the flow of water and salt through the outer skin of the hollow fibres may be represented by the equations:-

$$\text{Water flux, } J_1 = k_1 (\Delta P - \phi RT(C_w - C_d)) \qquad (1)$$

$$\text{Salt flux, } J_2 = k_2 (C_w - C_d) \qquad (2)$$

where the membrane constants $k_1$ and $k_2$ may at least be considered invariant at a fixed temperature and over the variations in pressure and brine concentrations that occur within the fibre bundle.

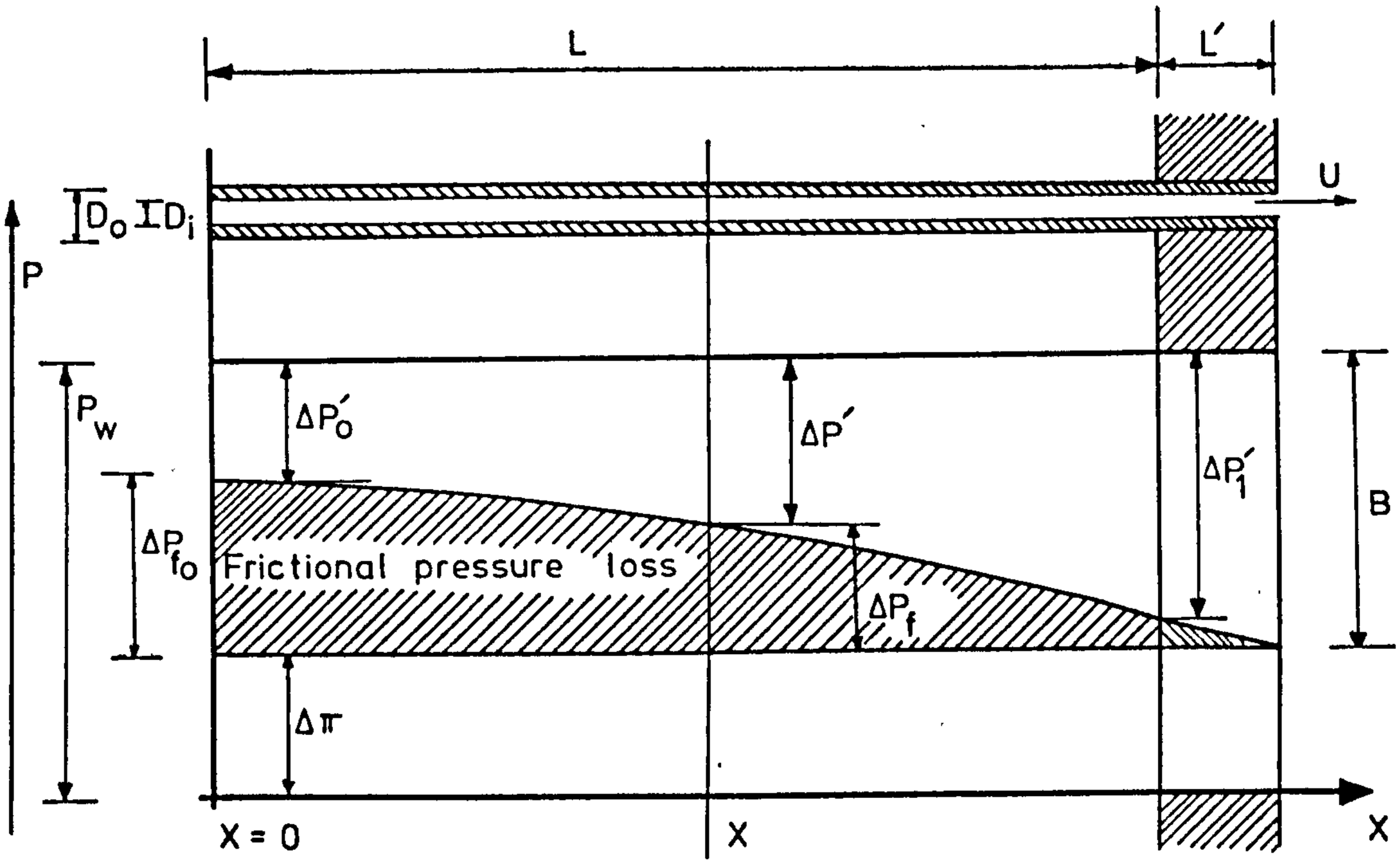


Figure 5.1 Pressure loss of the product flow in a hollow fibre.

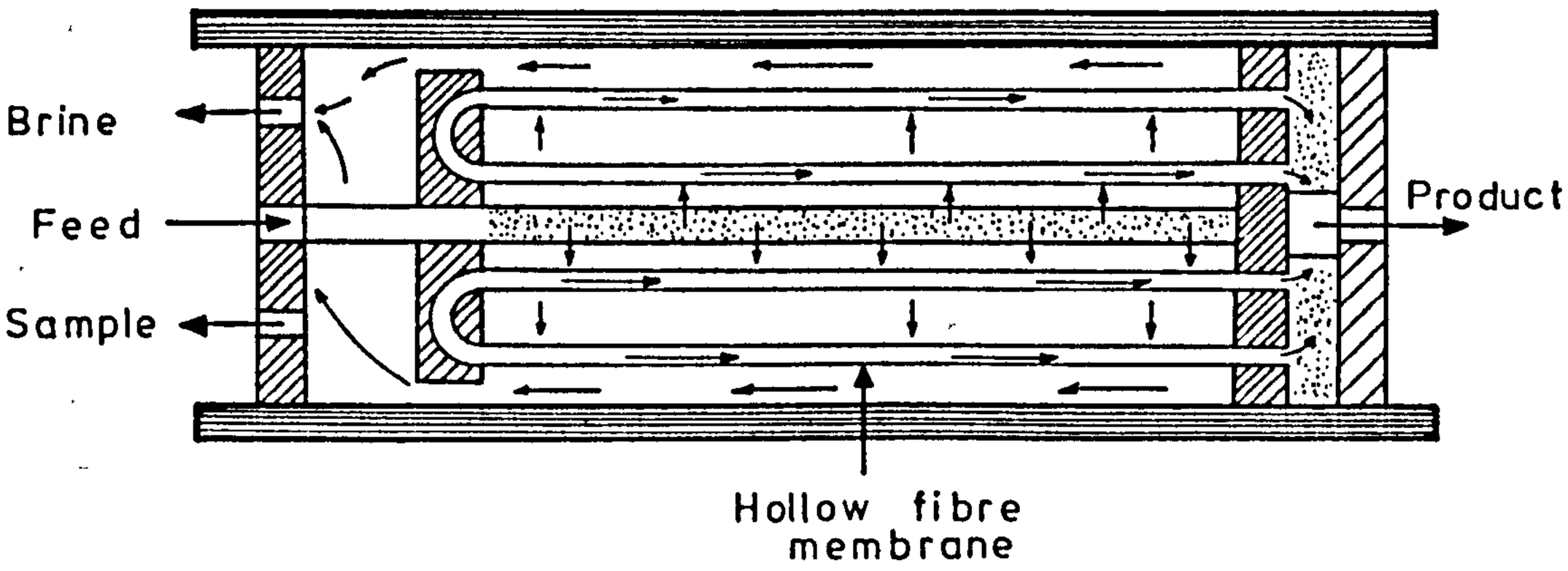


Figure 5.2 Illustration of hollow fibre reverse osmosis process.

## 5.3.1 Polarisation

The non-permeating component accumulates near the membrane surface due to the water permeation. The accumulation of salts on the membrane surface, called concentration polarisation, increases the concentration difference on both sides of the membrane resulting in a lower flux. This is a serious problem on the flat membranes. One of the reasons that makes the hollow fibre membranes attractive is the negligible concentration polarisation. There are two factors reducing the polarisation; a - the permeability of hollow fibre membranes is usually less than that of flat membranes, b - the distance over which diffusion takes place is very small in hollow fibre membraes. However, the analyses in the literature usually neglected this phenomenon (14, 15, 23, 39) and a detailed theoretical analysis of this may be found in Herman's (24) analysis. The concetration polarisation is therefore assumed to be negligible. The interface concentrations, $C_w$, in equations 1 and 2 above may be replaced by the local brine concentrations, $C_b$. Provided the rejection is good the salt flux may be written:-

$$J_2 = J_1 . C_d/\rho$$

Hence equations 1 and 2 are reduced to

$$J_1 = k_1(\Delta P - \phi RT(C_b - C_d)) \quad (3)$$

$$J_1 = k_2\rho(C_b - C_d)/C_d \quad (4)$$

which lead to the quadratic for the water flux, $J_1$, in terms of the local brine concentration and pressure difference across the membrane wall:-

$$J_1^2 + (k_1\phi RTC_b - k_1\Delta P + k_2\rho)J_1 - k_1k_2\rho\Delta P = 0 \quad (5)$$

With tight membranes such as those used for seawater a further approximation may be made by ignoring the product concentration in comparison to that of the brine. Equation 3 and 4 may then be reduced to:-

$$J_1 = k_1(\Delta P - \phi RTC_b) \quad (6)$$

$$J_1 = k_2 \rho C_b / C_d \qquad (7)$$

In this case equation 6 may solved directly for the water flux.

5.3.2 Pressure losses

There are generally two significant pressure losses. One is the radial pressure drop in the brine flow and the other is axial pressure drop in the product flow along the fibre bore.

The brine flow

The feed solution is distributed from a central feeder and moves radially outward through the bundle. The concentration of feed solution changes as a result of the permeation.

If the module is not operating at a very high recovery ratio, the axial component of the brine flow within the fibre bundle will not be significant and the flow can be considered to be purely radial. In that case, the radial distribution of the radial brine velocity will not vary significantly axially along the bundle. This is similar to Sullivan and Hertel's (49) work that used solid fibres instead of hollow fibres used here in calculations. In terms of the fibre bundle pressure drop measurements, pressure drop in the bundle will not couple with the osmotic fluxes.

The brine pressures at the inner and outer surfaces of the fibre bundle may be considered to be uniform axially. It therefore remains to establish the form of the pressure loss profile radially. The dependence of the profile form on the solution of the flux distributions can be shown to be small. This may be done by comparing the profile produced by the assumption of a uniform water flux throughout the entire bundle with that produced by assuming a negligible recovery ratio. The forms of these profiles are given by:-

$$\Delta P_b = A\left[\left[1 + R_c \frac{r_i^2}{r_o^2 - r_i^2}\right]\ln r - \left[\frac{R_c}{r_o^2 - r_i^2}\right]r^2\right] + B \qquad \text{where A \& B are constants}$$

and $R_c$ is the recovery ratio at that axial position.

Putting in typical bundle dimensions and comparing the profiles for zero and typical finite recovery ratios shows that there is seldom more than one or two percent difference. Hence it is a valid approximation to assume the radial brine pressure profile to be of the form:-

$$P_{bi} - P_b = (P_{bi} - P_{bo})\ln(r/r_i) \;/\; \ln(r_o/r_i) \qquad (8)$$

Thus the problem of the brine side pressure loss may virtually be uncoupled from the solution to the osmotic fluxes.

The product side pressure losses

The solute (salt) flux through the membrane is essentially pressure independent (depends on the concentration difference) and therefore it is uncoupled to the pressure to which the fibre is exposed. The water flux through the membrane varies linearly with the net driving force, ($\Delta P - \Delta\pi$). The pressure drops along the fibre bores are highly dependent on the water flux distribution and therefore coupled with the solution to the osmotic equations. However a useful analytical solution to the coupled problem may be found for cases where the product concentration, $C_d$, is small compared with that of the brine and the brine concentration does not vary significantly in the axial direction. In all cases the pressure gradient in the fibre bore is assumed to be given by the equation:-

$$\frac{d\Delta P_f}{dx} = - \frac{32\mu U}{D_i^2}$$

This is obtained from the Hagen-Poiseuille equation for pressure drop for laminar flow in a pipe. It should be recognised that "U" is a function of axial position, since the fluid is fed into the fibre along its entire length.

### 5.3.3 An Analytical Solution

The situation to be analysed is depicted in Figure 5.1. The water mass balance ($m = \rho.A.U$) over an elemental length of fibre, dx, gives:-

$$\frac{dU}{dx} = \frac{4J_1 D_o}{D_i^2 \rho} \qquad (9)$$

The water flux, $J_1$, is given by equation 6. Now, the osmotic pressure of the brine is assumed constant along the fibre length, so $\phi RTC_b$ may be written as $\Delta\pi$, a constant. Using the notation of Figure 5.1, the nett driving pressure difference for the water flux may be written:-

$$\Delta P' = P_W - \Delta P_f - \Delta\pi$$

and it varies from $\Delta P'_o$ at the closed end of the fibre to $\Delta P'_1$ at the point where the fibre enters the resin tube plate.

Since $P_W$ and $\Delta\pi$ are constant, the axial gradient in the net driving pressure may be written:-

$$\frac{d\Delta P'}{dx} = - \frac{d\Delta P_f}{dx} = \frac{32\mu U}{D_i^2} \qquad (10)$$

if the exposed length of the fibre is L then at x=L $P' = P'_1$ and

Combining equations 9 and 10 and substituting $k_1 \Delta P'$ for $J_1$

$$\frac{d\Delta P'}{dU} = \frac{8\mu\rho}{D_o k_1 \Delta P'} \frac{U}{}$$

Separating the variables and integrating over the exposed length of the fibre:-

$$\int \Delta P' d\Delta P' = \frac{8\mu\rho}{D_o k_1} \int U dU \quad : \quad \Delta P_1'^2 - \Delta P_o'^2 = \frac{8\mu\rho}{D_o k_1} U_1^2 \qquad (11)$$

This equation connects the conditions at either end of the exposed fibre. For any point along the fibre the net driving pressure and product velocity in the fibre bore are related by:-

$$\Delta P'^2 - \Delta P_o'^2 = \frac{8\mu\rho}{D_o k_1} U^2 \qquad (12)$$

The product velocity, U, may be eliminated between equations 10 and 12 to give an equation for the driving pressure, $\Delta P'$ :-

$$\frac{d\Delta P'}{dx} = \frac{32\mu}{D_i^2} \left[\frac{D_o k_1}{8\mu\rho}\right]^{\frac{1}{2}} \left[\Delta P'^2 - \Delta P_o'^2\right]^{\frac{1}{2}}$$

This may be integrated, with the boundary condition that at x=0 $\Delta P' = \Delta P'_o$, to give:-

$$\ln\left[\frac{\Delta P'}{\Delta P_o'} + \left[\left[\frac{\Delta P'}{\Delta P_o'}\right]^2 - 1\right]^{\frac{1}{2}}\right] = \left[\frac{128\mu D_o k_1}{D_i^4 \rho}\right]^{\frac{1}{2}} x \qquad (13)$$

$$\ln\left[\frac{\Delta P_1'}{\Delta P_o'} + \left[\left[\frac{\Delta P_1'}{\Delta P_o'}\right]^2 - 1\right]^{\frac{1}{2}}\right] = \left[\frac{128\mu D_o k_1}{D_i^4 \rho}\right]^{\frac{1}{2}} L \qquad (14)$$

Equations 11 and 14 describe the overall performance of the exposed part of the fibre. There will be an additional pressure drop in the product as it flows through the portion of the fibre buried in the resin tube plate. The net driving pressure at the location where the fibre enters the tube plate will be given by:-

$$\Delta P_1' = P_W - \Delta\pi - \frac{32\mu U_1}{D_i^2} L' \qquad (15)$$

where L' is the fibre length buried in the tube plate.

Equations 11, 14 and 15 describe the overall performance of the fibre. These equations may be simplified and cast in a non-dimensional form using the charecteristic length, G, given by:

$$G^2 = \frac{D_i^4 \rho}{128\mu D_o k_1}$$



and seeing that $\frac{}{e^{(L/G)} + e^{-(L/G)}} = \operatorname{sech}(L/G)$

The equations then become respectively:-

$$\frac{\rho U_1^2}{\Delta P_1'} = \frac{D_o k_1}{8\mu} \tanh^2\left(\frac{L}{G}\right) \qquad (16)$$

$$\frac{\Delta P_o'}{\Delta P_1'} = \frac{J_{1o}}{J_{11}} = \operatorname{sech}\left(\frac{L}{G}\right) \qquad (17)$$

$$\left(1 - (L'/G)^2 \tanh^2(L/G)\right)\left[\frac{\Delta P_1'}{B}\right]^2 - 2\frac{\Delta P_1'}{B} + 1 = 0 \qquad (18)$$

where $B = P_W - \Delta\pi$.

Hence the fibre production, product quality and water flux distribution:-

$$m_d = GD_o k_1 \pi \Delta P_1' \tanh(L/G) \qquad (19)$$

$$\frac{C_d}{C_b} = \frac{k_2 \rho}{k_1 \Delta P_1'} (L/G) \coth(L/G) \qquad (20)$$

$$\frac{J_1}{J_{11}} = \frac{\Delta P'}{\Delta P_1'} = \frac{\cosh(x/G)}{\cosh(L/G)} \qquad (21)$$

Equations 16 to 21 thus represent the solution for a fibre with constant brine pressure and concentration along its exposed length for the case where the product concentration is small compared with that of the brine - i.e. for a tight membrane.

Equation 17 is the critical relation of the solution, giving the fall off in net driving pressure, and hence also in water flux, due to pressure losses in the fibre bore. If sech(L/G) is near to unity then conditions along the fibre will vary only slightly and the radial brine concentration profile will not vary significantly in the axial direction. In such cases if the brine pressure drop is small compared to the driving pressure the analytical solution may be taken a stage further and expressions produced for the productivity and product quality of the bundle as a whole, which would in most practical cases lead to some loss of accuracy. This is particularly so when feeds of high concentration are used and the brine concentration starts to vary appreciably along the fibre length and the product concentration may become significant.

The primary use of this analysis is as an aid in the development of numerical solutions for conditions throughout the fibre bundle and for the performance of complete bundles.

## 5.4 Numerical analysis

In the analytical solution, the brine concentration variation along the fibre length and product concentration were neglected. A numerical iterative solution has been developed taking into account these two effects on the performance of a fibre and the bundle as a whole. The analytical solution is used as an approximate solution to speed up the iteration.

### 5.4.1 Solution for a single fibre

Equations 5, 9 and 10 are solved for an individual fibre by dividing it up into a number of finite elements and then proceeding as follows:-

The brine pressure $P_W$ and the distribution of the brine concentration along the fibre are taken as known (see later). The analytical solution is used to make an initial guess at the product pressure at the closed end of the fibre. Starting at the closed end equation 5 is solved to find the water flux for the first element of the fibre - hence the bore velocity at the end of the first element and the frictional pressure drop in the product flow. Decreasing the initial value of the bore pressure by the pressure loss in the previous element equation 5 is solved for the second element to give the water flux, increase in bore velocity and bore pressure loss. This process is repeated along the length of the fibre and then the pressure loss in the portion of the fibre sealed in the tube plate is added on to arrive at the total pressure loss along the fibre. This loss is compared to the initial guess for the bore pressure (to which it should be equal) and the guess readjusted accordingly. If $P_{d1}$ is the product static pressure on emerging from the fibre then the pressure at the closed end is adjusted by an amount - $E.P_{d1}$ and the solution along the fibre recalculated. This process is repeated until the error, $P_{d1}$, is sufficiently small. The convergence is fairly fast, each iteration reducing $P_{d1}$ by an order of magnitude.

Once the solution has converged the resulting water flux distribution is used to get the product quality distribution.

## 5.4.2 Solution for the fibre bundle

The fibre bundle is divided up radially into a number of annular elements. As the feed comes into the bundle it passes over the fibres in the innermost element first. These fibres are thus assumed to experience a uniform brine concentration at the feed pressure. The single fibre solution for this condition is then calculated and the result used to estimate the axial brine concentration distribution for the next annular element (radially outwards). The brine pressure drop through the first element is also estimated - hence the brine pressure for the next element. This process is repeated radially out through the bundle to complete the solution. As the solution progresses outwards from the centre so the axial brine distribution along the fibres becomes less uniform.

A computer program (Appendix 5) using this solution technique was written and used to compare the numerical solution both with the analytical solution and with experimental results.

NOTATION USED IN THIS CHAPTER

| | | |
|---|---|---|
| $B$ | atm | Nett driving pressure for zero bore pressure drop. |
| $C$ | gm/cc | Concentration. |
| $D_i$ | cm | Fibre bore diameter. |
| $D_o$ | cm | Fibre outside diameter. |
| $E$ | | sech(L/G). |
| $G$ | cm | characteristic length of fibre. |
| $J_1$ | $gm/cm^2s$ | Water flux. |
| $J_2$ | $gm/cm^2s$ | Salt flux. |
| $k_1$ | $gm/cm^2s.atm$ | Membrane water permeability constant. |
| $k_2$ | cm/s | Membrane salt permeability constant. |
| $L$ | cm | Exposed fibre length. |
| $L'$ | cm | Fibre length encased in tubeplate. |
| $P$ | atm | Pressure. |
| $\Delta P'$ | atm | Nett driving pressure ($J_1 = k_1.\Delta P'$). |
| $R$ | | Universal gas constant. |
| $R_c$ | | Recovery ratio. |
| $r$ | cm | radial position in bundle. |
| $T$ | K | Temperature. |
| $U$ | cm/s | Product mean velocity in fibre bore. |
| $x$ | cm | Axial position in bundle. |
| $\phi$ | | Osmotic pressure coefficient. |
| $\rho$ | gm/cc | Solution density. |
| $\mu$ | atm.s | Water viscosity. |
| $\pi$ | atm | Osmotic préssure. |

Suffices

| | |
|---|---|
| b | brine |
| d | product |
| i | initial |
| o | closed end of fibre or outside of bundle. |
| w | membrane/solution interface. |
| 1 | station where fibre enters tubeplate. |

# CHAPTER 6: EXPERIMENTAL WORK

## 6.1 Introduction

Hollow fine fibre membrane design for desalination by reverse osmosis was started early 1960's. The first commercial hollow fibre membrane, B-9, to desalt brackish waters, was introduced by Du Pont in 1970 . Since then research work has continued seeking to improve membranes, hardware and plant operating procedures. Different hollow fibre membrane modules are now available from a number of companies in the world. Very large surface to volume ratios, negligible concentration polarisation and self supporting strength has made them very attractive for many applications e.g. desalination of saline waters, waste water treatment, food industries etc.

In the design of hollow fibre membrane systems, the physical fibre parameters should be chosen to obtain an optimum bundle performance. A number of hollow fibre analyses upon which such optimisations could be based can be found in the literature (14) (15) (20) (23) (24). These concern mainly mass transport, the fibre diameter, length, wall thickness, packing density and fluid flow inside and outside of the fibre.

The assumptions upon which these analyses are based vary. A constant rejection model was assumed in Gill and Bansal's (20) analysis. Dandavati et al (15) extended these studies and assumed a diffusion model, instead of constant rejection model, to describe the salt transport and to predict the product concentration. Hermans (24) reported an analysis of hollow fibre system, paying special attention to concentration polarisation. Analytical solutions of Dandavati et al (15) and Hermans (24) for the detailed performance of complete bundles with radial brine flow are limited by assumptions of uniform brine concentration distribution along the outside of the fibre and the effect of permeate concentration in reducing the osmotic pressure difference across the membrane wall. Chen and Petty (14) analysed the flow characteristics inside the outside of hollow fibres with different length and proposed the coupled model (coupling between the osmotic fluxes and the bore flow) for any active length of hollow fibre. An analysis of hollow fibre systems was made by Ohya et al (38) neglecting the pressure drop in the bore of hollow fibre. A complete-mixing model was suggested by Soltanieh and Gill (46) assuming a uniform shell-side brine concentration equal to the reject (brine) concentration.

A summary of the assumptions used in these analyses may be seen in Table 6.1.

However, all the analyses (14-15-20-24-46) above assumed the fibre cross-section, where there is a very dense skin outside and a porous wall underneath, to remain undistorted under working conditions.

In the experimental literature (12) (15) (27) (36) (38) (46) there is ample evidence suggesting that the water (solvent) and salt (solute) permeabilities (based on constant fibre geometry) vary considerably with both temperature and pressure. The purpose of this work was to attempt to find out how much of this variation can be attributed to changes in the fibre geometry under the influence of external pressure. Since the theoretical solution to the performance of a fibre is particularly sensitive to changes in the bore diameter it was thought that measurements of the pressure drops along the fibre bores, under working conditions might provide some evidence of changes in the bore diameter. To this end a small 4" B-9 and B-10 hollow fibre modules were disassembled and pressure tapping holes drilled into the resin blocks supporting the looped, 'closed', ends of the fibres (Figure 6.3, 6.4, 6.16). These holes had to be drilled very exactly so as just to break into the "U" bends of a few fibres within the resin without allowing leakage of the high pressure brine into the tappings. In the experiments only one such tapping on B-9 module and three tappings on B-10 module proved to be sound. These tappings however have produced some interesting measurements.

Analyses of Hollow Fibre Membranes

TABLE 6.1

| Factors taking into account | | Radial brine distribution | Axial brine distribution | Fibre bore pressure | Fibre bore shrinkage |
|---|---|---|---|---|---|
| Dandavati et al | (15) | Yes | No | Yes | No |
| Ohya et al | (38) | Yes | No | No | No |
| Hermans | (24) | Yes | No | Yes | No |
| Chen & Petty | (14) | Yes | No | Yes | No |
| Soltanieh and Gill | (46) | No | No | Yes | No |
| Hanbury et al | (23) | Yes | Yes | Yes | Yes |


Fig. 6.1 The elements of B-9 Hollow Fibre Membrane

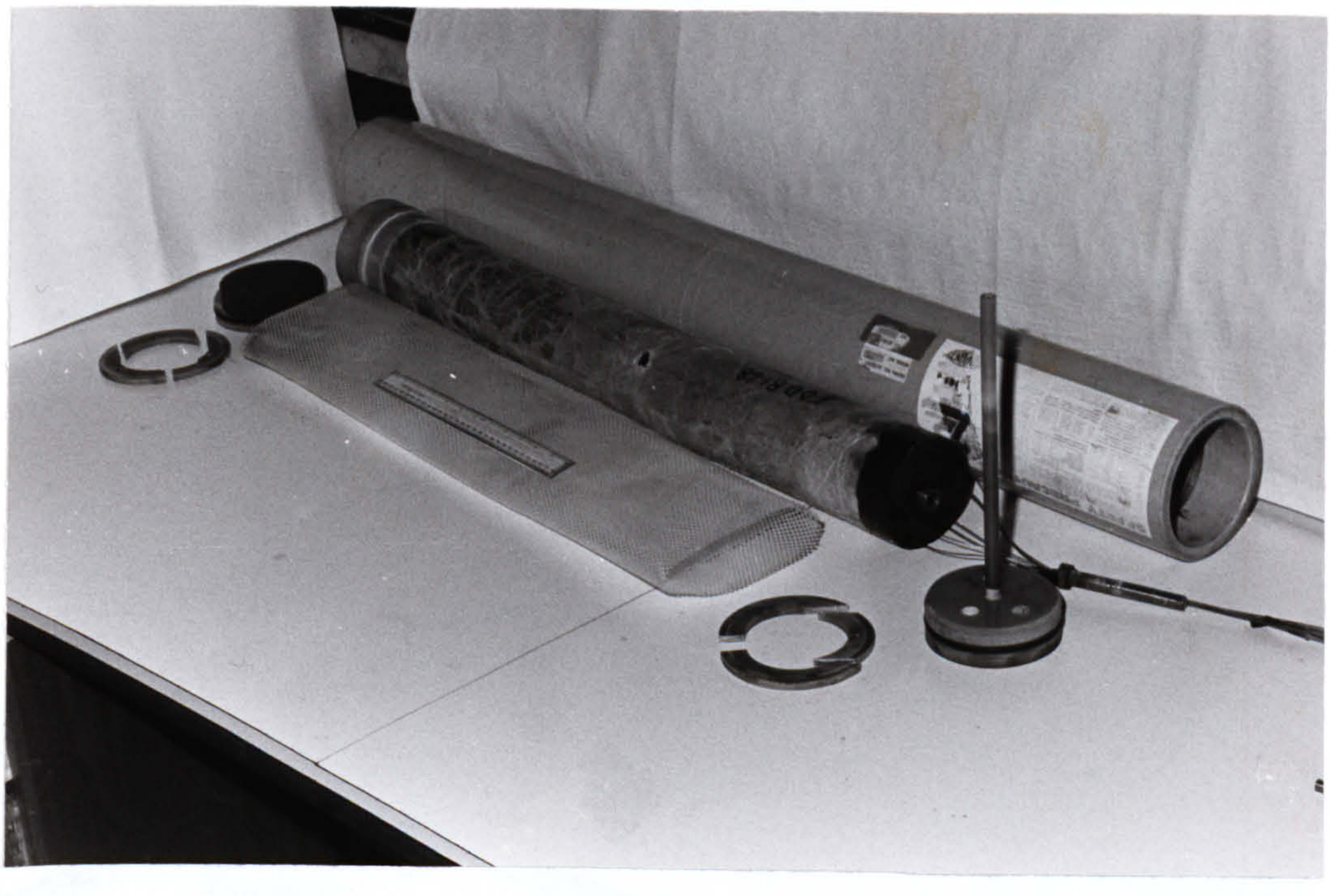

Fig. 6.2 The elements of B-10 Hollow Fibre Membrane

Fig. 6.3 Picture showing the pressure tappings on B-9 membrane closed end tube.



Fig. 6.4 Picture showing the pressure tappings on B-10 membrane closed end tube.

Fig. 6.5 Open end of Hollow Fibre Bundle

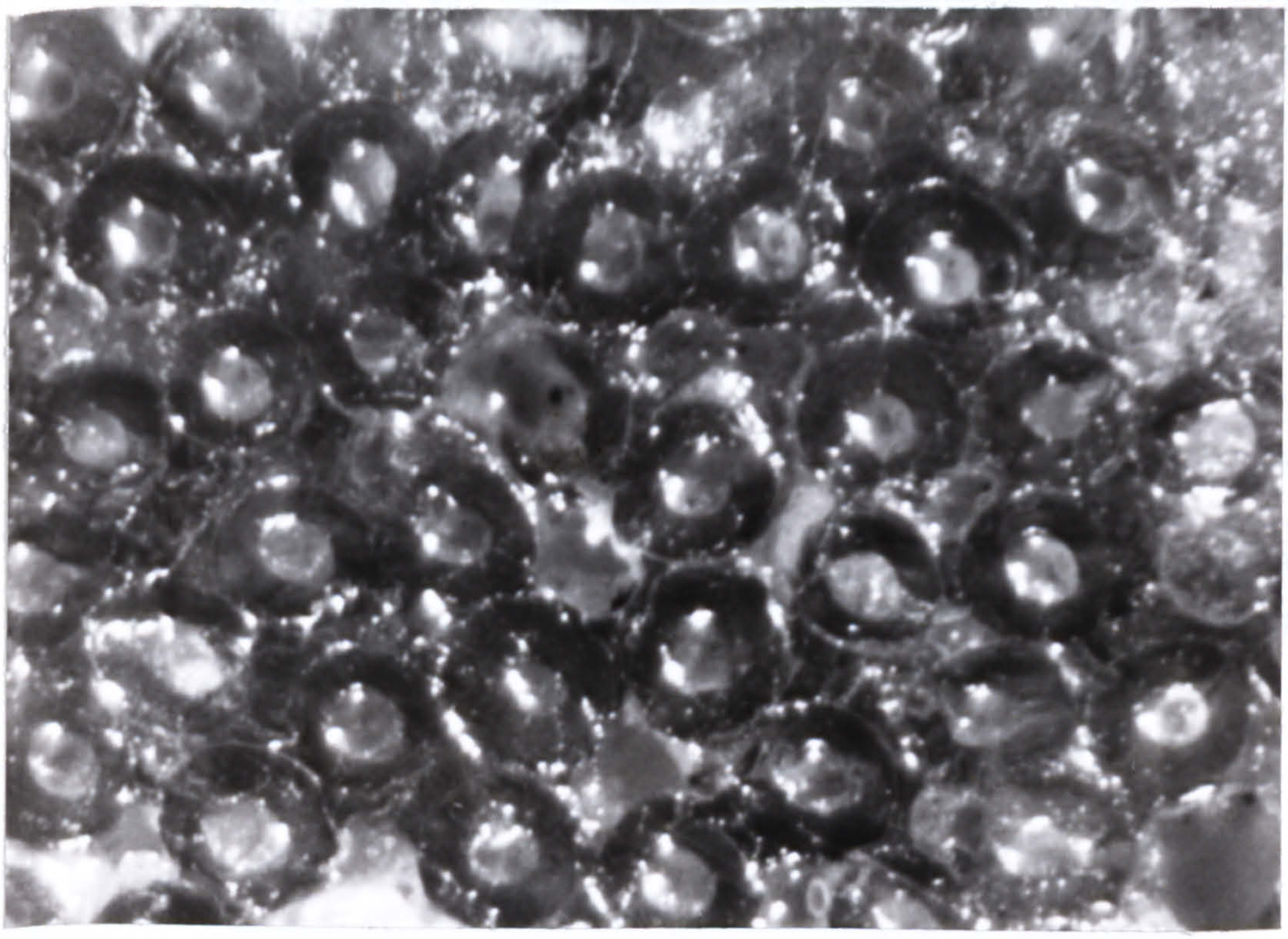

Fig. 6.6 Open end of Hollow Fibre Bundle under microscope

## 6.2 Du Pont hollow fibre membranes

Du Pont introduced the first "Permasep" hollow fibre membranes in 1970. The B-9 permeator was to desalt the brackish waters. Later, in 1973 the B-10 permeators were introduced for desalting the seawater in a single pass. The construction of these two permeators are almost the same except for the modification of the B-10 fibres to withstand higher operating pressures.

These membrane fibres, of dimensions similar to human hair, are made of aromatic polyamide. They are asymmetric in structure with a very dense skin on the outside, supported on the inside by a porous structure of the same chemical composition.

The hollow fibre yarns are wound around a flat porous web and this web with the layers of fibre on both of its sides is rolled around a central distributor tube which forms the axis of the fibre bundle. Both ends are sealed with epoxy resin and one end of the bundle is precisely cut so that the U-bends in the fibres are removed from one end exposing the opened fibre ends and allowing the product water to be discharged from the bore of the fibres, Figure 2.7.

The feed water is introduced into a central distributor tube where it is forced out radially through the bundle of fibres. As pressurised feedwater contacts the outside of the fibres, pure water is forced through the walls of each hollow fibre into the bore. The permeate (pure water - product water) moves along the bores of hollow fibres and comes out at the open end. The brine flows radially to the outer surface of the bundle and out of the permeator.

Aromtic polyamide fibres are reasonably chemically stable (except to chlorine attack), can tolerate a broad range of pH conditions and are relatively impervious to biologic attack.

The figures (6.1 and 6.2) show the elements of B-9 and B-10 hollow fibre membranes and the figures (3 and 4) the closed end tubes. The figure (6.5) shows the open end tube of B-10 hollow fibre membrane (same as B-9) and the figure (6.6) the fibre open ends under the microscope. The table (6.2) shows the dimensions of B-9 and B-10 hollow fibre membrane modules.

TABLE 6.2

Dimensions of Du Pont Hollow Fibre Membrane Modules

| Membrane module | B-9 | B-10 |
|---|---|---|
| Shell length, cm | 63.5 | 123.2 |
| Shell diameter, cm | 13.3 | 14.4 |
| Active bundle length, cm | 30.0 | 70.0 |
| Bundle sealed length, cm | 6.64 | 11.8 |
| Bundle outside diameter, cm | 9.80 | 10.5 |
| Bundle inside diameter, cm | 2.20 | 2.5 |
| No of fibres /$cm^2$ | 10000 | 10000 |
| Fibre inside diameter, micron | 42.0 | 45.0 |
| Fibre outside diameter, micron | 85.0 | 95.0 |

Microscopic studies of polyamide hollow fibre membrane structure

The purpose of this study was to investigate the structure of the hollow fibre membrane. The fibre structure was described by the manufacturers (PEM) as to be a very dense skin layer on the outside, 0.1 to 1 micron thick, and a porous wall underneath. There is also a thin skin layer inside the bore of hollow fibre. These hollow fibre membranes (B-10) can stand pressures as high as 70 atm. without any additional support. The experiments in Chapter 6, indicated that the hollow fibres were compressed under typical operating pressures. Hence the smaller bore size increased the product side pressure losses which reduces the performance of the hollow fibre membrane. Therefore, it was thought that these studies of the structure of the hollow fibres might throw some light on the compression phenomenon under working conditions.

Generally, in the literature (10) (20) (40) (50) the structure of reverse osmosis membranes were studied by using flat membranes (membrane specimen). Sthrathmann and Kock (50) reported a comprehensive theory of the membrane formation on the basis of thermodynamic and kinetic relations of phase separation processes. Guanghu et al (22) studied the structure of aromatic polyamide type asymmetric membranes and reported that the needle-like porous membranes had higher water fluxes than sponge-like

structures. Blais (10) studied the polyamide membrane structures on the basis of the improvement of the barrier layer and the underlying support structure to ensure useful product rates.

However, the high permeate flow rate is not the only factor in the selection of membrane structure and material. The other characteristics (factors) have also effects on selecting the membrane structure and material such as salt flux, chemical and biological stability etc. and the self supporting strength in the case of hollow fibre membranes.

Panar et al (40) studied the asymmetric membranes and reported that the polyamide membranes were composed of polymeric spheres (micelles). These sphere elements have 400 to 800 angstrom (Å) diameter and 75 to 100 Å voids between them. The surface layer was compressed by surface tension forces which were tended to fuse the micelles on the surface. These spheres are deformed and partly fused so that few permanent pores remain. The permeation occurs through free volume (dynamic pores) rather than permanent pores. The micelles directly below and in the bulk experienced no such forces and remain only poorly fused and relatively spherical. The product water moves through the 100 A gaps between the spheres with little impedence.

Preparation of Hollow fibre samples for microscopic examination

Initially samples were produced simply by cutting or breaking the fibres at room temperature. However, these two methods of preparation, were found to distort the structure of fibre cross sections and were therefore considered unsatisfactory.

Subsequently, a small bundle of wet fibres was immersed in liquid nitrogen and broken while still frozen. The fibre cross sections, thus produced, were investigated under a scanning electron microscope (SEM). As seen on Figure (6.7) laminar or plate-like structures were observed which were suspected to be freeze fractures.

Later, air-dried fibres were buried in araldite resin and broken. As seen on Figure (6.8) the fibre wall structure was seen to be different to those of Figure (6.7). Close examination of the fibre cross sections indicated that the wall structure had been stretched and sheared. However, as seen from Figure (6.8) the fibre skin was clearly visible. After that, air-dried fibres were immersed in liquid nitrogen and broken. These

air-dried cryogenically fractured fibre cross sections were smoother than the others under the same magnifications, Figure (6.9). Sphere elements were seen on the fibre cross sections at higher magnifications (80 000 x). As seen from Figure (6.10-12), these spherical elements were seemed to be fused. However, the detailed structure was found to vary slightly from sample to sample, as can be seen from Figures (6.10-12).

The membrane manufacturer (PEM) reported that the fibres had to be kept wet to retain the reverse osmosis characteristics. This phenomenon was explained by Panar et al (40) that dehydration leads to complete fusion of the micelles. When the membranes (fibres) are dehydrated these spherical elements are fused together irreversibly loosing the reverse osmosis characteristics.

However, it was possible to see the spherical elements with this simple method of sample preparation. The structure (fused elements) was the same all over the fibre cross section except the dense skin layer or just beneath. The studies in the literature (10) (22) (40) (50) all involved showing the dense skin structure. However, there is an indication that the very dense wall structure of these fibres are similar to skin structure of the flat polyamide membranes. It may be one of the reasons that these hollow fibre membranes have lower permeate fluxes than the flat membranes and also having self supporting strength.

As seen from the results of B-9 and B-10 membrane performances, the water permeability constant, $k_1$, did not change considerably with pressure at lower temperatures. But, however, in both experiments the $k_1$ values decreased with pressure at higher temperatures such as $30^{o}C$. This phenomenon may be due to the compaction of these spherical elements at higher temperatures and pressure. Decrease in the apparent fibre bore diameter with increasing temperature may also be due to the compaction of the spherical elements (where the elasticity increases with temperature).

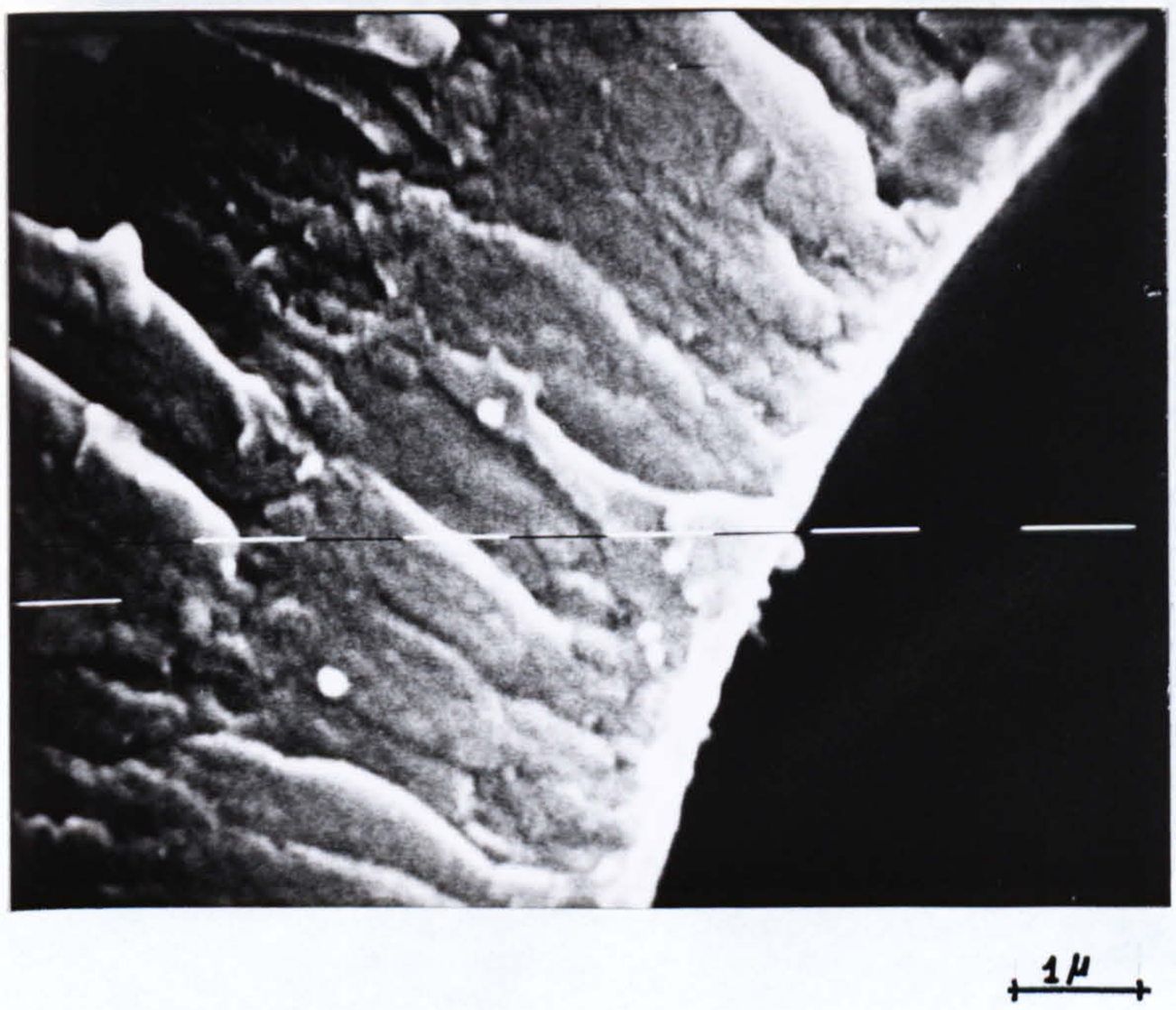


Fig. 6.7 Cross-section of a wet fibre cryogenically broken

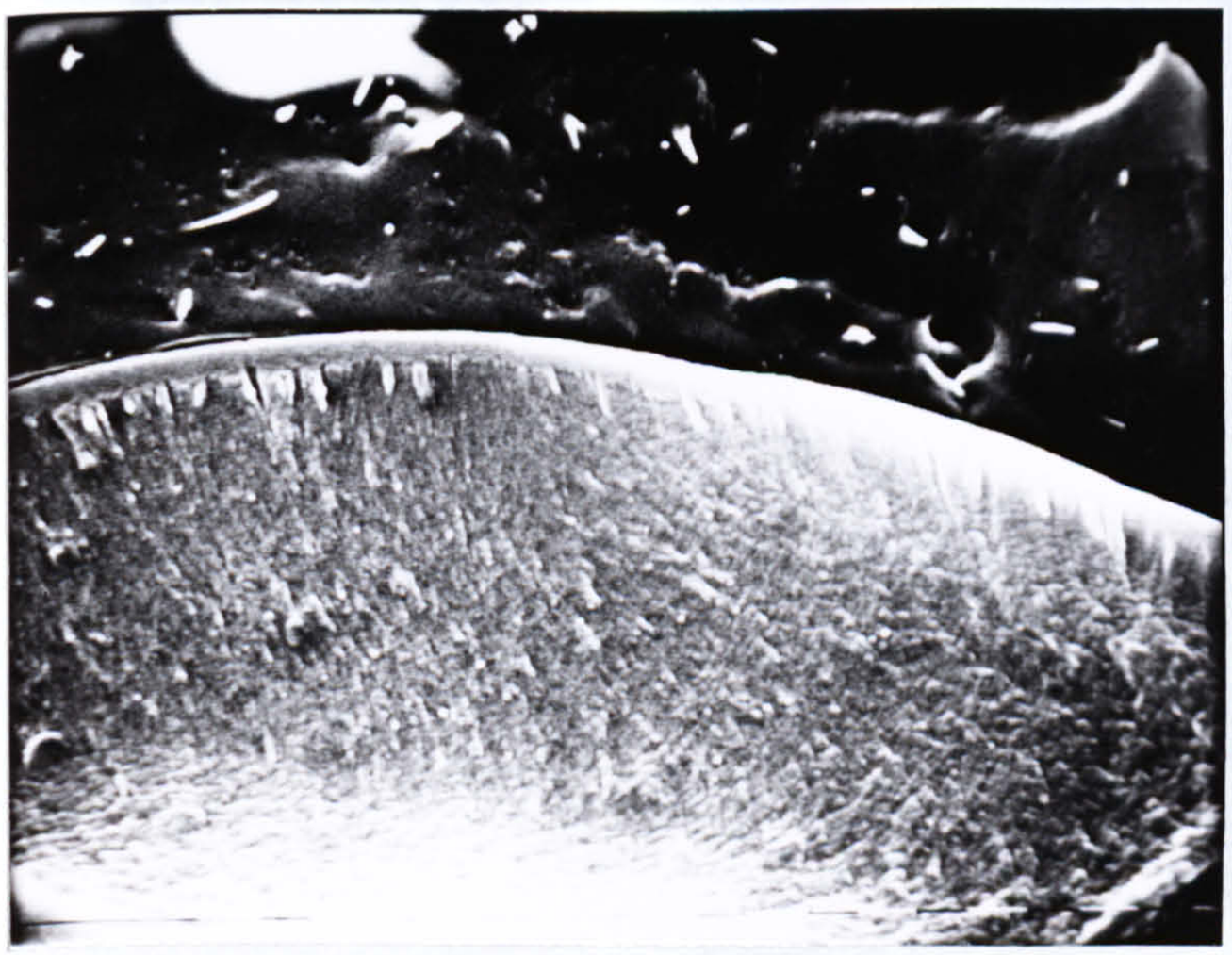


Fig. 6.8 Cross-section of an air dried fibre buried in araldite resin and broken


Fig. 6.9 Cross-section of an air dried fibre cryogenically broken

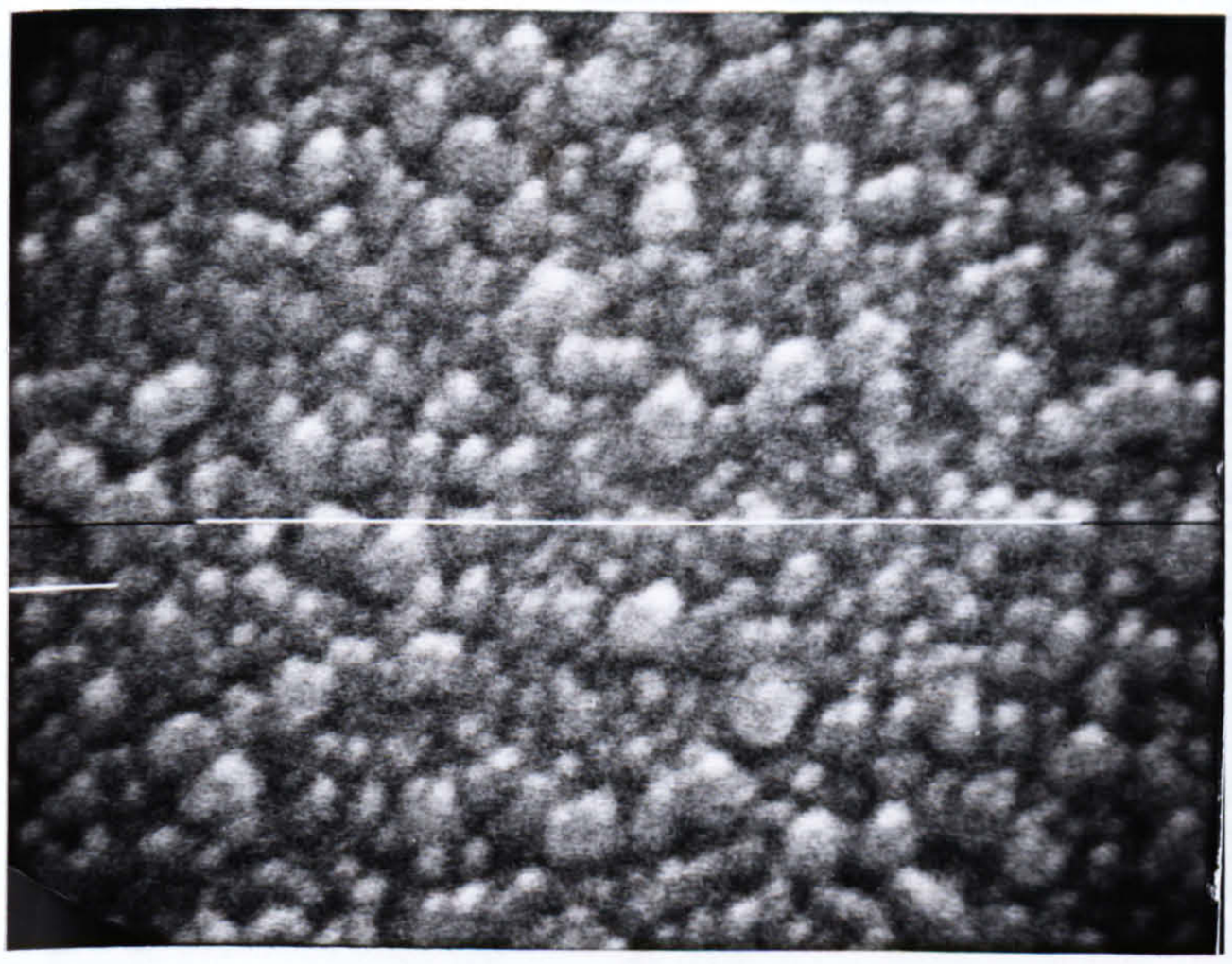


Fig. 6.10 Cross-section of a fibre wall structure showing spherical elements

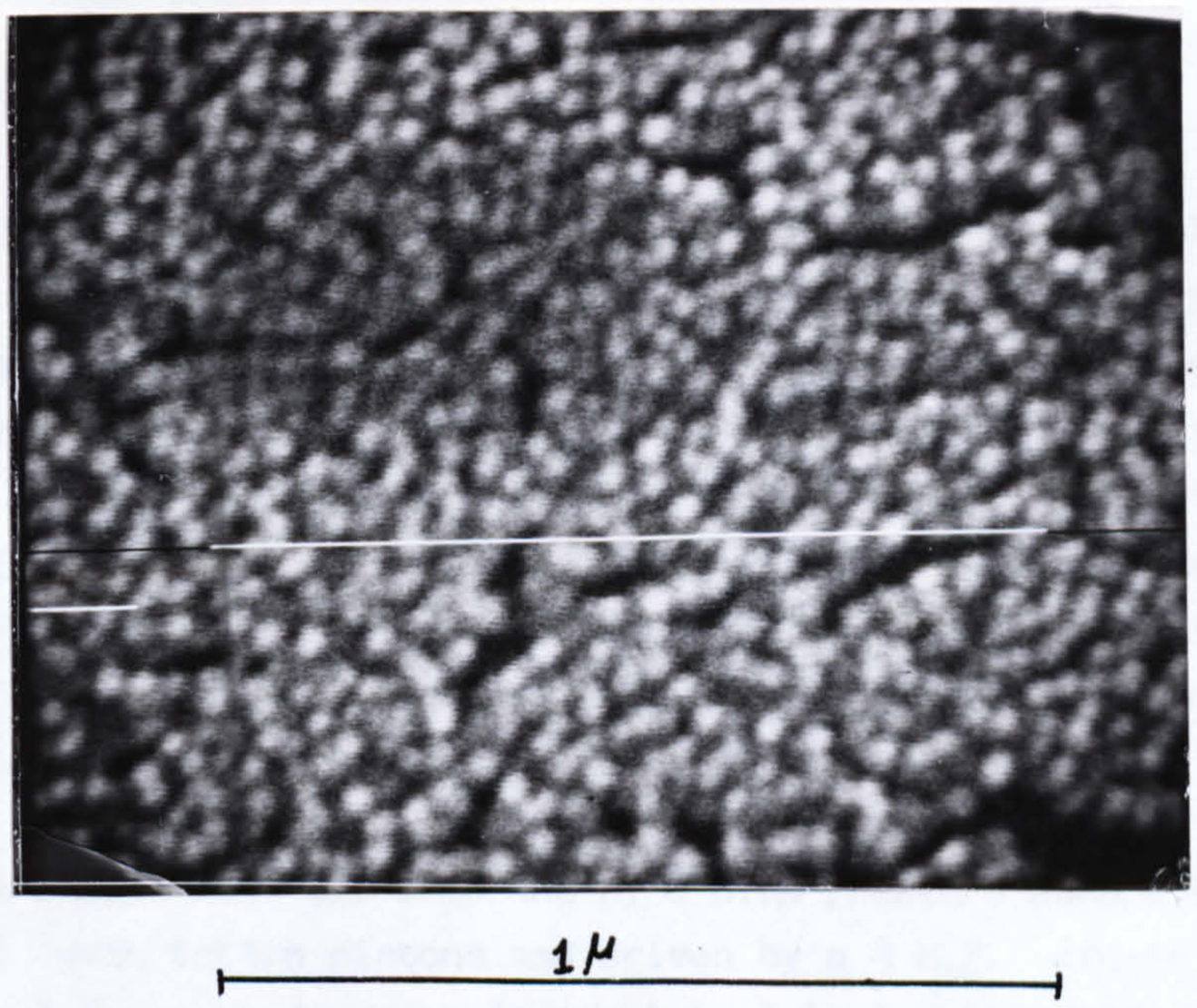


Fig. 6.11 Cross-section of a fibre wall structure showing spherical elements

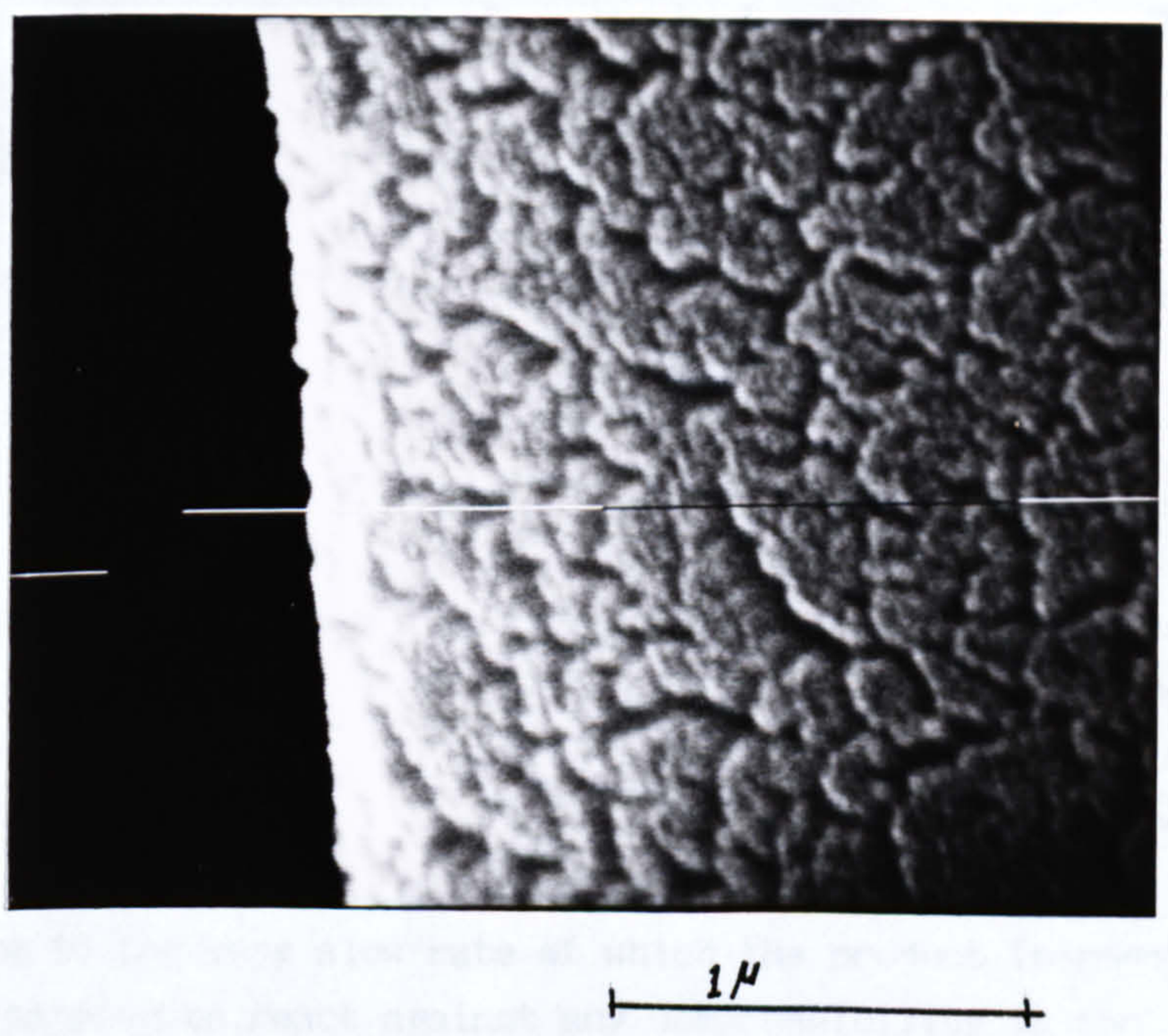


Fig. 6.12 Cross-section of a fibre structure showing fused spherical elements

## 6.3 Experimental rig

The experimental rig is a recirculation system mainly consisting of a feed tank, high pressure pump (H.P.P.) and a membrane unit, see Figure 6.13 and 15. The feed solution tank has a cooler and a heater to keep the desired feed temperature. Feed solution is first pumped into the system by a priming pump. The pump has two roles, one is to fill the system with water purging any air from the system and the second is to supply the high pressure pump with a sufficiently pressurised water at about 20 psi. After the priming pump there is a flow meter, a 10 micron cartridge filter and a cooling device to help maintain a constant feed temperature.

The feed is pumped into the membrane by a high pressure pump which was made of 316 S.S. with teflon pistons and driven by a 3 H.P. single phase electric motor. A pressure dampener (accumulator) is incorporated into the outlet of the high pressure pump to give a smoother flow into the membrane (to eliminate the pulsation caused by the high pressure pump).

The by-pass and pressure control valves are used to control the flow rates and the applied pressures. The pressure gauges were placed on the reject stream, and also before and after the high pressure pump. The brine pressure drop across the membrane is measured by a differential pressure gauge connected to the inlet and outlet of the membrane module.

The temperatures of the incoming and outgoing streams are measured by thermocouples (type K) connected to a data logger, Figure 6.14.

## 6.4 Experimental procedure

For each set of conditions investigated the rig was run at least five hours to allow a steady state to be reached. This run settling time was required for two reasons. Firstly it takes about that length of time for the membrane to relax under the operating pressure, and secondly, it took a similar time for the bore pressure measurement to stabilise. This later effect being due to the very slow rate at which the product (permeate) can issue from the tapping to react against any compressibility in the measurement system.

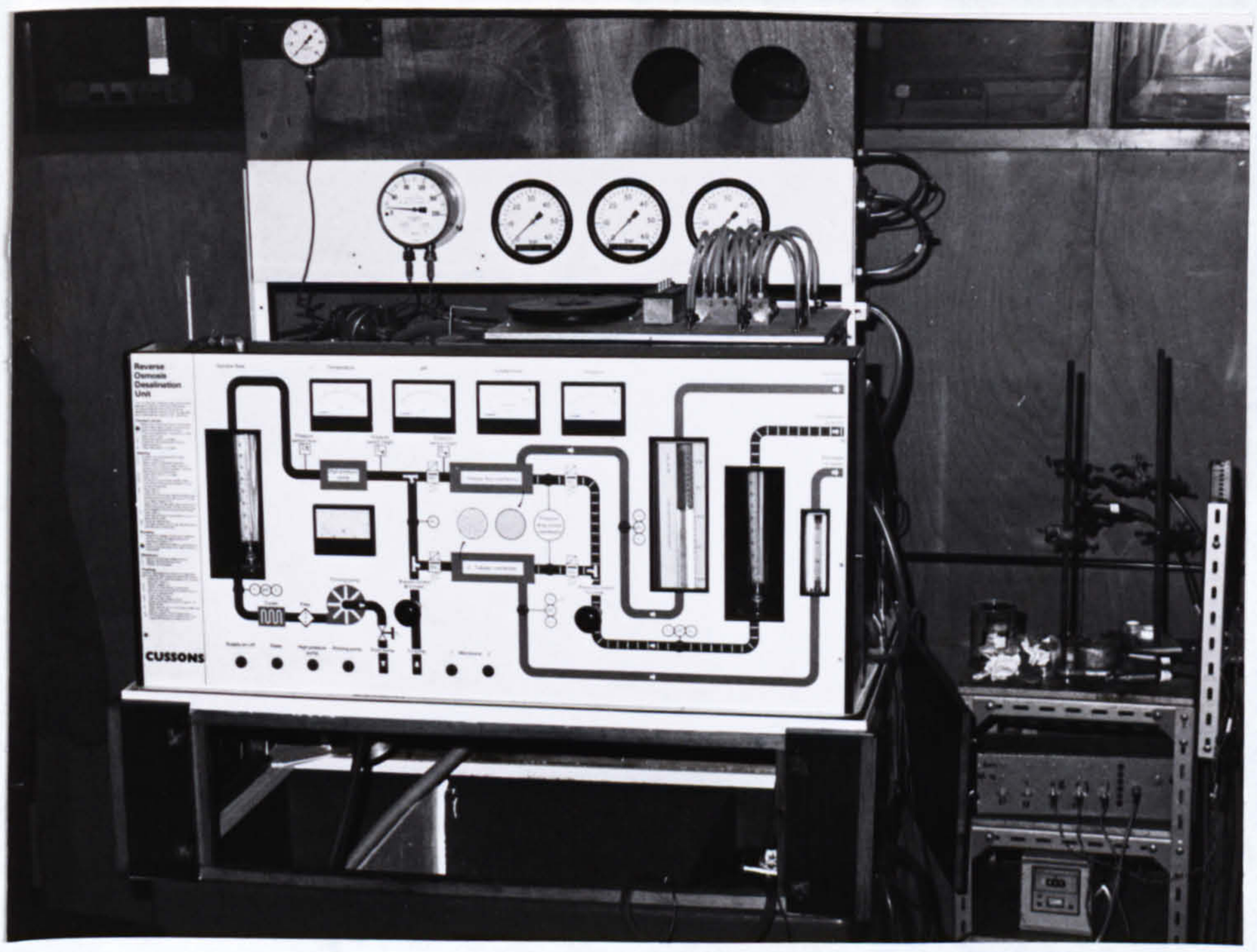


Fig. 6.13 The Reverse Osmosis Test Rig


Fig. 6.14 The Data Logger

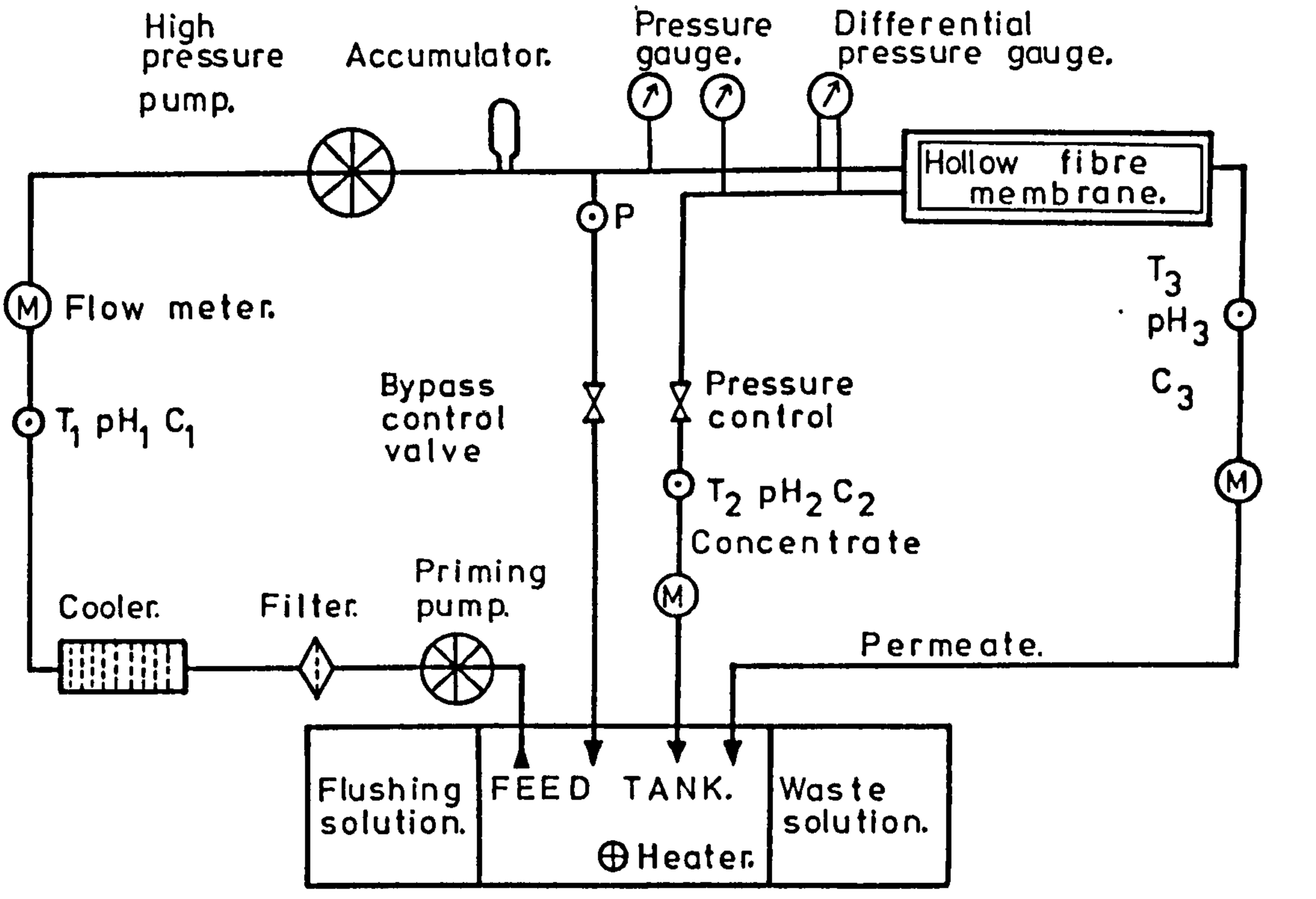


Figure 6.15 Flow diagram of reverse osmosis test rig.

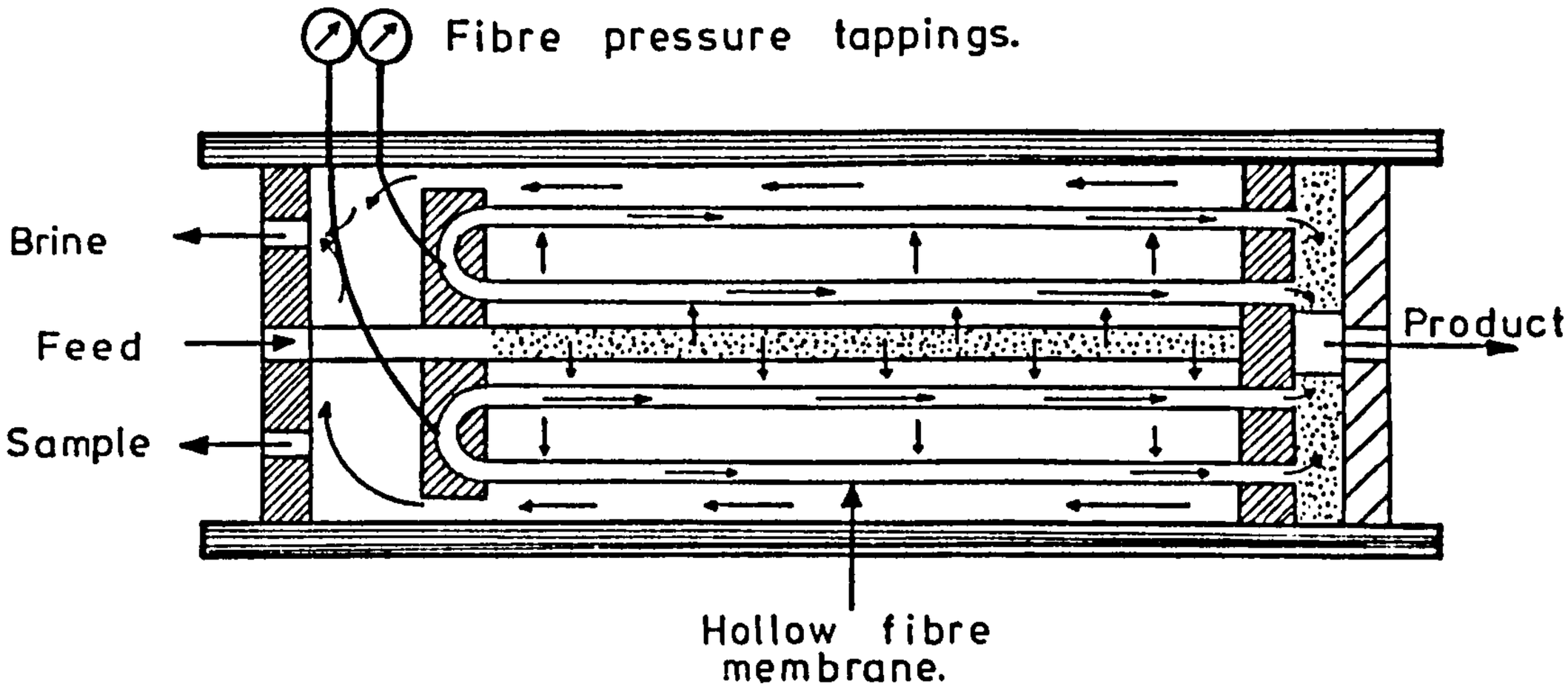


Figure 6.16 Pressure tappings in hollow fibre bundle.

Once the experimental rig is started, the conditions are adjusted such as desired temperature and pressure. After about one hour of running, the measurements of flow rates, temperatures, pressures and conductivities are taken every thirty minutes.

They system is assumed to be stablised when the fibre bore pressure and te product concentration are stable. The rig is shut down after at least two hours of stable running. After that the system is flushed with distilled water for at least five minutes to prevent direct osmosis and crevice corrosions.

During the experiments the pressure gauges and transducers were checked at regular intervals by using a dead-weight tester. The thermocouple calibrations were also regularly checked.

## 6.5 The Experiments

Measurements of pressure drops along the bores of hollow fibres in B-9 and B-10 fibre bundles have been made under various ranges of operating conditions.

The membrane modules were disassembled and pressure tapping holes drilled into the resin tube plate to break the fibre walls at the "U" bends. Stainless steel hypodermic tubes were inserted into the tappings to be enable to measure the product pressure at the closed ends of the fibres, see Figure (6.3 and 4 ). The hypodermic tubes were taken through the pressure vessel wall and were connnected to pressure transducers.

The sodium chloride feed solution was made up with sodium chloride and distilled water in the measuring containers. The feed tank was filled with about 150 litres of sodium chloride solutions. The feed solutions of salt water and distilled water were changed every two or three days of experiments.

The system was flushed with distilled water at the end of each experiment.

The readings of product conductivity, flow rates, temperaturtes and pressures were taken every 30 minutes during each run.

### 6.5.1 Experiments with the B-9 permeator

The small B-9 membrane module was disassembled and three tapping holes were drilled into the resin tube plate. The stainless steel hypodermic tubes were taken out through the pressure vessel (shell). The integrity of these tappings was established by running the rig on a feed of 5000 ppm Sodium chloride (NaCl) solution and allowing liquid to issue freely from the ends of the pressure tapping tubes. The samples were collected at the end of the tubes and conductivity measurements made. Only one of the tappings was found to be entirely secure giving a conductivity slightly less than that for the overall permeate. This was the one at a radius of 2.4 cm from the module axis.

The fibre bundle performance, including the measurement of the closed end bore pressure (at r = 2.4 cm) was investigated for two feeds, one of pure (distilled) water and the other of a 4500 ppm NaCl solution. Three feed temperatures were looked at, 20°C, 25°C and 30°C. At each temperature a series of working pressures were investigated between the values of 14 and 25 atms. The feed flow rate was kept constant at 0.225 l/sec.

#### 6.5.1.1 The results (B-9)

Computer Programs: Each set of experimental conditions, both pure water and salt solutions, was numerically analysed using a computer program. The details of the procedure used to analyse the results can be found in Chapter 5, numerical analysis. Two programs were used.

1. The first program (FD-9), assumed a fixed fibre geometry with a bore diameter of 39 microns and, given the overall bundle performance, determined the appropriate values for the membrane constants $k_1$, $k_2$ and the bore pressure at the closed end of the fibre.

2. The second program (VID-9) used the measured value of the bore pressure to predict an effective bore diameter, Dia, and the modified membrane constants $k_{1eff}$ and $k_{2eff}$ to fit the experimental data.

## Analysis of Experimental Results

The results for pure water feeds are shown in Table (6.3) and those for sodium chloride feeds in Table (6.4). Plots of the resulting membrane constants $k_1$, $k_{1eff}$, $k_2$ and effective bore diameters, Dia, are shown in Figure 6.17 to 21. From the membrane performance it was seen that:-

1. The permeate flow rate increased with increasing temperature and pressure.

2. The increase in permeate flow rate was proportional to that of the net driving pressure.

3. The permeate concentration increased with increasing temperature but decreased with increasing pressure.

A. Using the first program (FD-9), the $k_1$ and $k_2$ values and the fibre bore pressures at the closed end were determined. However, as seen from Figure 6.18 and 20, the results indicate that:-

1. The water permeability constant, $k_1$ increased with increasing temperature.

2. Increasing pressure did not show much variation on $k_1$ at 20°C and 25°C. However, $k_1$ decreased with increasing pressure at 30°C.

3. The salt permeability constant, $k_2$ increased with increasing temperature and pressure and it was approximately proportional to the net driving pressure.

B. The effective bore diameter and the modified values of membrane constants $k_{1eff}$ and $k_{2eff}$ based on the effective bore diameter were determined by using the second program (VID-9). As seen on Figure 6.19 and 21 the results indicate that:-

1. The modified values of water permeability constant ($k_{1eff}$) were found to be higher than the values of $k_1$ for the fixed diameter.

2. The salt permeability constants ($k_2$ and $k_{2eff}$) from two methods of calculation were found to be identical because the same membrane surface area or fibre O.D. was used in the calculations.

3. The effective fibre bore diameter decreased with increasing pressure and temperature.

6.5.1.2 Discussion of the B9 Results

Fibre cross section measurements were made both on the fibres at the open end (embedded in the resin tube plate) and on fibres taken from the outer surface of the bundle. The fibre diameters on the open end were in the range of 35 to 46 micron internal diameter (ID) and 72 to 88 micron outer diameter (OD). The average values were ID:39 microns and OD:80 microns. The free fibre diameters on the outer surface of the bundle were in the range of 78 to 91 microns OD and 38 to 47 microns ID. The average free fibre diameters were ID:42 microns and OD:85 microns.

However, in the experimental literature (38) (42) (15) (46) the nominal bore of the B-9 fibres is usually taken to be 42 microns. The difference between this and measured average value of 39 microns may well be due to the fact that the measurements were made on the exposed ends of the fibres embedded in the resin tube plate. However, as may be seen, on looking at Figure 6.21, the effective bore diameters vary from just over 39 microns at lower pressures to as low as 37.5 microns at the higher pressures. A bore dimeter of 42 microns at zero applied pressure would be more consistent with trend shown by the effective bore diameters than the value of 39 microns. The scatter of the effective bore diameter results make it difficult, but if anything, it would appear that the bore diameter decreases with increasing temperature, suggesting that the fibres become weaker at high temperatures and hence more easily compressed.

The pure water permeability constants obtained, at 20°C and 25°C, using the first program (FD-9, assuming a fixed fibre geometry), as seen on Figure (6.18), do not show much variation with pressure. Those for 30°C, however show a tendency to decrease with increasing pressure.

Dandavati et al (15) Ohya et al (38) and Soltanieh and Gill (46) (S and G,) carried out experiments on standard B-9 membranes (La = 75 cm). A small B-9 membrane (La = 30 cm) was also used in S and G's (46) experiment which was the same as the module used here. However, the structural differences between the small and standard B-9 membrane units were reported by S and G (46) to result in differing responses to condition changes and to give differing values for the membrane constants, $k_1$ and $k_2$.

The $k_1$ values were determined in Dandavati et al (15) and S and G's (46) experiments in the same way but the assumptions were different considering the feed concentration distributions radially in the shell. Dandavati et al's experiments the feed concentration increased radially outward but in S and G's experiments the feed concentration was assumed to be the same in the shell which was equal to the brine (reject) concentration (complete-mixing model). In Ohya et al's (38) experiments the $k_1$ values were determined neglecting the fibre bore pressure which was reported to be maximum 1 atm. or less than 5% of the operating pressure.

The experimental $k_1$ and $k_2$ values in Ref. (15) and (38) were similar but however, the values of $k_1$ and $k_2$ in S and G's (46) experiments were higher than those Ref. (15) and (38). S and G (46) explained this to be due to the different water permeability of the membrane modules used.

Generally, in the above experiments (15) (38) (46), the effect of pressure on the $k_1$ was found to be small in the pressure range between 12 atm. and 30 atm. at 25°C. This is also true of the results of the small B-9 membrane module in S and G's (46) experiments.

Hence, comparing the experimental results obtained here with those of the above experimental workers (15) (38) (46) it may be concluded that the water permeability constants, $k_1$, of B-9 membranes are not a strong function of nominal applied pressure at 25°C (even though these workers obtained different absolute values due to the differences in the way they analysed their results).

In Dandavati et al (15) and S and G's (46) experiments, the effect of pressure on $k_2$ was reported to be small. However, an increase in $k_2$ with increasing pressure was reported by Ohya et al (38) and it was suggested that this phenomenon was due to the some imperfections on the surface of the B-9 membranes. The experimental results here are in agreement with Ohya et al's (38) results where $k_2$ increased with increasing pressure.

In the experiments here, the membrane performance obtained from the small B-9 membrane was well within the makers specifications.

All the experiments with B-9 membranes (15) (38) (46) and the analysis of hollow fibre systems (24) (14) determined the membrane constants by assuming that the fibre geometry remained unchanged under working conditions.

Using the second program, (VID-9 assuming the fibre bores shrink under pressure), the modified values of $k_{1eff}$ were found to be higher than the values of $k_1$ for the fixed diameter, Figure 6.19. The increase in $k_{1eff}$ over $k_1$ would be expected since the effective bore diameter, Dia, which was smaller than the fixed value Di, was used when determining the $k_{1eff}$ values. It is well known that the solution to a fibre performance is very sensitive to changes in bore diameters. Therefore the difference between the $k_1$ and $k_{1eff}$ values would have been higher if the bore diameter had been taken to be 42 microns in the calculations instead of 39 microns Figure 6.19.

The values of $k_1$ determined from the pure water and salt solution experiments were found to be similar, see Figure 6.19. Hence, the $k_1$ values may be determined by operating the membrane with pure water feed for a few applied pressures as was done by Dandavati et al (15) and Ohya et al (38). However, as seen on Figure 6.19 $k_{1eff}$ values differ from the $k_1$ values, therefore the bore shrinkage should be taken into account when determining the $k_1$ values.

The salt permeability constants ($k_2$) from two methods of calculation were found to be identical, and hence $k_2$ appears to be independent of allowance for bore shrinkage as would be expected because the assumed fibre surface area remains constant.

TABLE 6.3

Experimental results for pure water feeds.

| Run number | 1 | 2 | 3 | 4 | 5 | 6 | 7 | 8 | 9 |
|---|---|---|---|---|---|---|---|---|---|
| Temperature C | 20.0 | 20.0 | 20.0 | 25.0 | 25.0 | 25.0 | 30.0 | 30.0 | 30.0 |
| Feed Press.atm. | 13.8 | 18.74 | 23.67 | 13.8 | 18.74 | 23.67 | 13.8 | 18.74 | 23.67 |
| Feed flow cc/s. | 226 | 225 | 224 | 226 | 224 | 223 | 225 | 225 | 222 |
| Permeate cc/s. | 45 | 64 | 82 | 54 | 77 | 101 | 66 | 91 | 116 |
| DPB atm. | 2.86 | 2.86 | 2.86 | 2.86 | 2.76 | 2.66 | 2.76 | 2.76 | 2.66 |
| Fibre press.atm | 2.56 | 3.55 | 4.83 | 2.86 | 4.24 | 6.12 | 2.76 | 4.04 | 5.43 |

Calculated values.

| | | | | | | | | | |
|---|---|---|---|---|---|---|---|---|---|
| k1,39 x $10^6$ | 9.37 | 9.07 | 8.79 | 11.2 | 10.8 | 10.8 | 13.6 | 12.8 | 12.4 |
| Fibre press.atm | 2.57 | 3.58 | 4.55 | 2.74 | 3.83 | 4.97 | 3.01 | 4.08 | 5.15 |
| Dia microns | 39.13 | 39.20 | 38.38 | 38.55 | 38.10 | 37.08 | 39.86 | 39.13 | 38.48 |
| k1eff.x $10^6$ | 9.35 | 9.04 | 8.88 | 11.3 | 11.1 | 11.3 | 13.3 | 12.8 | 12.6 |

TABLE 6.4

Experimental results for 4,500 ppm NaCl solution feeds.

| Run number | 1 | 2 | 3 | 4 | 5 | 6 | 7 | 8 |
|---|---|---|---|---|---|---|---|---|
| Temperature C | 20.0 | 25.0 | 30.0 | 20.0 | 25.0 | 30.0 | 20.0 | 25.0 |
| Feed Press.atm. | 13.8 | 13.8 | 13.8 | 16.3 | 16.3 | 16.3 | 18.7 | 18.7 |
| Feed flow cc/s. | 228 | 227 | 227 | 227 | 226 | 225 | 226 | 225 |
| Permeate cc/s. | 30 | 35 | 45 | 40 | 47 | 57 | 46 | 58 |
| Permeate ppm. | 380 | 420 | 388 | 345 | 370 | 395 | 335 | 350 |
| DPB atm | 2.96 | 3.06 | 2.91 | 3.06 | 2.96 | 2.88 | 3.06 | 3.01 |
| Fibre press.atm | 1.77 | 1.87 | 2.27 | 2.47 | 2.57 | 2.71 | 2.86 | 2.98 |

Calculated values.

| | | | | | | | | |
|---|---|---|---|---|---|---|---|---|
| k1,39 x $10^6$ | 9.03 | 11.0 | 14.5 | 9.36 | 11.2 | 14.1 | 8.62 | 11.3 |
| k2x$10^6$ cm/s | 4.05 | 5.13 | 5.87 | 4.74 | 5.82 | 7.24 | 5.19 | 6.51 |
| Fibre press.atm | 1.81 | 1.89 | 2.18 | 2.37 | 2.49 | 2.72 | 2.70 | 3.04 |
| Dia microns | 39.26 | 39.14 | 38.60 | 38.58 | 38.66 | 39.05 | 38.40 | 39.24 |
| k1eff.x $10^6$ | 9.00 | 10.9 | 14.6 | 9.45 | 11.3 | 14.1 | 8.73 | 11.2 |

Experimental results for 4,500 ppm NaCl solution feeds.

| Run number | 9 | 10 | 11 | 12 | 13 | 14 | 15 |
|---|---|---|---|---|---|---|---|
| Temperature C | 30.0 | 20.0 | 25.0 | 30.0 | 20.0 | 25.0 | 30.0 |
| Feed Press.atm. | 18.7 | 21.2 | 21.2 | 21.2 | 23.7 | 23.7 | 23.7 |
| Feed flow cc/s. | 224 | 226 | 224 | 224 | 224 | 224 | 224 |
| Permeate cc/s. | 66 | 59 | 67 | 79 | 68 | 77 | 86 |
| Permeate ppm. | 360 | 310 | 340 | 360 | 310 | 325 | 365 |
| DPB atm. | 3.00 | 3.06 | 2.96 | 2.90 | 3.06 | 3.06 | 3.01 |
| Fibre press.atm | 3.38 | 3.75 | 3.85 | 4.14 | 4.19 | 4.34 | 4.74 |

Calculated values.

| | | | | | | | |
|---|---|---|---|---|---|---|---|
| k1,39 x $10^6$ | 13.0 | 9.40 | 10.8 | 13.1 | 9.34 | 10.7 | 12.2 |
| k2 x $10^6$ | 7.38 | 5.86 | 7.06 | 8.37 | 6.53 | 7.45 | 8.96 |
| Fibre press.atm | 3.12 | 3.43 | 3.48 | 3.71 | 3.93 | 3.99 | 4.02 |
| Dia microns | 38.24 | 38.15 | 38.02 | 37.96 | 38.35 | 38.18 | 37.45 |
| k1eff.x $10^6$ | 13.3 | 9.58× | 11.1 | 13.5 | 9.48 | 10.9 | 12.7 |

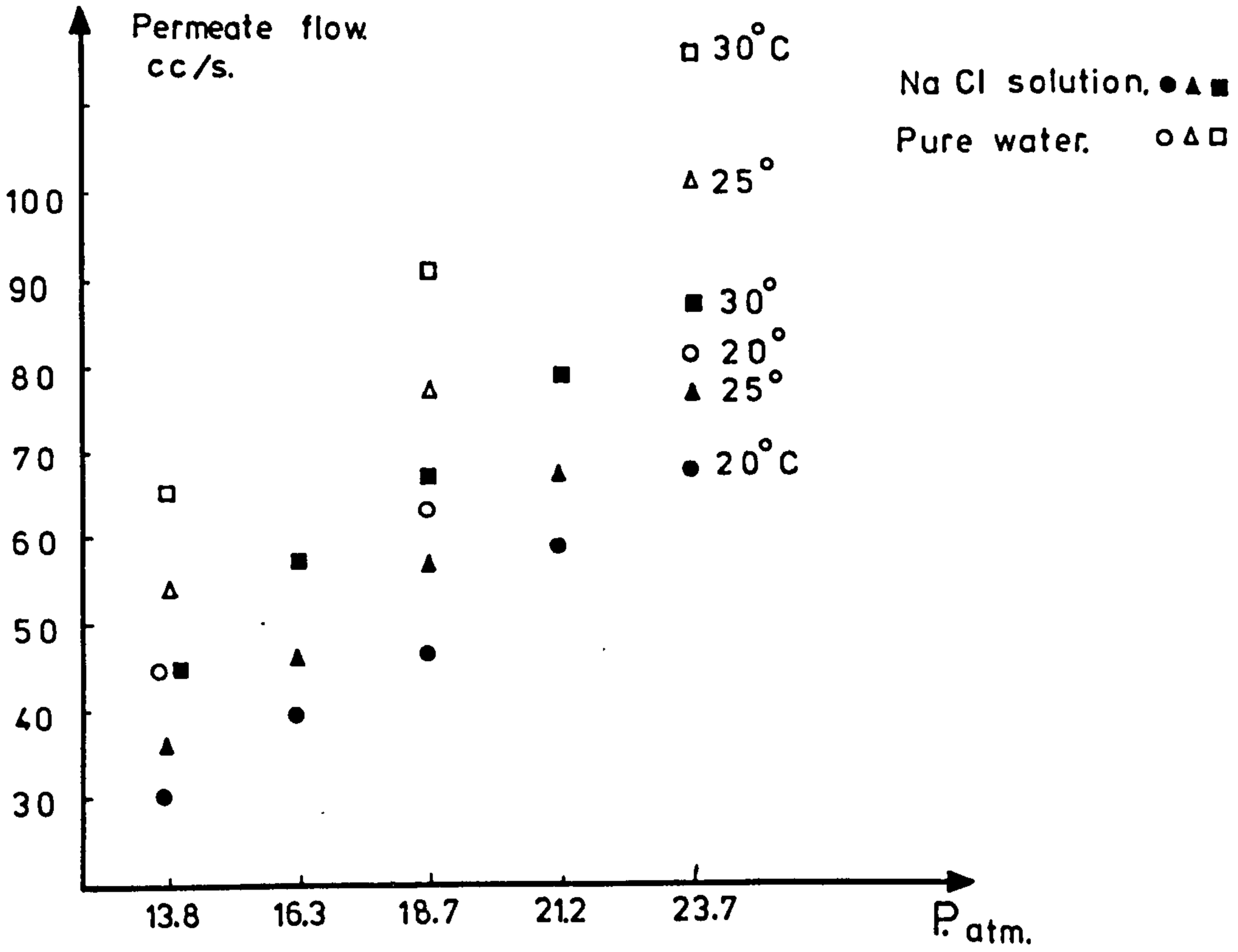


Figure 6.17. Variation of (B-9) permeate flow rate with temperature and pressure.

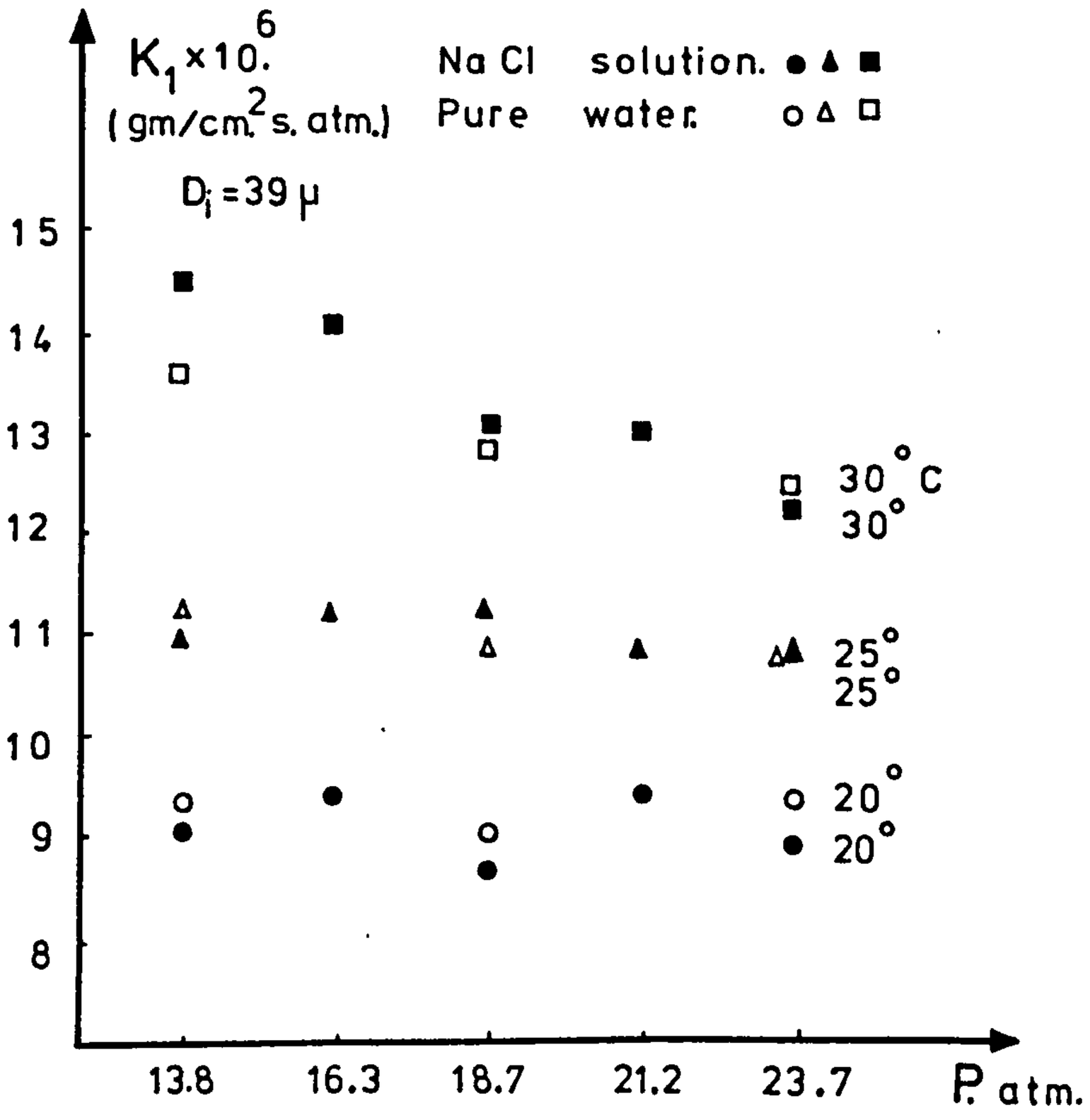


Figure 6.18. Variation of (B-9) water permeability constant with temperature and pressure.

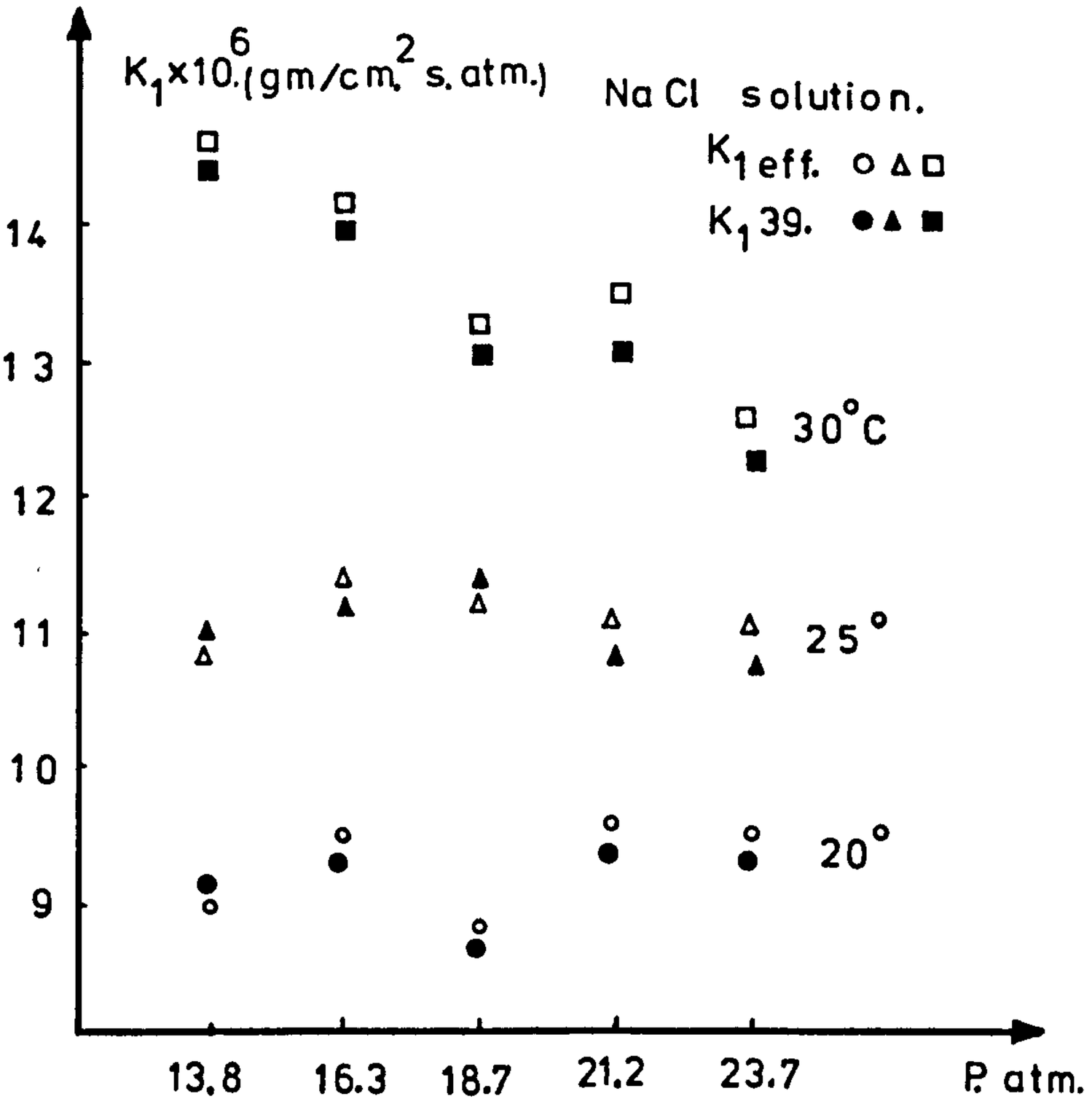


Figure 6.19. Comparison of (B-9) water permeability constants with ($K_{1eff.}$) and without ($K_{139}$) taking into account the fibre bore shrinkage vs. applied pressure.
(Above NaCl solution, below pure water as feed)

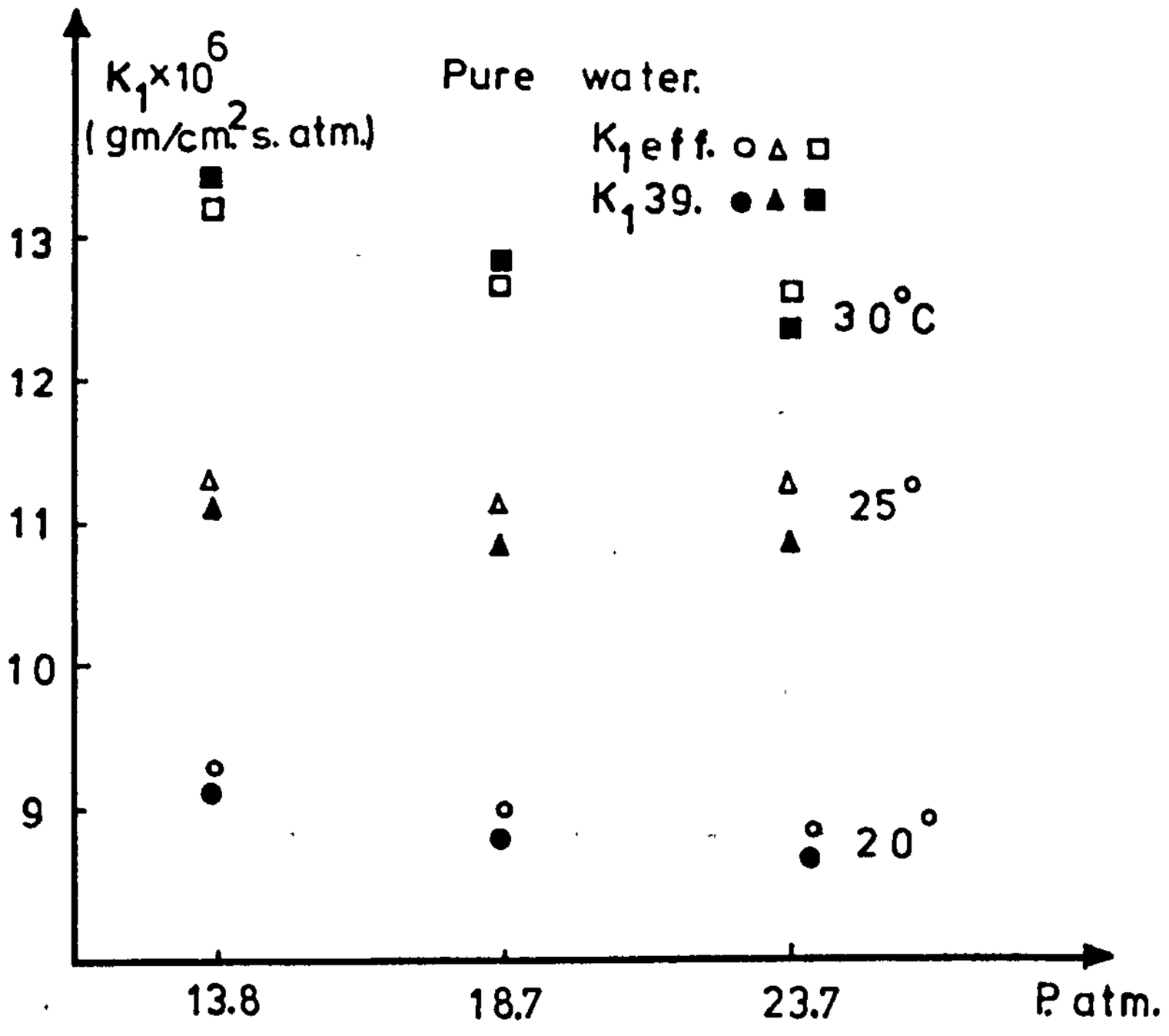

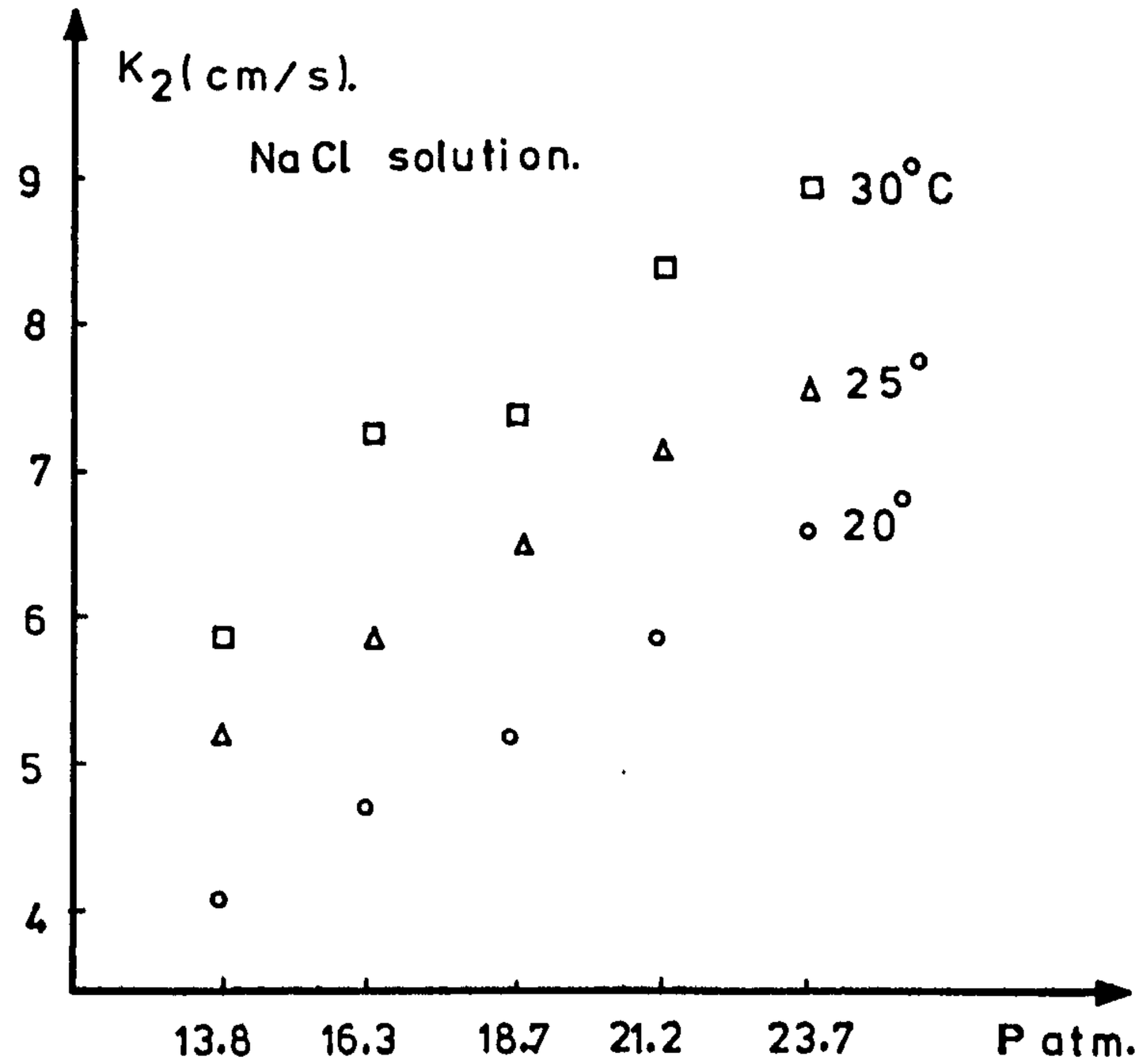


Figure 6.20. Salt permeability constant ( B-9 ) vs. applied pressure and temperature.

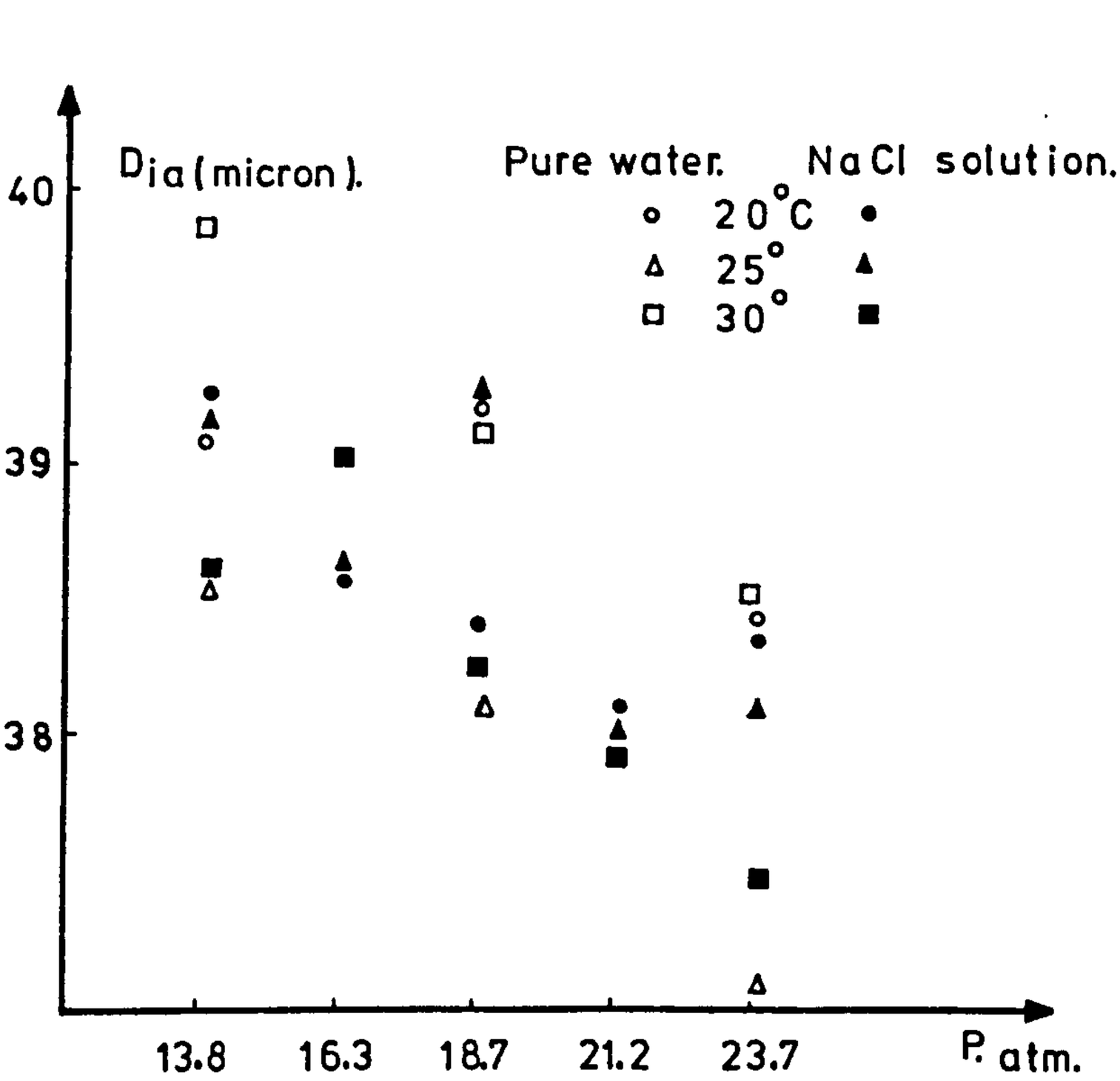


Figure 6.21. Variation of ( B-9 ) effective fibre bore diameter, $D_{ia}$, with applied pressure and temperature.

## 6.5.2. Experiments with the B-10 Membrane Module

The B-10 hollow fibre membranes were introduced to desalt highly brackish and sea waters in a single pass. They are modified version of B-9 membranes with thicker fibres and much smaller permeabilities. The very high rejections of these fibres are achieved by chemically treating the fibre surface with a solution of tannic acid. This 'post-treatment' as it is referred to by the makers must be carried out both on a newly installed membrane and also at regular intervals during the membrane life - particularly after any form of membrane cleaning operation. The post-treatment helps restore the membrane rejection which is usually significantly reduced by such operations.

Preparation of the B10 Module and Fresh Water Tests.

The newly installed B-10 membrane unit was first flushed with distilled water to discharge the sterilising solution. The experimental rig was run with distilled water for a set of conditions. After that the membrane was post-treated with PT-B (tannic acid) powder and run for another set of conditions. These two sets of conditions, before and after post-treatment, are compared on a graph, shown in Figure 6.28, where the permeate flow rate is plotted against the operating pressure. As seen in Figure 6.28, the permeate flow rate decreased after the PT-B post- treatment.

Salt Water Tests.

Following these pure water tests the rig was run with a feed of 3.2% (32,000 ppm) sodium chloride solution. As seen from the results in Table 6.13, the membrane was post-treated with PT-B to increase salt rejection after each set of experimental conditions. The salt rejection above 98% with 27% recovery was thus achieved and product concentration kept below 500 ppm for a single pass. The result was similar to the permeator characteristics under the the manufacturer's standard test conditions (feed 30,000 ppm NaCl, 30% convertion at 25°C) reported in PEM (42). These results demonstrated the dependence of the B10 rejection on the post-treatment history of the membrane.

Insertion of Pressure Tappings.

The membrane module was disassembled to drill the tapping holes at the closed ends of the fibres, so as just to break into the 'U' bends of a few fibres in order to be able to measure the fibre bore pressures. Seven tapping holes were drilled at different locations and stainless steel hypodermic tubings were set into the resin block, Figure 6.4. The drilling operation had to be done very carefully because the fibres are so small. The main difficulty was to break into the fibres without disturbing the seal between the fibre and the resin tube plate and allowing high pressure brine to leak through into the tapping. It was found that the high pressure feed solution could sometimes leak into the sealed end tube plate through the web or through gaps between the fibres which were not filled with resin thoroughly. If the fibre ends are properly embedded in the resin, the flow from the tappings should be pure permeate.

Test of tappings.

The rig was run with 20,000 ppm sodium chloride solution and samples were collected from each tapping. At the beginning of the experiments, four out of seven tappings were giving water with a concentration less than the overall permeate indicating that the tappings were sound. The rest of them gave salt water with concentrations similar to that of the feed solution and the pressure at the end of tappings was a couple of atmospheres less than the applied pressure, indicating that they were not sound.

Some experiments were carried out with these four tappings but however, later one of the tappings at r = 30 mm started leaking and giving salt water and high pressure readings. The remaining experiments were carried out using only three tappings at 23 mm, 24 mm and 37 mm away from the distributor. The concentration of the water issuing from each tapping was checked after each run, to ensure their integrity. They were found to remain sound (giving pure permeate) during the remainder of the experiments.

Post treatment and cleaning.

One of the problems encountered during the experiments was the day by day increase in permeate concentration and brineside pressure drop across the fibre bundle. The reason for this was thought to be exhaustion or removal of the PT-B (tannic acid) film on the fibre surfaces. The experiments were

carried out daily and at the end of a day's experiments the membrane unit was flushed with distilled water and kept in distilled water overnight or over the weekend. The membrane was flushed again with distilled (pure) water just before starting the next experiment.

The B-10 membrane was post-treated with PT-B powder to decrease product concentration and brineside pressure drop across the bundle. After 4 or 5 post-treatments, the post-treatment became less effective in decreasing the pressure drop across the bundle but it was still effective in reducing the product concentration. At this stage the brineside pressure drop had risen above 3 atmospheres. The reason was thought to be membrane fouling and a 'Biz-cleaning' (detergent wash) was used to reduce the bundle pressure drop. The pressure drop came down to just less than one atmosphere after 'Biz-cleaning' followed by PT-B treatment. This dependance of the membrane rejection on the post-treatment history made it very difficult to get repeatable results from one set of experiments to another.

The experimental program.

The hollow fibre membrane performance, including the measurements of closed end fibre bore pressures (at r = 23 mm, 24 mm, 30 mm and 37 mm) were investigated for two feeds, distilled (pure) water and a 20,000 ppm NaCl solution.

The applied pressures and temperatures were kept under the manufacturers safety limits of 54 atm. and 35°C maximums.

In these experiments four different working pressures of 35 atm., 40 atm., 45 atm. and 50 atm. were used at feed temperatures of 20°C, 25°C and 30°C.

6.5.2.1 The Experimental Results for the B-10 Module.

A series of tests, as described above, were made on a 4" B-10 membrane module. The results of membrane performance including measured values of fibre bore pressures under different experimental conditions are shown on Table 6.10 and 11 for pure water and Table 6.7 to 9 for 20,000 ppm sodium chloride solution.

The experiments were repeated at least two or three times. The feed flow rate was kept constant at about 350 $cm^3$/sec (0.35 l./s).

From the resulting membrane performance with sodium chloride and pure water, it was seen that,

1. The permeate flow rate increased with increasing pressure and temperature. The permeate flow rates were almost identical in the repeated experiments (i.e. relatively unaffected by the post-treatment history).

2. The increase in permeate flow rate was proportional to the increase in the net driving pressure.

3. The permeate concentrations may be found to be different in the repeated experiments (i.e. were not repeatable). This would appear to have been due to differences in the lapse of time since post-treatment.

4. Comparing sets of experiments carried out at 30°C between which there was a large variation in rejection, indicated that a large increase in salt flux was accompanied by a smaller, but significant, increase in water flux. It would thus appear that the post-treatment may have a slight effect on the water flux at higher temperatures.

5. Increasing temperature and pressure increased the fibre bore pressures. The fibre bore pressures were found to be almost identical in the repeated experiments, as were the water fluxes.

6. The pressures at the end of the fibre bores decreased with radial distance from the central of the bundle.

Computer programs used for analysis of results.

Water and salt permeabilities, $k_1$ and $k_2$, for each experiment, were determined using the following computer programs:-

1. The first program (F.D.) used the overall bundle performance to determine the membrane constants $k_1$, $k_2$ and the fibre bore pressures at the closed end by assuming a fixed fibre geometry of OD = 95 microns and with bore diameters of 42 and 45 microns. The results are shown on Tables 6.5 to 11 and Figure 6.22 to 29.

2. The second program (VID), allowing the bore diameter to float, used the overall bundle performance together with the measured values of bore pressures to predict the effective bore diameters, Dia, and modified membrane constants $k_{1eff}$ and $k_{2eff}$. The outside fibre diameter was kept constant at 95 microns (i.e. underformed).

3. The third program (VIDOD), allowed both the outside and bore diameters to float together, maintaining a constant wall thickness, and used the overall bundle performance to determine the new modified water and salt permeability constants $k_{1A}$ and $k_{2A}$.

Analysis of Experimental Results.

1. Using the first program (FD) for sodium chloride solution and pure water experiments gave the results in Figure 6.23, 26 and 27, from which it can be seen that:-

(a) The water permeability constant, $k_1$ increased with increasing temperature.

(b) Increasing the working pressure did not have much effect on $k_1$ at $20^oC$ and $25^oC$. However, $k_1$ decreased with increasing pressure at $30^oC$.

(c) The water permeabilities, $k_1$ values, were found to be higher in the pure water experiments than in the salt solution experiments.

(d) The scatter of salt permeability constants, $k_2$, results make it difficult to detect a consistent temperature or pressure effect.

(e) The decrease of bore diameter in calculations from 45 microns to 42 microns makes about 4% increase in water permeability, $k_1$, but has little effect on the salt permeability, $k_2$.

2. The results obtained by using the second program (VID) and third program (VIDOD) on both the pure water and sodium chloride experimental results, may be seen in Figure 6.24, 25 and 29.

(a) The effective water permeability constants, $k_{1eff}$ and $k_{1A}$ increased with increasing temperature. As expected $k_{1A}$ values were higher than $k_{1eff}$ values due to the smaller values used for the calculated membrane area.

(b) The effect of increasing pressure on $k_{1eff}$ and $k_{1A}$ at the lower temperatures, 20°C and 25°C, was only small, but at the higher temperature of 30°C, the $k_{1eff}$ and $k_{1A}$ decreased with increasing pressure.

(c) The values of $k_{1eff}$ and $k_{1A}$ decreased as the fibre position moved radially outward from the central of the bundle, mainly because of the radial variation in the calculated bore diameter.

(d) The values of $k_{1A}$ and $k_{1eff}$ were higher than the values of $k_1$ for the fixed diameter.

(e) The salt permeability constants $k_2$ and $k_{2eff}$ were identical, but $k_{2A}$ was found to be higher than the values assuming a fixed fibre outside diameter. This was to be expected due to the change in the assumed membrane surface area.

(f) The effective fibre bore diameters decreased with increasing temperature and pressure. The effective bore diameters, Dia and DiA were found to be identical in both calculations because they were based on the same fibre performances.

(g) The effect of increasing working pressure in increasing the fibre bore shrinkage tends to be lower at high tempeatures. In other words the higher the temperature the smaller the values of the effective bore diameters, and the less their variation with the working pressure.

(h) The values of the effective bore diameters determined in pure water experiments were smaller than those for the salt water experiments.

(i) The apparent fibre bore shrinkage becomes lower as the fibre position moves radially outward from the central of the bundle.

(k) The values of $k_{1eff}$ and $k_{1A}$ determined in pure water experiments were higher than the values found in salt solution experiments.

6.5.2.2 Discussion of the B-10 Results.

Experiments were carried out on a 4" B-10 hollow fibre membrane. The plots of the resulting membrane constants $k_1$, $k_2$ and effective bore diameters are shown in Figure 6.22 to 29. According to the experimental literature (12) (15) (27) (36) (38) (46) using hollow fibre membranes the $k_1$ and $k_2$ are both varied with temperature and pressure. The purpose of this work was to attempt to find out how much of this variation was due to changes in the B-10 fibre geometry under the influence of external pressure. This is very important because the theoretical solution to the performance of a fibre is very sensitive to changes in bore diameter. Sensitivity analyses were made using the computer program (VID), Figure 6.30 shows the effect of assumed fibre bore diameter on the variation of the water permeability constant, $k_1$, and the fibre bore pressure. For example, reducing the fibre bore diameter in the calculations from 45 microns to 42 microns made about 4% increase in water permeability constant, $k_1$. In the literature on hollow fibre membranes, water permeability constant, $k_1$, was obtained by using different assumptions Table 6.1. As seen on Table 6.1 all the calculations, however, assumed fibre cross section remained contant under working conditions except Hanbury et al's (23) work where the fibre bore shrinkage under the effect of external pressure was taken into account when determining the water permeability constant, $k_1$.

Before looking at the effect of pressure and temperature on the fibre bore diameter under working conditions, the bundle performance was investigated with a fixed fibre geometry. The reason for this to make comparison between the values of $k_1$ and $k_2$ determined here and those of the experimental literature. Reported results using B-10 hollow fibre membranes are rather limited. However, there are some experimental reports (1) (45) (54) (36) (27) using B-10 membranes but these reports are mainly concerned with the long term performance and service life characteristics of the hollow fibre module.

Considering the permeate flow rate, whatever the transport model is used, it is in direct proportion with the effective pressure, $j_1 = k_1 (\Delta P - \Delta \pi)$. As seen on Figure 6.22 the permeate flow rate is proportional to the net driving pressure in both salt solution and pure water experiments. The membrane constant $k_1$, in both experiments Figure 6.24, did not show much variation with pressure at lower temperatures such as 20°C and 25°C but decreased with increasing pressure at 30°C. However, the average $k_1$ increased with increasing temperature. Murayama et al (36) carried out experiments on a 4" B-10 membrane and reported that the pressure dependence of $k_1$ could be negligible within the applied pressure range from 10 atm. to 54 atm. at a temperature around 25°C. Thus, the experimental results here where the $k_1$ is practically independent of applied pressure at 25°C, is in agreement with the experimental results of Murayama et al (36).

In the experiments of Murayama et al (36) $k_1$ was determined to be $2 \times 10^{-6}$ $g/cm^2.s.atm.$ with seawater at 25°C. However, this figure is higher than the values of $k_1$ found here. One of the reasons may be due to the effect of the assumed membrane surface area used in their calculation which was reported to be. 139 $m^2$ by Kunisada et al (27) in the continuing experiments. However, the surface area of the B-10 membrane was determined to be 170 $m^2$ in this experiment. Sensitivity analyses, using the computer program VID, shows the effect of assumed fibre packing density (which determines the membrane surface area) on the variation of water permeability constant, $k_1$, and the fibre bore diameter, Di, Figure 6.31. Analyses of these experiments (27) (36) were made by Ohya (37) and the values of $k_1$ were simply determined by using pure water feed and moreover the fibre bore pressure was neglected in the calculations. However, a decrease in the productivity of the B-10 membrane with time was reported by Ohya (37) and Winters et al (54).

The water permeability constant $k_1$, in pure water experiments, were found to be higher than the values of $k_1$ in the salt solution experiments, Figure 6.23. In the literature (37) (15), the water permeability constant, $k_1$, of a hollow fibre membrane is obtained by measuring the productivity for a few values of the applied pressure. The water permeability constant, $k_1$, is the property and characteristics of the membrane itself. Different membranes may give different water transport depending on their chemical nature and the fabrication technique. However, the prediction of $k_1$ by

using pure water feed solution, as seen on Figure 6.23, may lead to an overestimate on B-10 membrane model used here.

When the salt permeability constant, $k_2$, or product concentration is considered, the direct comparison of the effect of pressure and temperature on $k_2$ was difficult. Because the B-10 membranes are post-treated with PT-B (tannic acid) to decrease the salt passage by time. The PT-B treatment causes a thin film on the fibre surfaces (membrane) which markedly improves the salt rejection. In the PEM (42) it was reported that one of the possible reasons for declining the salt passage was the exhaustion of this tannic acid film. This phenomenon was also reported in the experimental literature (27) (54) in that the high salt rejection (above 98%) was maintained by treating the membrane with PT-B (tannic acid).

During this experimental program the experiments were carried out daily and at the end of the day's experiments the permeator was flushed with distilled water and left overnight, weekend or for some days when the faults occurred on the experimental rig. This procedure may be one of the reasons responsible for the apparent loss of effectiveness of the tannic acid film on the membrane surface. However, generally, satisfactory product water quality (less than 500 ppm) was maintained by the application of PT-B treatment during these experiments. The experiments were repeated time to time and product concentrations, in the repeated experiments, were sometimes found to be quite different, while the water fluxes remained constant. This was probably due to the differences in time elapsed since the last PT-B treatment. This heavy dependence of rejection on post-treatment history made it difficult to detect any consistent effect of pressure or temperature on $k_2$. However, in continuous operation with B-10, a decrease in salt permeability, $k_2$, with increasing pressure was reported by Murayama et al (36). In this work, salt rejections of over 98% were obtained and the average salt permeability constant, $k_2$, was in the range of 0.57 to 0.96 x $10^{-6}$ cm/sec. This is in contrast to the range of 1.8 to 2.4 x $10^{-7}$ reported by Murayama et al (27) - where obviously better rejections were achieved.

In the literature (11) (7) (42) (43), the B-10 fibre bore diameters are taken to be between 38 microns to 46 microns with outside diameters of 93 microns to 98 microns. However, the measured average value here was 45 microns ID and 95 microns OD. It was one of the reasons for looking at the

fibre performance for two different fibre bore diameters of 42 and 45 microns. As seen on Figure 6.26, decreasing the fibre bore diameter in calculations from 45 to 42 microns made about 4% increase in $k_1$. As would be expected from the theoretical analysis the estimated water permeability constant, $k_1$, increases proportionally with decreasing assumed values for the fibre bore diameter, Figure 6.30.

Fibre cross section measurements were made both on the open end of the bundle where the fibres were buried in the resin tube plate and on the bundle surface where the fibres were free. The fibre outside diameters were in the range of 87 to 94 microns and inside diameters 40 to 47 microns. However, an average outside diameter of 92 microns and inside diameter of 44 microns were found from the measurements made on the open end tube plate. Some fibres were cut out from the outer surface of the bundle to be able to measure the bore diameters in a free, wet state. The fibre outside diameters, in these samples, were in the range of 86 to 107 microns and inside diameters 42 to 48 microns. The average free fibre outside diameter was 95 microns and inside diameter 45 microns.

Using the first program (F.D.), assuming fixed fibre bore diameters, values for $k_1$, $k_2$ and the fibre bore pressures were determined. However, the theoretically determined values of fibre bore pressures assuming a fixed fibre geometery (45 microns) were found to be significantly less than the measured fibre bore pressures. The major reasons for this difference was thought to be the decrease in the fibre bore diameter under the working conditions. Studies on the capability of hollow fibre membranes to withstand high pressures by Orofino (39) suggested that the maximum compaction occurs at the inner surface, thus supporting the concept of bore shrinkage. Hence the measured values of fibre bore pressures, Table 6.7 to 11, were used to predict the effective fibre bore diameters by using the second program (VID). As seen on Figure 29, the effective bore diameter was found to be as low as 31.5 microns compared to the atmospheric measured values of 45 microns.

Fibre bore pressure measurements were made at the closed end of the bundle at radius 23 mm, 24 mm, 30 mm and 37 mm away from the distributor tube. The computer program (VID) was run for each tapping separately using the measured value of the bore pressure to estimate an effective bore diameter, uniform throughout the bundle. The fibre bundle was analysed as a whole and the fibre bore pressures, at the other tappings, based on the

effective bore diameter were predicted. However, these theoretical values of the bore pressure for the other tappings were found to differ from the measured values of the bore pressure.

The results of these computations may be seen on Figure 6.29. The effective bore diameter increased as the position of the tapping upon which it was based moved radially outwards from the axis of the bundle. In other words, the apparent (uniform) fibre bore shrinkage decreased radially outwards.

Looking for some possible explanations for this phenomenon, it may be seen that the brine concentration increases due to the permeation as it moves radially outwards through the bundle and this causes a higher osmotic pressure and reduces the net driving force. Also, the brine pressure drop reduces the applied pressure difference acrosss the fibre wall. But these facts cannot account for the radial differences in apparent bore shrinkage.

As seen on Figure 6.29, the apparent fibre bore shrinkages in the pure water experiments was higher than those in the salt water experiments. It should be appreciated, when making this comparison, that the water permeabilities, $k_1$'s, for the pure water experiments are higher than those for equivalent conditions in the salt water experiments.

Considering the pure water experiments, theoretically, there is virtually no pressure drop radially other than the small bundle pressure drop. Therefore the effective bore diameters would be expected to be the same radially in all over the bundle in pure water experiments. On the other hand, in the salt water experiments, since the fibre production would be expected to decrease radially it would be expected that the bore pressure losses would also decrease radially and hence the fibre bore shrinkages should increase radially. However the opposite effect is observed in these experimental results.

As seen on Figure 6.29 the apparent fibre bore shrinkage decreased radially outward in both experiments. Detailed measurements on B-10 hollow fibres showed that the fibre diameters were not uniform and also microscopic examination of the fibre structure tended to suggest that the porosity of fibre structure might not be entirely uniform in the fibres studied. The differences in apparent fibre shrinkage in the pure water experiments

suggested that the fibres at each tapping might have different diameters or that the fibre structure resistances to compression under external pressure might be different. In the above calculations the fibre bore diameters were assumed to be uniform axially. However, the variation of the pressure difference across the fibre wall along the fibre becomes significant when the axial bore pressure drop is taken into account. Therefore the fibres towards the open end tube plate are exposed to the highest net pressure difference and hence would be expected to undergo the greatest bore shrinkage. Thus the fibres may become non-uniform axially or slightly conical in shape. This would tend to distort the pressure distribution along the fibre bore and could also cause a higher pressure at the closed end of the fibre in pure water experiments.

The fibre bore shrinkage increased with increasing temperature, see Figure 6.29 suggesting that the fibres become weaker at higher temperatures and hence more easily compressed. The effect of increasing pressure on fibre bore shrinkage tends to be lower at higher temperatures. For example, as seen on Figure 6.29 increasing pressure from 35 atm. to 50 atm. at 20°C (23 mm tapping) decreased the fibre bore 0.7 micron however, at 30°C increasing pressure from 35 atms. to 50 atm. the fibre bore decreased only 0.3 micron. Moreover, in pure water experiments it seems that increasing pressure from 35 atm. to 45 atm. has a relatively small effect on fibre bore shrinkage. It would tend to suggest that the fibre bore shrinkage is limited. As the fibres are compressed under increasing pressure and the fibre shrinkage tends to reach a point beyond which their stiffness increases dramatically and little further contraction takes place.

Summarising, evidence from the fibre bore pressure measurements tends to show that the fibre bore diameters shrink under pressure and this effect increses with increasing temperature and furthermore the compaction of the fibres may also be non-linear and limited.

The membrane constants $k_1$ and $k_2$ were recalculated (as $k_{1eff}$ & $k_{2eff}$), allowing for the fibre bore shrinkage. As seen on Figure 6.24, the modified effective water permeability constants ($k_{1eff}$) were found to be higher than the values neglecting the bore shrinkage effect. The increase in $k_{1eff}$ was probably due to the smaller fibre bore diameters taken into account under the same bundle performance. As explained earlier that the solution to a fibre performance is sensitive to changes in fibre bore diameter. However, the salt permeability constants, $k_2$ and $k_{2eff}$, were identical as expected, since the same fibre surface area was used in both calculations.

In the calculations above, the fibre outside diameter was assumed to be unchanged. If the fibre bores shrink under the influence of external pressure, there will obviously be another effect due to the compressive strain experienced by the outside skin of the fibre. If the fibre outside diameter is assumed to shrink by the same amount as the internal diameter, assuming the wall thickness unchanged, then new modified water and salt permeability constants, $k_{1A}$ and $k_{2A}$ can be determined. This was done using the third program (VIDOD). As seen on Figure 6.25, the new modified values of $k_{1A}$ and $k_{2A}$ were found to be higher than the values of $k_{1eff}$ and $k_2$. The reason for this is obviously due to the resulting reduction in the membrane surface area used in the calculations with the same bundle performance. However, the effective bore diameters (Dia) were identical in both calculations. The result was expected because the same fibre bore pressure and the bundle performance taken in the calculations.

The whole fibre bundle behaviour was analysed using the computer programs (FD) and (VID), then these two results were compared. An example of these results can be seen as computer outputs in Appendix 4B and 4C. One is for the fixed diameter of 45 microns and the other takes into account the fibre bore shrinkage. The variation of pressure difference across the fibre wall along the fibre becomes significant when the axial fibre bore pressure drop is considered. In the experiments with B-9 bundle, the measured fibre bore pressures were about two times higher than the theoretically predicted fibre bore pressures for the fixed fibre bore diameter. However, in the experiments with B-10 bundle, the measured values of fibre bore pressures were about 3 or 4 times higher than initially expected for a fixed bore diameter of 45 microns. Therefore, the fibres towards the open end tube plate are exposed to the highest net pressure difference and hence increasing the productivity and the local brine concentration. Thus the polarisation type effect is increased significantly.

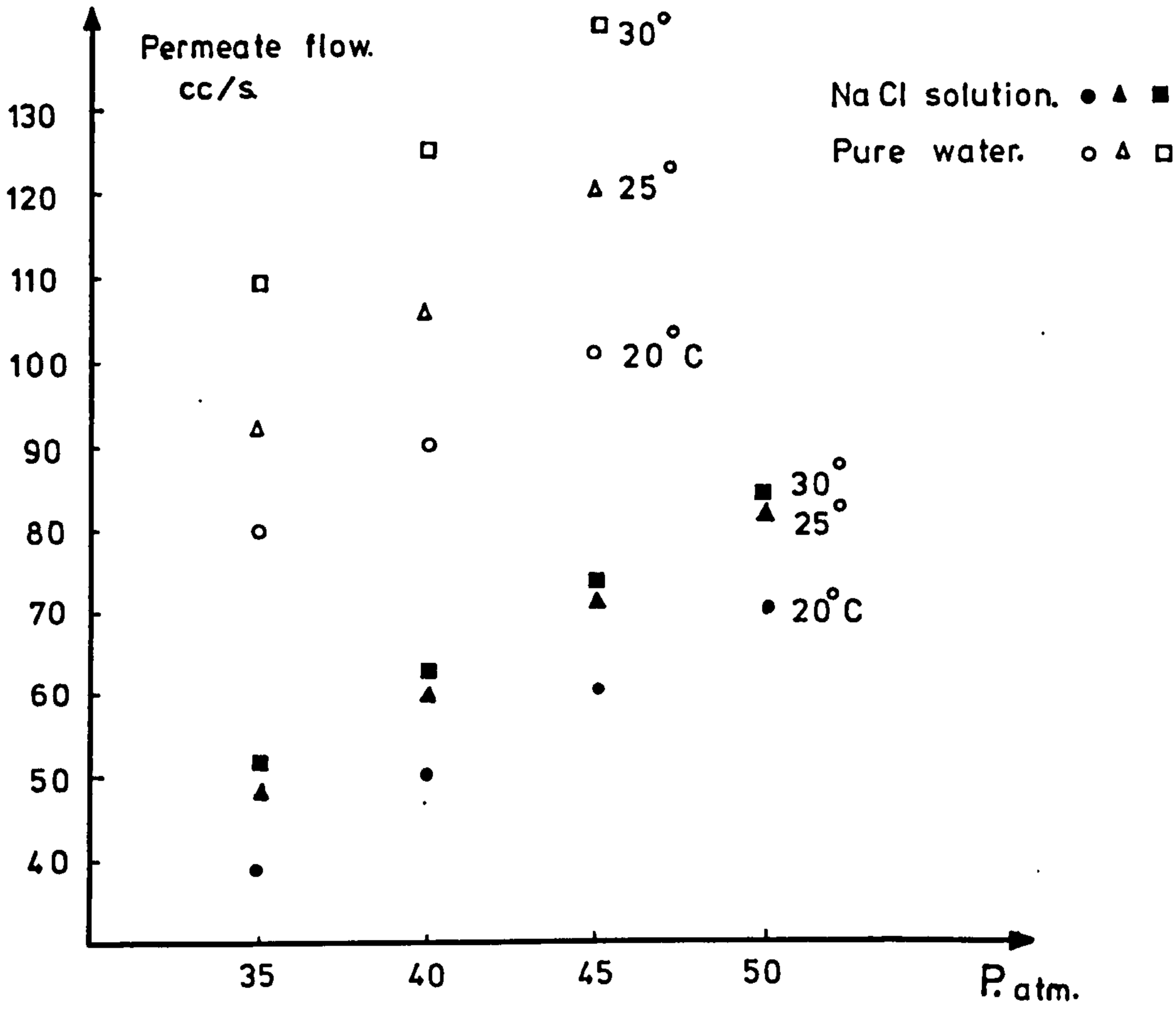


Figure 6.22. Variation of (B-10) permeate flow rate with temperature and pressure.

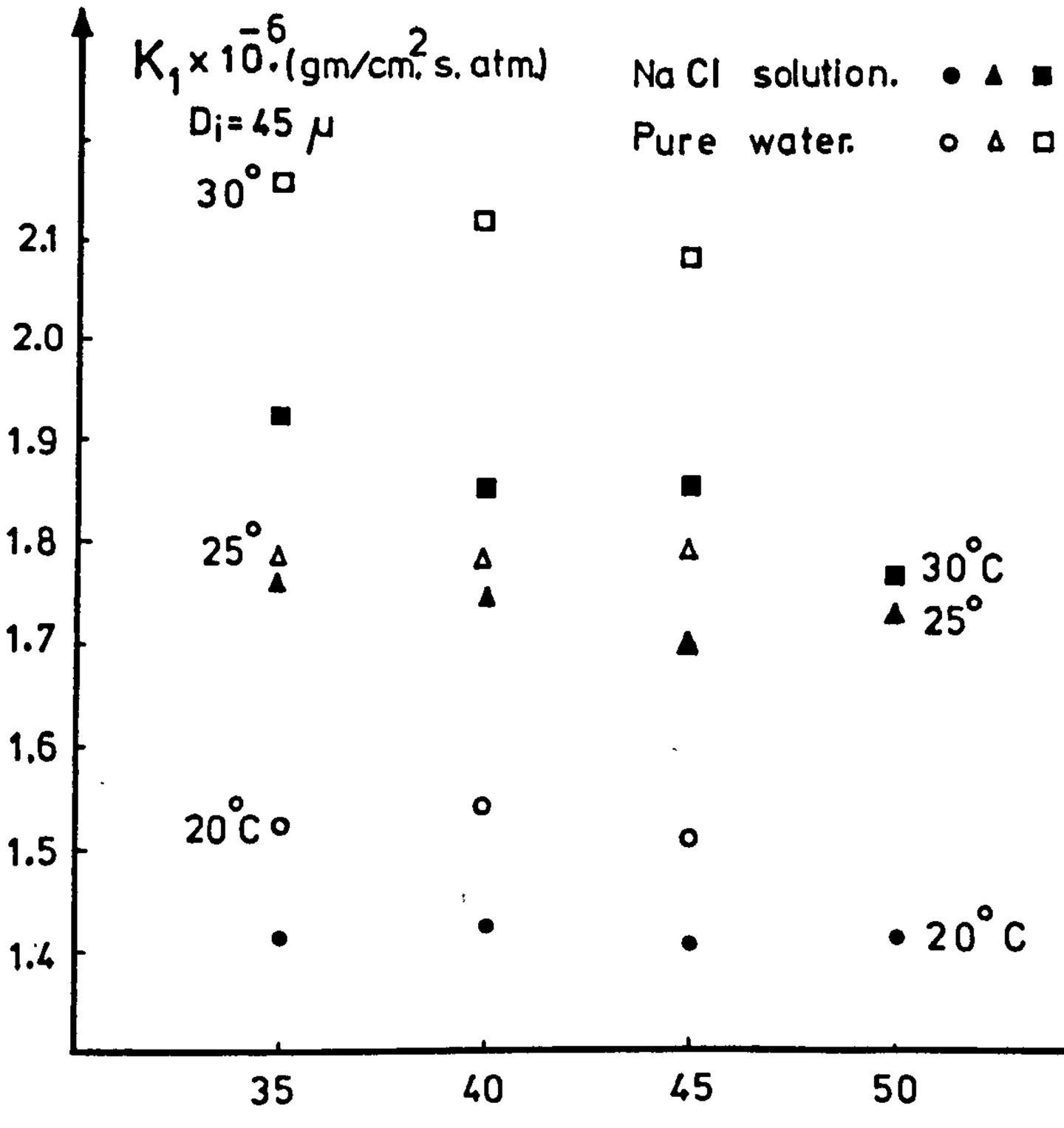


Figure 6.23. Water permeability constant (B-10) vs. temperature and pressure.

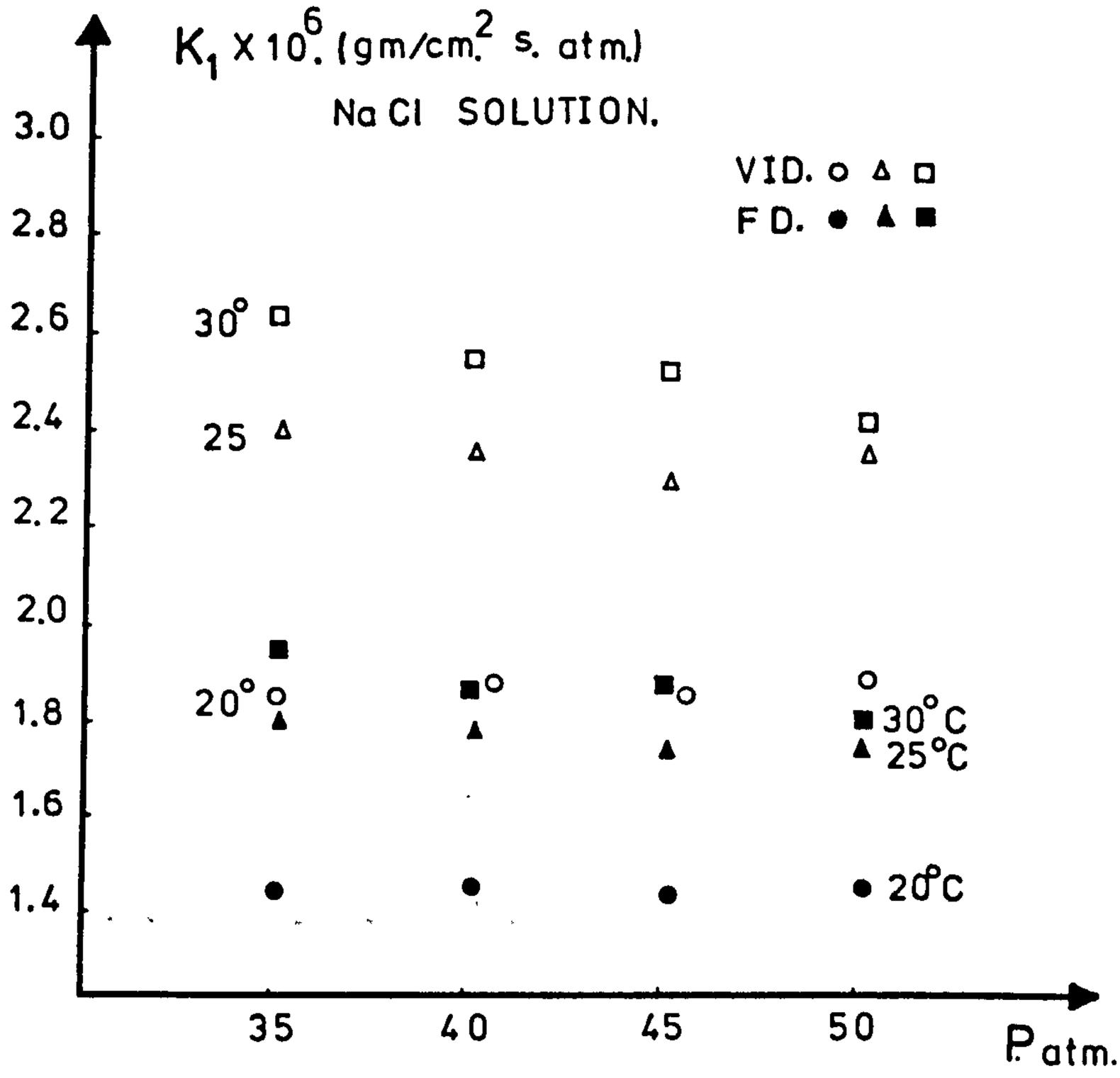


Figure 6.24. Comparison of B-10 water permeability constants with (VID), and without (FD) taking into account the fibre bore shrinkage vs. applied pressure (Above NaCl solution below pure water as feed).

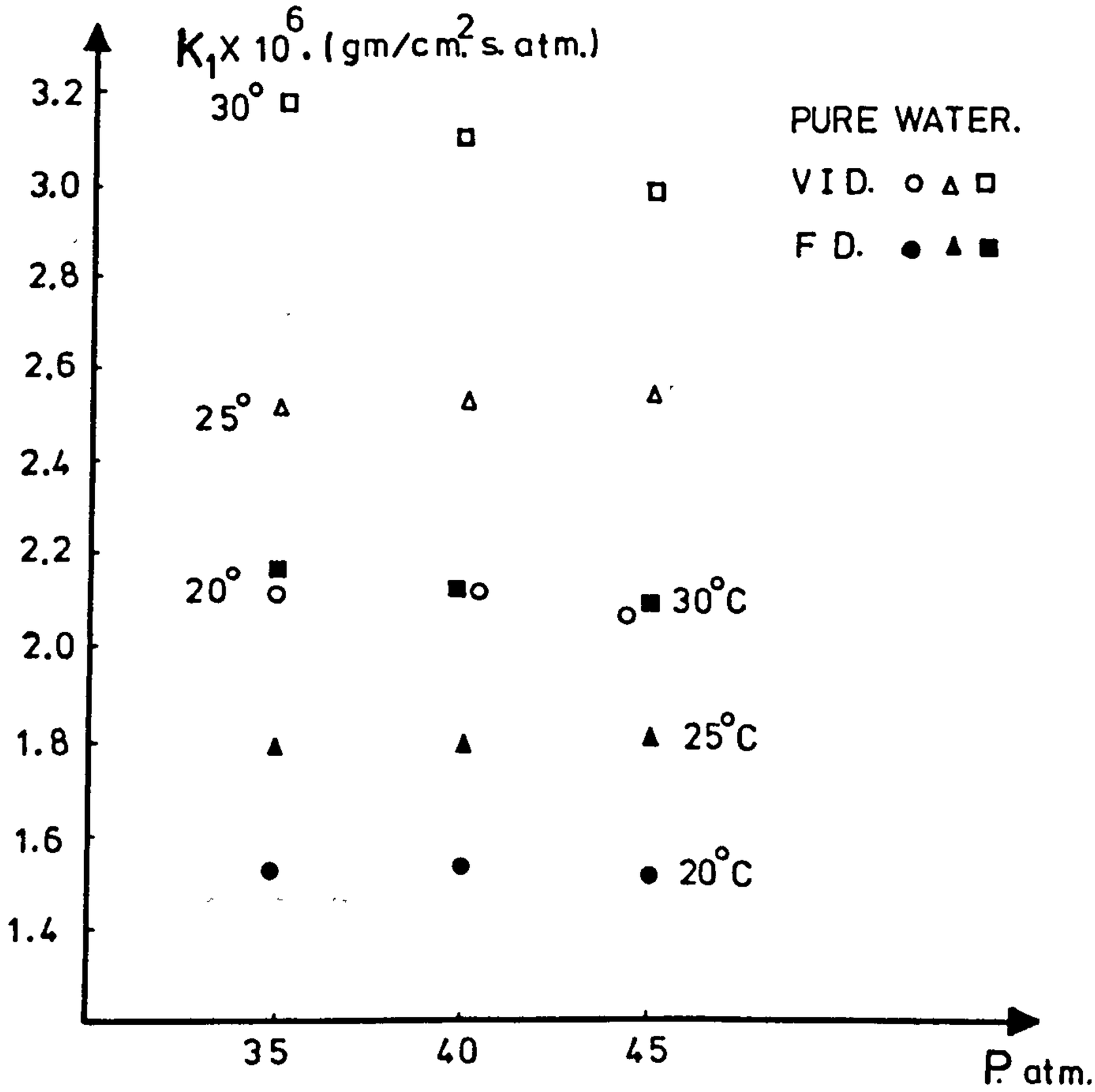

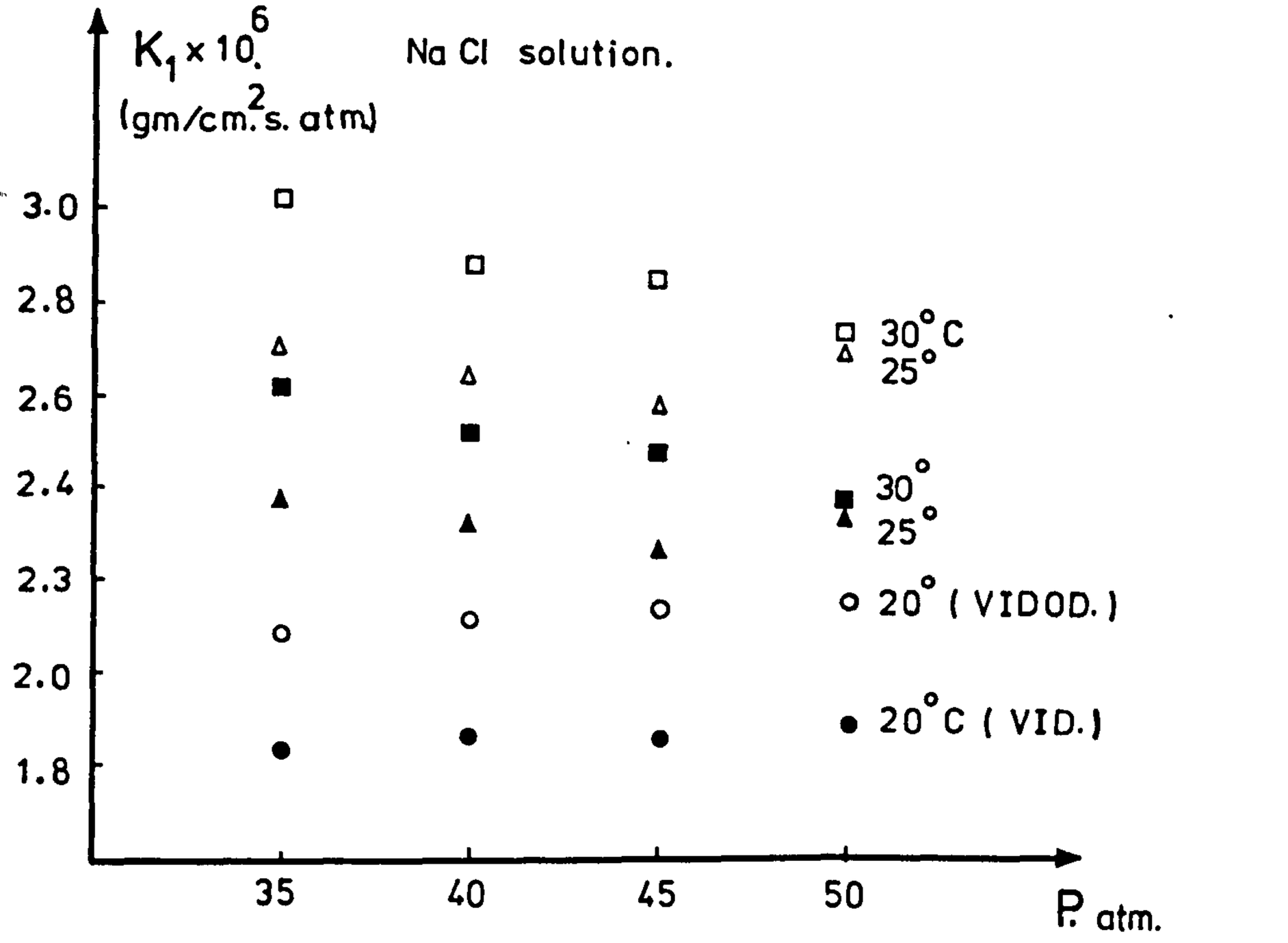


Figure 6.25. Comparison of B-10 effective water permeability constants with (VIDOD), and without (VID) taking into account the shrinkage of assumed fibre outside diameter.

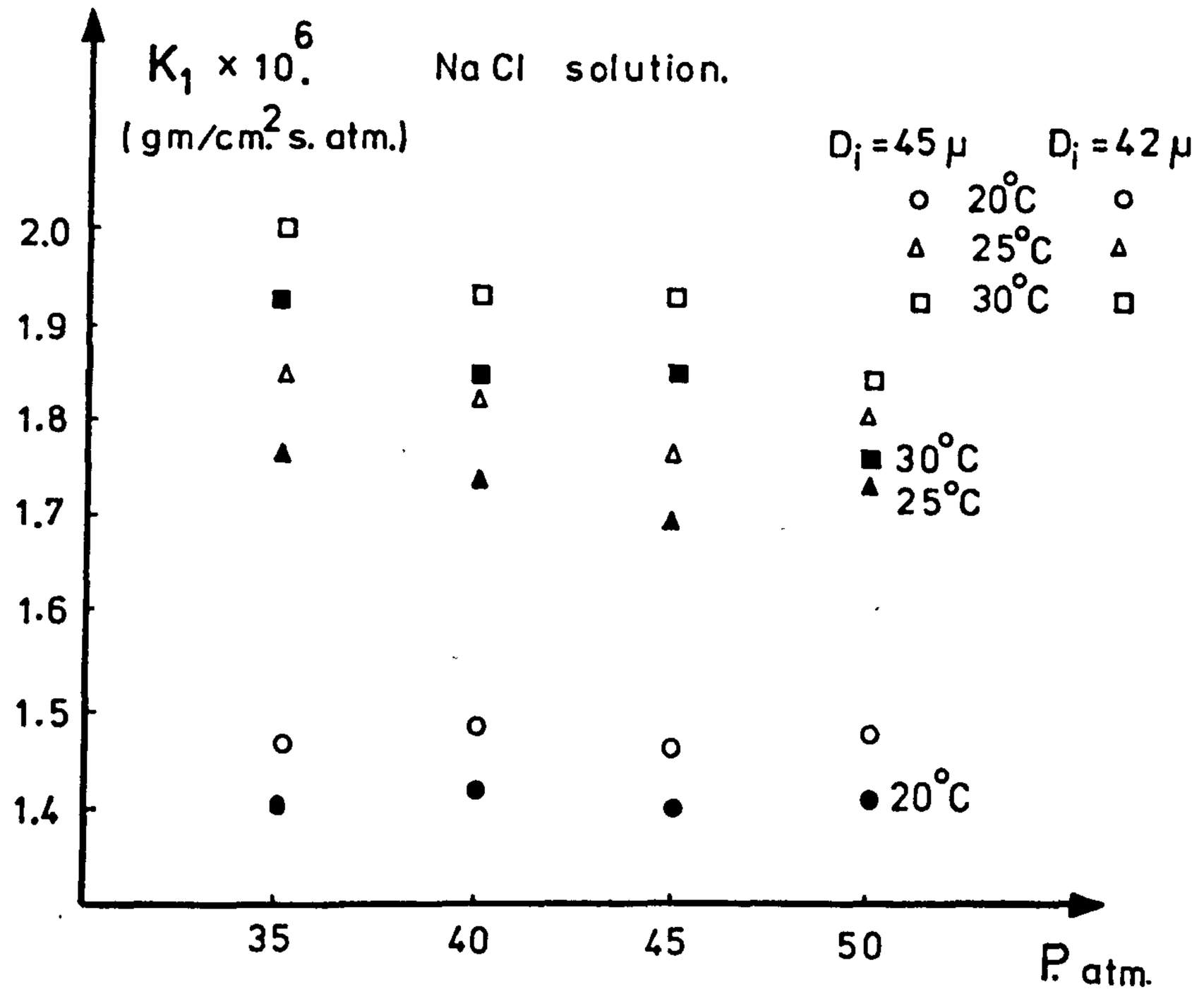


Figure 6.26. Variation of B-10 water permeability constant with assumed fibre bore diameters vs. applied pressure.

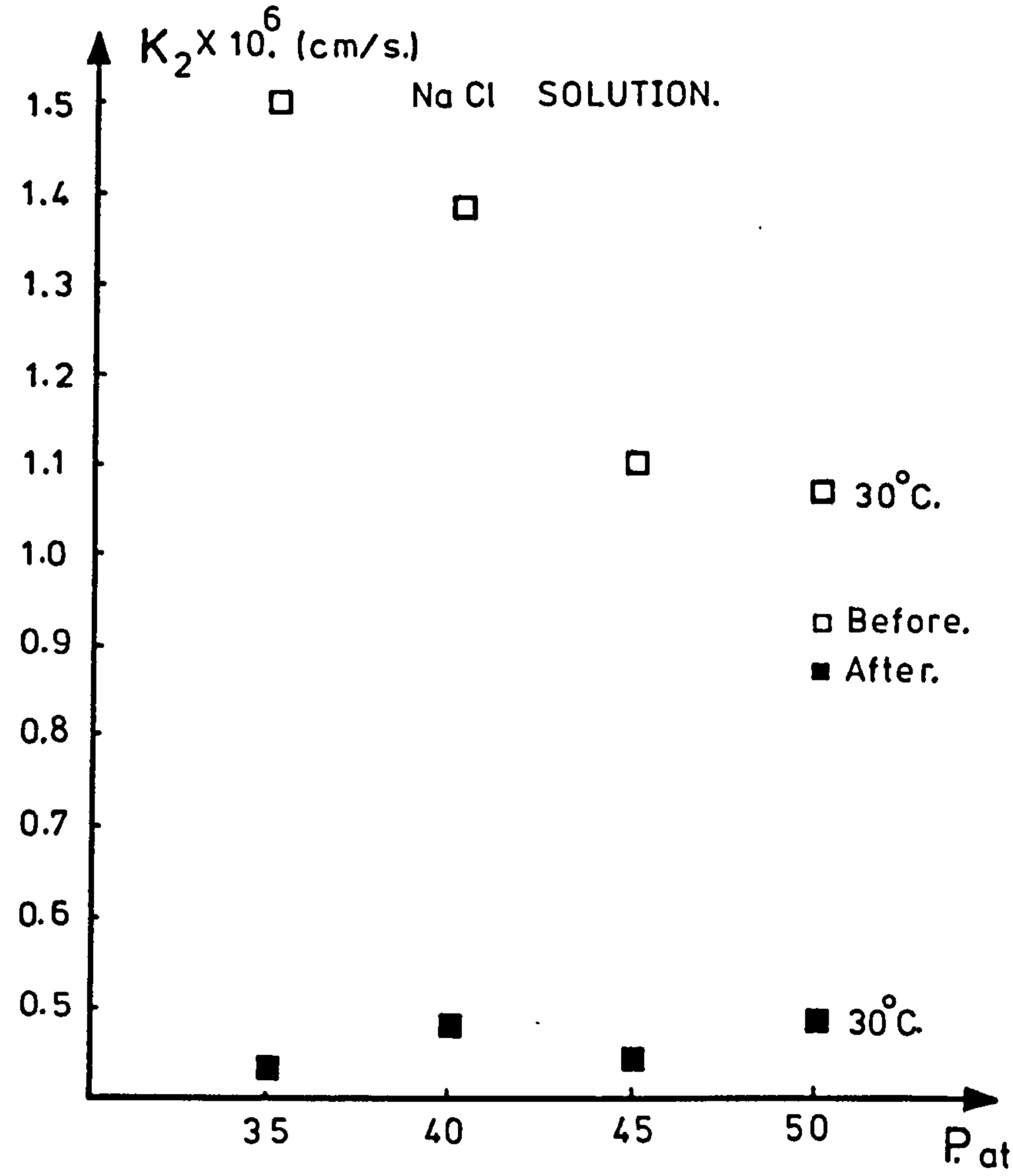


Figure 6.27. Variation of (B-10) salt permeability constant, $K_2$, with different time elapsed since the last PT-B posttreatment vs. applied pressure.

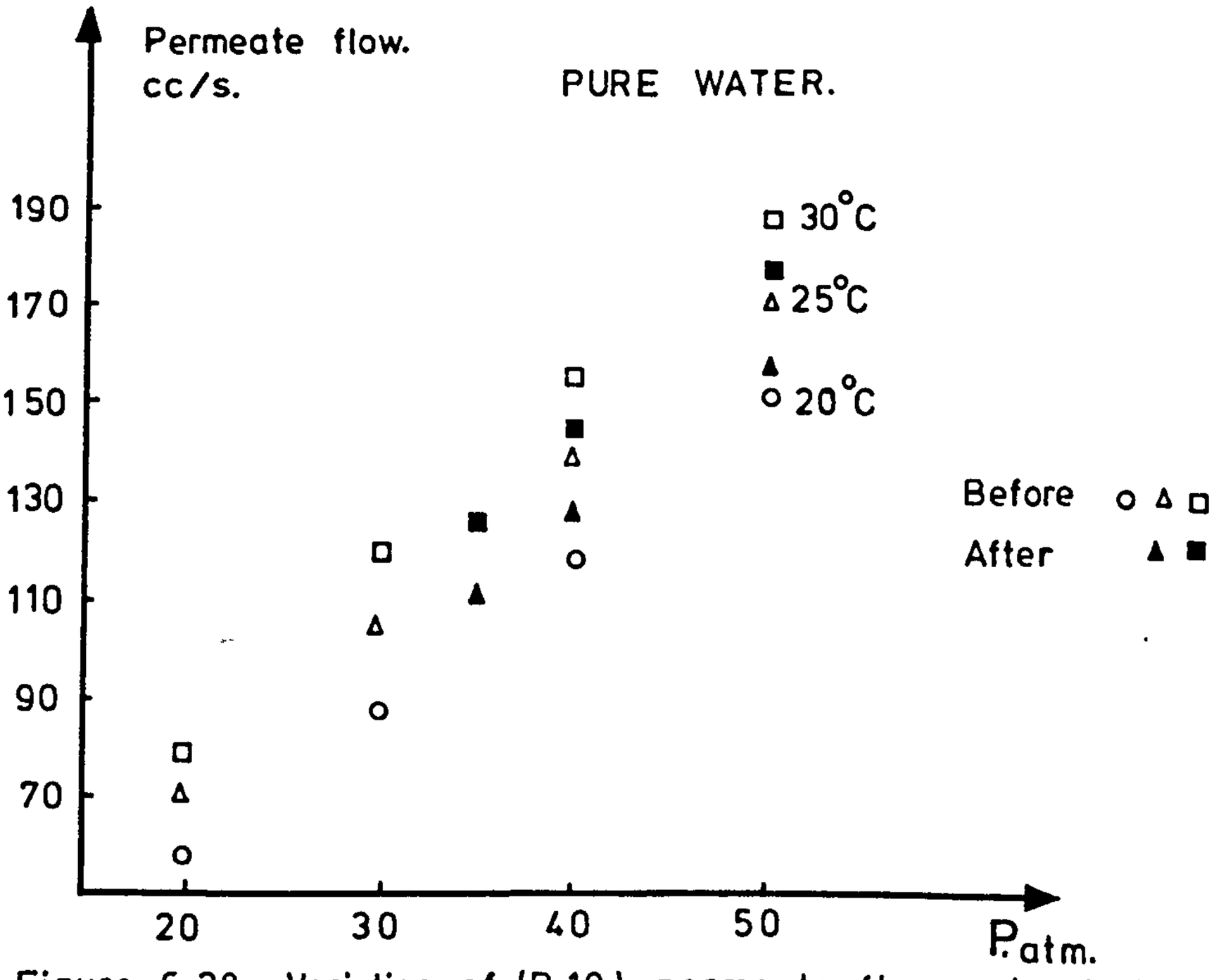


Figure 6.28. Variation of (B-10) permeate flow rate before and after posttreatment (PT-B) vs. applied pressure.

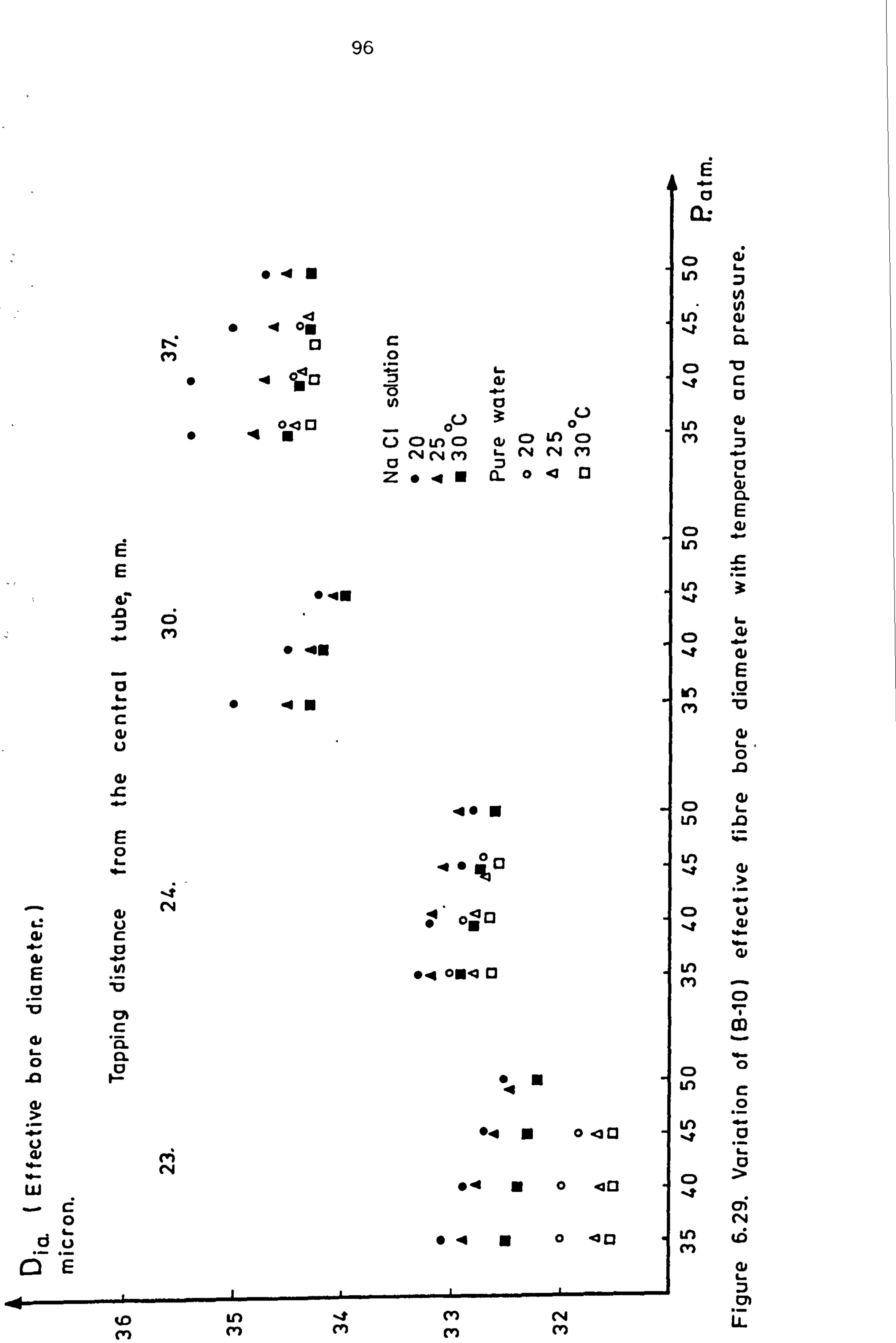
Dia. ( Effective bore diameter.)
microns.
36
35
34
33
32
35 40 45 50
Pressure in Atm.
Figure 6.29. Variation of (B-10) effective fibre bore diameter with temperature and pressure.
Tapping distance from the central tube, mm.
23.
24.
30.
37.
Pure water
20
25
30°C
Na Cl solution
20
25
30°C
35 40 45 50 P.atm.

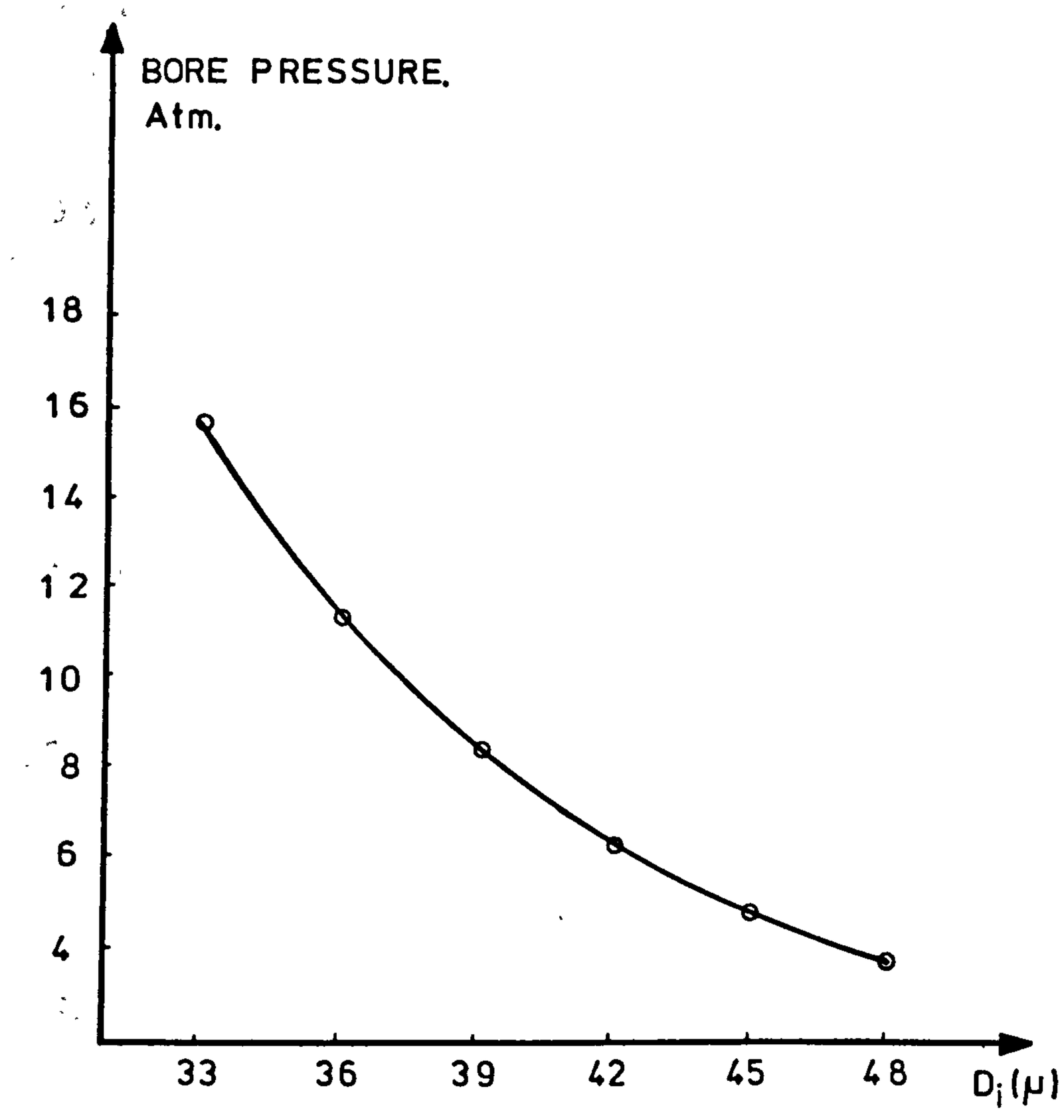


Figure 6.30. Calculated values for variation of fibre bore pressure (above) and water permeability constant (below) with fibre bore diameter.

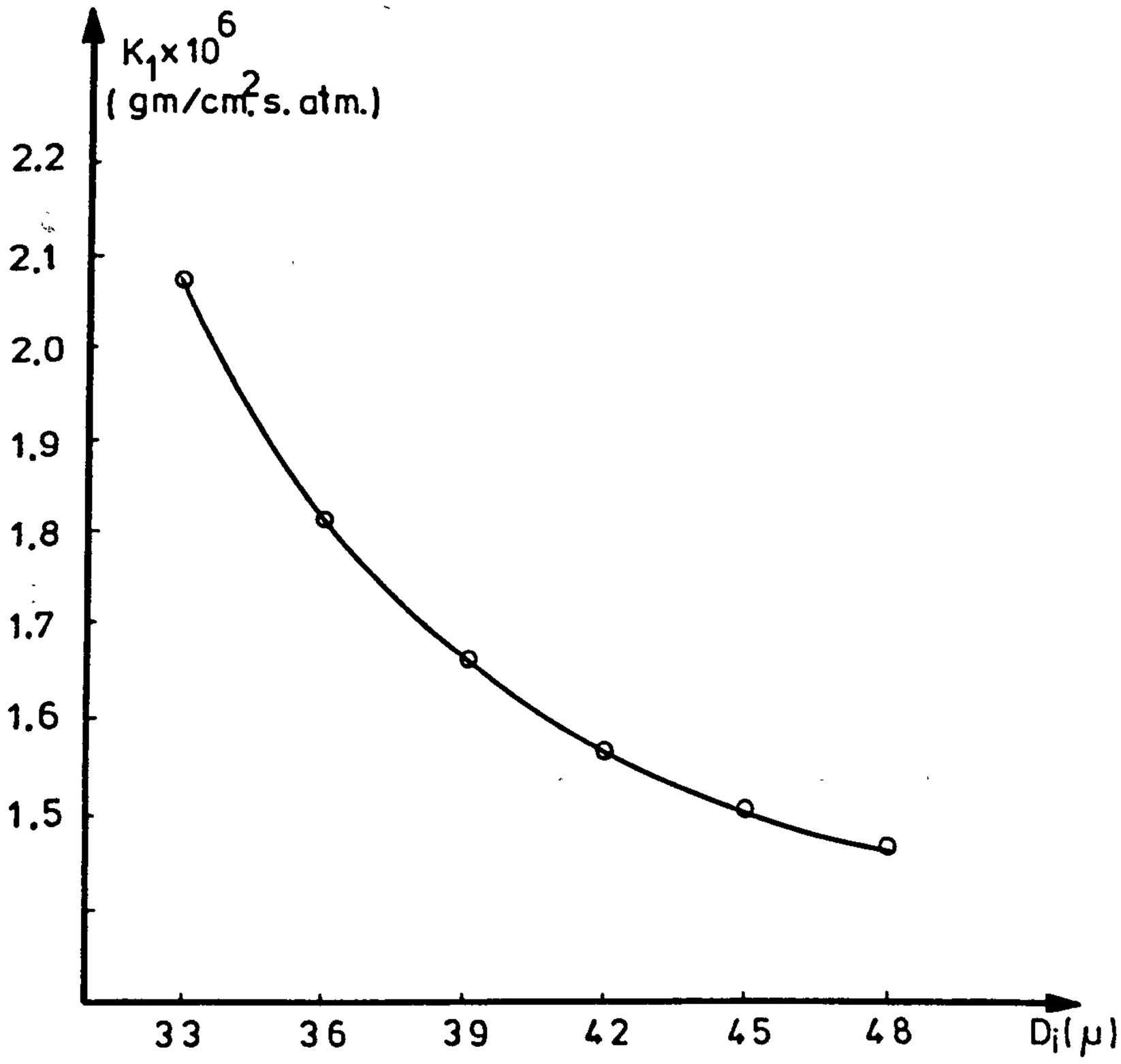

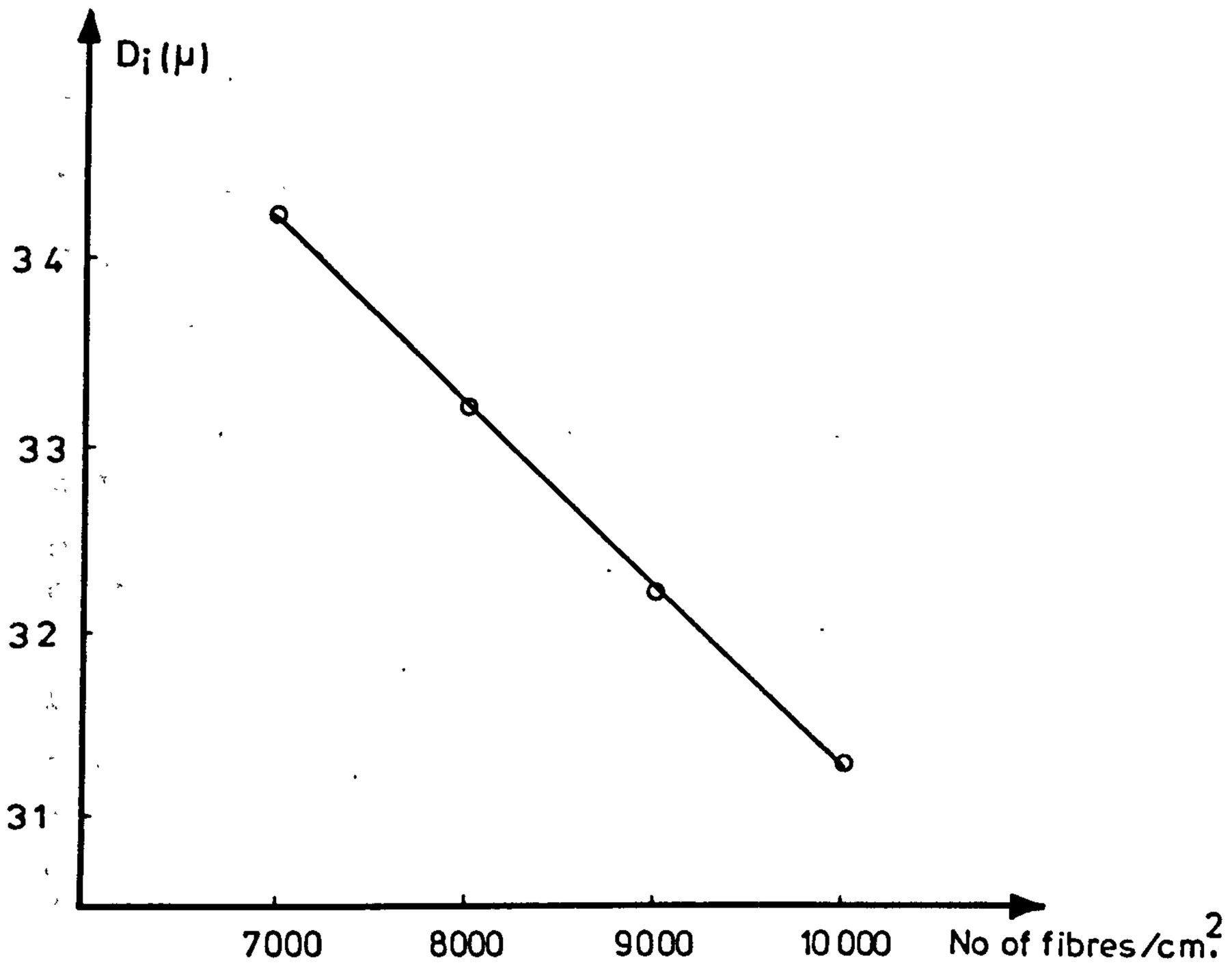


Figure 6.31. Calculated values for variation of effective bore diameter (above) and water permeability constant (below) with fibre packing density.

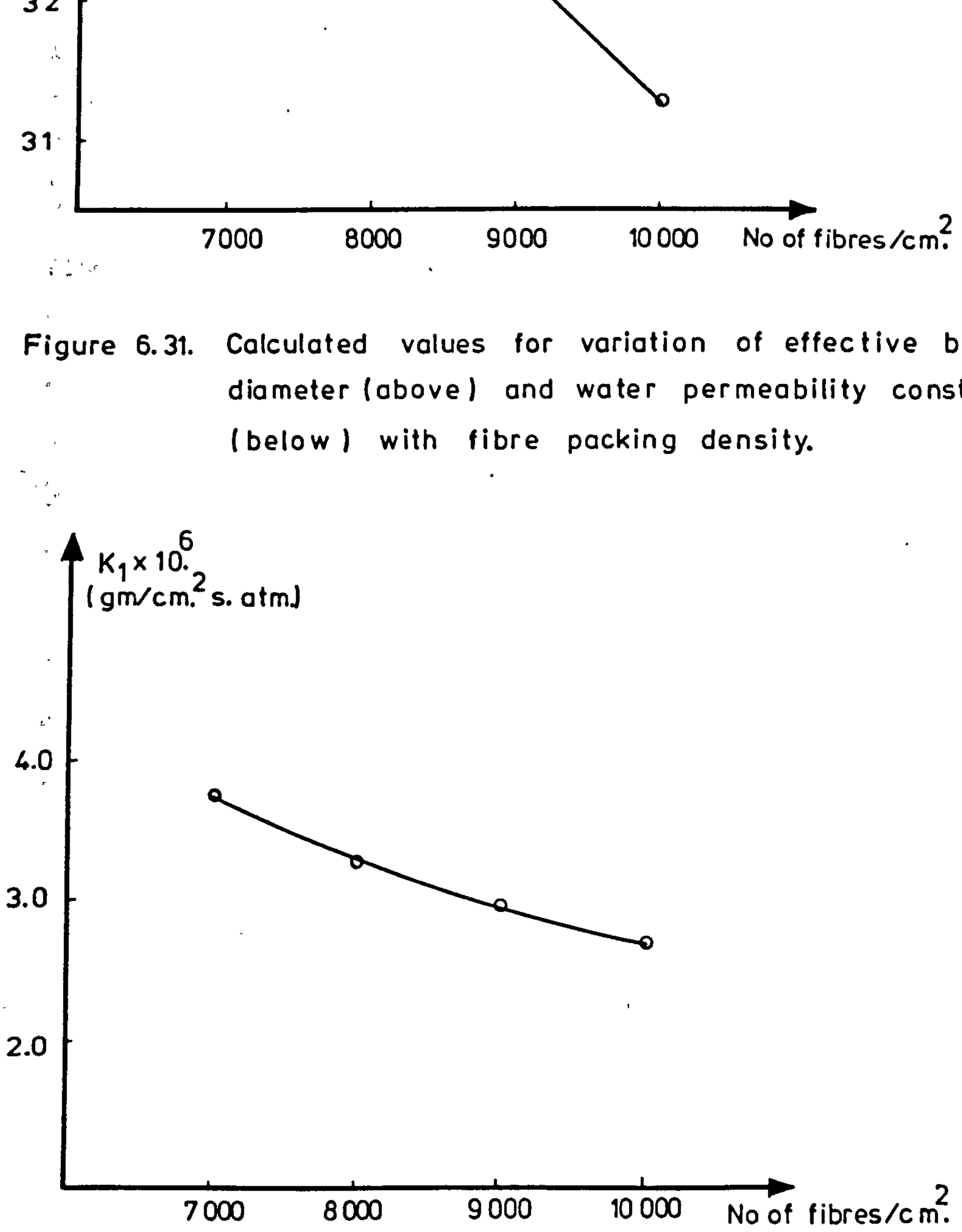

TABLE 6.5

Average values of experimental results for 20,000 ppm Na Cl solution feeds

| Run number | | | | | | | | | | | | |
|---|---|---|---|---|---|---|---|---|---|---|---|---|
| Temperature $^{o}C$ | 20 | 20 | 20 | 20 | 25 | 25 | 25 | 25 | 30 | 30 | 30 | 30 |
| Feed press. atm. | 35 | 40 | 45 | 50 | 35 | 40 | 45 | 50 | 35 | 40 | 45 | 50 |
| Feed flow, cc/s | 349 | 350 | 347 | 342 | 356 | 348 | 346 | 345 | 354 | 352 | 349 | 344 |
| Permeate flow, cc/s | 38 | 50 | 60 | 70 | 47 | 59 | 69 | 82 | 51 | 62 | 73 | 83 |
| Permeate loncn. ppm. | 670 | 630 | 530 | 465 | 443 | 515 | 455 | 3½0 | 685 | 555 | 400 | 368 |
| Bundle press. drop. atm. | 2.41 | 1.73 | 1.66 | 1.60 | 1.31 | 1.36 | 1.40 | 1.76 | 1.25 | 1.56 | 1.76 | 1.96 |
| Fibre press. at, (atm) | | | | | | | | | | | | |
| 23mm | 7.4 | 9.9 | 12.3 | 14.6 | 8.4 | 10.7 | 12.8 | 15.3 | 8.6 | 10.5 | 12.6 | 14.6 |
| 24mm | 7.2 | 9.5 | 11.8 | 14.0 | 7.9 | 9.8 | 12.0 | 14.5 | 8.1 | 10.0 | 12.0 | 13.7 |
| 37mm | 5.4 | 7.0 | 8.9 | 10.7 | 6.3 | 8.0 | 9.4 | 11.2 | 6.3 | 7.7 | 9.3 | 10.5 |
| Calculated values | | | | | | | | | | | | |
| $k_1, {}_{x10^6}(45)$ | 1.41 | 1.42 | 1.40 | 1.41 | 1.77 | 1.74 | 1.69 | 1.72 | 1.92 | 1.85 | 1.85 | 1.76 |
| $k_1, {}_{x10^6}(42)$ | 1.47 | 1.48 | 1.46 | 1.47 | 1.85 | 1.82 | 1.76 | 1.80 | 2.00 | 1.93 | 1.93 | 1.83 |
| $k_2 \times 10^6$ | 0.70 | 0.85 | 0.83 | 0.85 | 0.57 | 0.81 | 0.83 | 0.76 | 0.96 | 0.93 | 0.77 | 0.78 |
| Diameter at. (μ) | | | | | | | | | | | | |
| 23mm | 33.1 | 32.9 | 32.7 | 32.5 | 32.9 | 32.8 | 32.6 | 32.5 | 32.5 | 32.4 | 32.3 | 32.3 |
| 24mm | 33.3 | 33.2 | 32.9 | 32.8 | 33.2 | 33.2 | 33.1 | 32.9 | 32.9 | 32.8 | 32.7 | 32.6 |
| 37mm | 35.4 | 35.4 | 35.0 | 34.7 | 34.8 | 34.7 | 34.6 | 34.5 | 34.5 | 34.4 | 34.3 | 34.3 |
| $k_{1eff} \times 10^6$ | 1.83 | 1.86 | 1.85 | 1.88 | 2.38 | 2.32 | 2.25 | 2.36 | 2.62 | 2.53 | 2.50 | 2.38 |
| $k_{1A} \times 10^6$ | 2.07 | 2.11 | 2.13 | 2.14 | 2.72 | 2.64 | 2.59 | 2.70 | 3.01 | 2.89 | 2.86 | 2.73 |
| $k_{2A} \times 10^6$ | 0.80 | 0.97 | 0.97 | 0.97 | 0.65 | 0.93 | 0.92 | 0.87 | 1.11 | 1.07 | 0.89 | 0.90 |

TABLE 6.6

Average values of experimental results for pure water feeds

| | | | | | | | | | |
|---|---|---|---|---|---|---|---|---|---|
| Temperature oC | 20 | 20 | 20 | 25 | 25 | 25 | 30 | 30 | 30 |
| Feed press. atm. | 35 | 40 | 45 | 35 | 40 | 45 | 35 | 40 | 45 |
| Feed flow, cc/s | 355 | 351 | 349 | 358 | 356 | 353 | 352 | 351 | 349 |
| Permeate flow, cc/s | 79 | 91 | 101 | 92 | 106 | 120 | 111 | 125 | 139 |
| Bundle press. drop. atm. | 1.82 | 1.87 | 1.86 | 1.29 | 1.29 | 1.36 | 1.36 | 1.42 | 1.49 |
| Fibre press. at, (atm) | | | | | | | | | |
| 23mm | 17.1 | 19.7 | 22.3 | 18.4 | 21.4 | 23.9 | 19.7 | 22.4 | 24.7 |
| 24mm | 15.3 | 17.7 | 20.0 | 16.3 | 18.6 | 21.2 | 17.6 | 19.5 | 21.7 |
| 37mm | 12.6 | 14.7 | 16.7 | 13.3 | 15.6 | 17.6 | 14.4 | 16.2 | 18.4 |
| Calculated values | | | | | | | | | |
| $k_1$, (45) x $10^6$ | 1.53 | 1.54 | 1.51 | 1.77 | 1.78 | 1.79 | 2.16 | 2.12 | 2.09 |
| $k_1$, (42) x $10^6$ | 1.60 | 1.60 | 1.58 | 1.84 | 1.85 | 1.86 | 2.26 | 2.22 | 2.18 |
| Diameter at. (μ) | | | | | | | | | |
| 23mm | 32.0 | 32.0 | 31.8 | 31.7 | 31.6 | 31.6 | 31.6 | 31.6 | 31.5 |
| 24mm | 33.0 | 32.9 | 32.7 | 32.8 | 32.8 | 32.7 | 32.7 | 32.8 | 32.7 |
| 37mm | 34.6 | 34.5 | 34.4 | 34.5 | 34.4 | 34.3 | 34.4 | 34.4 | 34.3 |
| $k_{1eff}$ x $10^6$ | 2.12 | 2.13 | 2.09 | 2.52 | 2.54 | 2.54 | 3.18 | 3.10 | 3.02 |
| $k_{1A}$ x $10^6$ | 2.43 | 2.44 | 2.40 | 2.89 | 2.91 | 2.93 | 3.67 | 3.56 | 3.46 |

TABLE 6.7

Experimental results for 20,000 ppm Na Cl solution feeds

| Run number | 1 | 2 | 3 | 4 | 5 | 6 | 7 | 8 |
|---|---|---|---|---|---|---|---|---|
| Temperature $^{o}C$ | 20 | 20 | 20 | 20 | 20 | 20 | 20 | 20 |
| Feed press. atm. | 35 | 35 | 40 | 40 | 45 | 45 | 50 | 50 |
| Feed flow, cc/s | 350 | 347 | 349 | 352 | 346 | 347 | 341 | 342 |
| Permeate flow, cc/s | 38 | 38 | 47 | 52 | 57 | 62 | 67 | 72 |
| Permeate concn. ppm. | 700 | 640 | 600 | 660 | 555 | 505 | 480 | 450 |
| Bundle press. drop. atm. | 2.38 | 2.44 | 2.31 | 1.15 | 2.17 | 1.15 | 2.04 | 1.15 |
| Fibre press. at, (atm) | | | | | | | | |
| 23mm | 7.3 | 7.5 | 9.4 | 10.4 | 11.8 | 12.7 | 14.2 | 14.9 |
| 24mm | 7.1 | 7.3 | 9.1 | 10.0 | 11.4 | 12.1 | 13.6 | 14.3 |
| 37mm | 5.3 | 5.4 | 6.6 | 7.4 | 8.6 | 9.1 | 10.5 | 10.8 |
| <u>Calculated values</u> | | | | | | | | |
| $k_1$, (45) x $10^6$ | 1.41 | 1.42 | 1.37 | 1.48 | 1.34 | 1.47 | 1.37 | 1.46 |
| $k_1$, (42) x $10^6$ | 1.47 | 1.48 | 1.42 | 1.54 | 1.39 | 1.53 | 1.42 | 1.52 |
| $k_2$ x $10^6$ | 0.74 | 0.67 | 0.77 | 0.93 | 0.84 | 0.83 | 0.85 | 0.85 |
| Diameter at. (μ) | | | | | | | | |
| 23mm | 33.2 | 33.0 | 32.9 | 32.9 | 32.6 | 32.7 | 32.4 | 32.6 |
| 24mm | 33.4 | 33.2 | 33.2 | 33.2 | 32.8 | 33.0 | 32.7 | 32.9 |
| 37mm | 35.5 | 35.3 | 35.5 | 35.4 | 34.8 | 35.1 | 34.5 | 34.9 |
| $k_{1eff}$ x $10^6$ | 1.81 | 1.85 | 1.76 | 1.95 | 1.75 | 1.95 | 1.81 | 1.94 |
| $k_{1A}$ x $10^6$ | 2.04 | 2.10 | 2.00 | 2.21 | 2.04 | 2.22 | 2.07 | 2.21 |
| $k_{2A}$ x $10^6$ | 0.83 | 0.76 | 0.87 | 1.05 | 0.97 | 0.95 | 0.97 | 0.97 |

TABLE 6.8

| Run number | 9 | 10 | 11 | 12 | 13 | 14 | 15 | 16 | 17 | 18 | 19 |
|---|---|---|---|---|---|---|---|---|---|---|---|
| Temperature $^{o}C$ | 25 | 25 | 25 | 25 | 25 | 25 | 25 | 25 | 25 | 25 | 25 |
| Feed press. atm. | 35 | 35 | 35 | 40 | 40 | 45 | 45 | 45 | 50 | 50 | 50 |
| Feed flow, cc/s | 359 | 359 | 351 | 346 | 349 | 346 | 347 | 346 | 346 | 343 | 346 |
| Permeate flow, cc/s | 46 | 47 | 49 | 57 | 61 | 69 | 69 | 70 | 80 | 83 | 83 |
| Permeate concn. ppm. | 320 | 425 | 585 | 555 | 475 | 475 | 450 | 440 | 400 | 360 | 320 |
| Bundle press. drop. atm. | 0.88 | 1.83 | 1.22 | 1.36 | 1.36 | 1.36 | 1.49 | 1.36 | 1.49 | 2.04 | 1.76 |
| Fibre press. at, (atm) | | | | | | | | | | | |
| 23mm | 8.2 | 8.4 | 8.7 | 10.4 | 10.9 | 12.7 | 12.8 | 12.9 | 14.9 | 15.6 | 15.4 |
| 24mm | 7.8 | 8.0 | | 9.8 | | 11.9 | 12.0 | | 14.0 | 14.6 | 14.8 |
| 37mm | 6.2 | 6.2 | 6.5 | 7.9 | 8.1 | 9.6 | 9.2 | 9.4 | 11.0 | 11.4 | 11.2 |
| <u>Calculated values</u> | | | | | | | | | | | |
| $k_1$, (45) x $10^6$ | 1.69 | 1.80 | 1.83 | 1.67 | 1.82 | 1.68 | 1.68 | 1.71 | 1.66 | 1.76 | 1.75 |
| $k_1$, (42) x $10^6$ | 1.76 | 1.88 | 1.91 | 1.74 | 1.90 | 1.75 | 1.75 | 1.78 | 1.73 | 1.84 | 1.83 |
| $k_2$ x $10^6$ | 0.40 | 0.54 | 0.78 | 0.85 | 0.77 | 0.86 | 0.82 | 0.81 | 0.83 | 0.77 | 0.68 |
| Diameter at. ($\mu$) | | | | | | | | | | | |
| 23mm | 32.9 | 32.8 | 32.9 | 32.6 | 32.9 | 32.6 | 32.5 | 32.6 | 32.5 | 32.4 | 32.5 |
| 24mm | 33.2 | 33.2 | | 33.2 | | 33.2 | 33.0 | | 33.0 | 32.9 | 32.8 |
| 37mm | 34.8 | 34.8 | 34.8 | 34.5 | 34.8 | 34.4 | 34.7 | 34.7 | 34.5 | 34.4 | 34.6 |
| $k_{1eff}$ x $10^6$ | 2.25 | 2.45 | 2.46 | 2.23 | 2.45 | 2.24 | 2.25 | 2.26 | 2.22 | 2.44 | 2.42 |
| $k_{1A}$ x $10^6$ | 2.57 | 2.80 | 2.81 | 2.55 | 2.76 | 2.58 | 2.59 | 2.59 | 2.56 | 2.78 | 2.76 |
| $k_{2A}$ x $10^6$ | 0.46 | 0.62 | 0.88 | 0.97 | 0.87 | 0.98 | 0.93 | 0.92 | 0.94 | 0.87 | 0.78 |

TABLE 6.9

| Run number | 20 | 21 | 22 | 23 | 24 | 25 | 26 | 27 |
|---|---|---|---|---|---|---|---|---|
| Temperature $^{o}C$ | 30 | 30 | 30 | 30 | 30 | 30 | 30 | 30 |
| Feed press. atm. | 35 | 35 | 40 | 40 | 45 | 45 | 50 | 50 |
| Feed flow, cc/s | 352 | 356 | 350 | 353 | 350 | 348 | 347 | 341 |
| Permeate flow, cc/s | 49 | 53 | 59 | 65 | 71 | 76 | 81 | 85 |
| Permeate concn. ppm. | 320 | 1050 | 300 | 810 | 240 | 560 | 235 | 500 |
| Bundle press. drop. atm. | 1.15 | 1.36 | 1.63 | 1.49 | 1.90 | 1.63 | 2.17 | 1.76 |
| Fibre press. at, (atm) | | | | | | | | |
| 23mm | 8.2 | 8.9 | 10.0 | 10.9 | 12.3 | 12.9 | 14.3 | 14.8 |
| 24mm | 7.7 | 8.5 | 9.5 | 10.4 | 11.6 | 12.3 | 13.4 | 13.9 |
| 37mm | 6.0 | 6.6 | 7.4 | 8.0 | 9.0 | 9.6 | 10.2 | 10.8 |
| Calculated values | | | | | | | | |
| $k_1$, (45) x $10^6$ | 1.85 | 1.99 | 1.77 | 1.94 | 1.77 | 1.89 | 1.72 | 1.80 |
| $k_1$, (42) x $10^6$ | 1.93 | 2.07 | 1.85 | 2.02 | 1.85 | 1.97 | 1.79 | 1.87 |
| $k_2$ x $10^6$ | 0.42 | 1.50 | 0.47 | 1.39 | 0.44 | 1.10 | 0.49 | 1.08 |
| Diameter at. (μ) | | | | | | | | |
| 23mm | 32.4 | 32.5 | 32.4 | 32.4 | 32.2 | 32.4 | 32.1 | 32.2 |
| 24mm | 33.0 | 32.7 | 32.7 | 32.8 | 32.6 | 32.7 | 32.5 | 32.6 |
| 37mm | 34.5 | 34.4 | 34.3 | 34.5 | 34.2 | 34.3 | 34.3 | 34.2 |
| $k_{1eff}$ x $10^6$ | 2.50 | 2.75 | 2.38 | 2.69 | 2.39 | 2.60 | 2.32 | 2.44 |
| $k_{1A}$ x $10^6$ | 2.85 | 3.16 | 2.73 | 3.06 | 2.75 | 2.98 | 2.66 | 2.80 |
| $k_{2A}$ x $10^6$ | 0.48 | 1.72 | 0.54 | 1.60 | 0.51 | 1.27 | 0.56 | 1.25 |

TABLE 6.10

Experimental results for pure water feeds

| Run number | 1 | 2 | 3 | 4 | 5 | 6 | 7 | 8 |
|---|---|---|---|---|---|---|---|---|
| Temperature $^{o}C$ | 20 | 20 | 20 | 20 | 20 | 20 | 20 | 20 |
| Feed press. atm. | 35 | 35 | 35 | 40 | 40 | 40 | 45 | 45 |
| Feed flow, cc/s | 360 | 357 | 349 | 359 | 350 | 346 | 354 | 344 |
| Permeate flow, cc/s | 79 | 79 | 79 | 91 | 91 | 91 | 100 | 102 |
| Bundle press. drop. atm. | 1.15 | 1.83 | 2.50 | 1.22 | 1.90 | 2.50 | 1.29 | 2.44 |
| Fibre press. at, (atm) | | | | | | | | |
| 23mm | 17.6 | 16.7 | 17.0 | 19.8 | 19.3 | 19.8 | 22.0 | 22.5 |
| 24mm | 15.4 | 15.1 | 15.4 | 17.7 | 17.6 | 17.9 | 19.4 | 20.5 |
| 37mm | 13.0 | 12.6 | 12.3 | 15.1 | 14.6 | 14.4 | 16.8 | 16.5 |
| Calculated values | | | | | | | | |
| $k_1$, (45) x $10^6$ | 1.51 | 1.54 | 1.56 | 1.52 | 1.54 | 1.56 | 1.48 | 1.55 |
| $k_1$, (42) x $10^6$ | 1.57 | 1.61 | 1.62 | 1.58 | 1.61 | 1.62 | 1.54 | 1.61 |
| Diameter at. ($\mu$) | | | | | | | | |
| 23mm | 31.8 | 32.2 | 32.1 | 31.9 | 32.2 | 32.0 | 31.8 | 31.8 |
| 24mm | 32.9 | 33.1 | 32.9 | 33.0 | 33.0 | 32.8 | 32.8 | 32.6 |
| 37mm | 34.4 | 34.6 | 34.8 | 34.3 | 34.6 | 34.7 | 34.2 | 34.5 |
| $k_{1eff}$ x $10^6$ | 2.11 | 2.10 | 2.16 | 2.13 | 2.10 | 2.17 | 2.04 | 2.18 |
| $k_{1A}$ x $10^6$ | 2.40 | 2.41 | 2.47 | 2.42 | 2.43 | 2.48 | 2.35 | 2.48 |

TABLE 6.11

| Run number | 9 | 10 | 11 | 12 | 13 | 14 |
|---|---|---|---|---|---|---|
| Temperature $^{o}C$ | 25 | 25 | 25 | 30 | 30 | 30 |
| Feed press. atm. | 35 | 40 | 45 | 35 | 40 | 45 |
| Feed flow, cc/s | 358 | 356 | 353 | 352 | 351 | 349 |
| Permeate flow, cc/s | 92 | 106 | 120 | 111 | 125 | 139 |
| Bundle press. drop. atm. | 1.29 | 1.29 | 1.36 | 1.36 | 1.42 | 1.49 |
| Fibre press. at, (atm) | | | | | | |
| 23mm | 18.4 | 21.4 | 23.9 | 19.7 | 22.4 | 24.7 |
| 24mm | 16.3 | 18.6 | 21.2 | 17.6 | 19.5 | 21.7 |
| 37mm | 13.3 | 15.6 | 17.6 | 14.4 | 16.2 | 18.4 |
| Calculated values | | | | | | |
| $k_1$, (45) x $10^6$ | 1.77 | 1.78 | 1.79 | 2.16 | 2.12 | 2.09 |
| $k_1$, (42) x $10^6$ | 1.84 | 1.85 | 1.86 | 2.25 | 2.22 | 2.18 |
| Diameter at. (μ) | | | | | | |
| 23mm | 31.7 | 31.6 | 31.6 | 31.6 | 31.6 | 31.5 |
| 24mm | 32.8 | 32.8 | 32.7 | 32.7 | 32.8 | 32.7 |
| 37mm | 34.5 | 34.4 | 34.3 | 34.4 | 34.4 | 34.3 |
| $k_{1eff}$ x $10^6$ | 2.52 | 2.54 | 2.54 | 3.18 | 3.10 | 3.02 |
| $k_{1A}$ x $10^6$ | 2.89 | 2.91 | 2.93 | 3.67 | 3.56 | 3.45 |

TABLE 6.12

| Run number | 1 | 2 | 3 | 4 | 5 | 6 | 7 | 8 | 9 | 10 | 11 |
|---|---|---|---|---|---|---|---|---|---|---|---|
| Temperature oC | 20 | 20 | 20 | 20 | 20 | 25 | 25 | 25 | 30 | 30 | 30 |
| Feed press. atm. | 35 | 40 | 40 | 45 | 45 | 35 | 40 | 45 | 35 | 40 | 45 |
| Feed flow, cc/s | 334 | 338 | 338 | 328 | 332 | 333 | 336 | 336 | 331 | 334 | 339 |
| Permeate flow, cc/s | 40 | 49 | 50 | 58 | 58 | 45 | 56 | 68 | 50 | 66 | 78 |
| Permeate concn. ppm. | 350 | 350 | 260 | 220 | 220 | 300 | 350 | 300 | 590 | 410 | 350 |
| Bundle press. drop. atm. | 1.0 | 1.0 | 1.0 | 1.7 | 1.0 | 1.4 | 1.0 | 1.0 | 0.9 | 0.8 | 0.8 |
| Fibre press. at, (atm) | | | | | | | | | | | |
| 23mm | 7.0 | 9.3 | 9.5 | 11.3 | 11.2 | 7.8 | 9.8 | 12.0 | 8.1 | 10.8 | 13.2 |
| 24mm | — | — | — | 11.0 | — | — | — | — | 7.9 | — | — |
| 30mm | 6.1 | 8.0 | 8.0 | 9.8 | 9.6 | 6.4 | 8.3 | 10.3 | 6.5 | 8.8 | 10.6 |
| 37mm | — | 7.0 | — | — | — | 5.7 | 7.7 | 9.7 | — | 8.2 | 10.0 |
| <u>Calculated values</u> | | | | | | | | | | | |
| $k_1 \times 10^6$, g/cm$^2$.sec.atm. | | | | | | | | | | | |
| $k_2 \times 10^6$, cm/s | 0.38 | 0.46 | 0.35 | 0.34 | 0.34 | 0.36 | 0.52 | 0.53 | 0.79 | 0.71 | 0.70 |
| Effective fibre diameter, (μ) | | | | | | | | | | | |
| 23mm | 34.1 | 33.4 | 33.4 | 33.1 | 33.3 | 32.3 | 33.1 | 33.0 | 32.8 | 32.7 | 32.4 |
| 24mm | — | — | — | 33.3 | — | — | — | — | 33.0 | — | — |
| 30mm | 35.0 | 34.4 | 34.6 | 34.1 | 34.3 | 34.5 | 34.3 | 34.0 | 34.3 | 34.2 | 34.0 |
| 37mm | — | 35.4 | — | — | — | 34.9 | 34.6 | 34.3 | — | 34.5 | 34.2 |
| $k_{1eff} \times 10^6$ (average) | 1.80 | 1.73 | 1.83 | 1.82 | 1.75 | 2.21 | 2.10 | 2.15 | 2.50 | 2.65 | 2.59 |

TABLE 6.13

| Temp. °C | Flow rates $cm^3/s$ Feed | Permeate | Pressure Atm. Feed | Drop bundle | Permeate concn. mg/L | Salt reject % | Recovery % |
|---|---|---|---|---|---|---|---|
| 25 | 224 | 27 | 35 | 0.65 | 650 | 97.9 | 12 |
| 25 | 224 | 38 | 40 | 0.70 | 510 | 98.4 | 17 |
| 25 | 223 | 61 | 50 | 0.75 | 460 | 98.6 | 27.4 |
| 30 | 224 | 28 | 35 | 0.80 | 1550 | 95.3 | 12.5 |
| 30 | 223 | 41 | 40 | 0.83 | 1360 | 95.9 | 18.2 |
| 30 | 222 | 62 | 50 | 0.82 | 1100 | 96.6 | 27.9 |
| The permeator was post-treated to increase salt rejection | | | | | | | |
| 25 | 227 | 23 | 35 | 0.55 | 650 | 97.9 | 10 |
| 25 | 226 | 36 | 40 | 0.88 | 460 | 98.6 | 16 |
| 25 | 225 | 56 | 50 | 1.00 | 450 | 98.5 | 25.9 |
| 30 | 224 | 25 | 35 | 1.00 | 1200 | 96.2 | 11 |
| 30 | 224 | 37 | 40 | 1.05 | 850 | 97.3 | 16.5 |
| 30 | 223 | 57 | 50 | 1.30 | 720 | 97.7 | 25.6 |
| The permeator was post-treated to increase salt rejection | | | | | | | |
| 25 | 227 | 23 | 35 | 1.10 | 910 | 97.1 | 10 |
| 25 | 224 | 33 | 40 | 1.15 | 675 | 97.9 | 14.7 |
| 25 | 223 | 52 | 50 | 1.42 | 585 | 98.1 | 23.3 |
| 30 | 225 | 24 | 35 | 1.00 | 920 | 97.1 | 10.6 |
| 30 | 224 | 35 | 40 | 1.00 | 690 | 97.8 | 15.6 |
| 30 | 224 | 61 | 50 | 1.05 | 535 | 98.6 | 27.2 |

32,000 ppm NaCl solution as feed

TABLE 6.14

The experiments started after the brand new permeator was flushed with distilled water for 10 hours

| Temp. | Flow rates ($cm^3/s$) | | | Pressure (atm) | |
|---|---|---|---|---|---|
| $^oC$ | Feed | Concnt. | Permeate | Feed | Drop across membrane |
| 20 | 224 | 166 | 58 | 20 | 0.65 |
| 20 | 220 | 132 | 88 | 30 | 0.75 |
| 20 | 216 | 99 | 117 | 40 | 0.80 |
| 20 | 222 | 71 | 151 | 50 | 0.80 |
| 25 | 225 | 155 | 70 | 20 | 0.55 |
| 25 | 225 | 121 | 104 | 30 | 0.57 |
| 25 | 224 | 85 | 139 | 40 | 0.60 |
| 25 | 226 | 55 | 171 | 50 | 0.68 |
| 30 | 226 | 148 | 78 | 20 | 0.50 |
| 30 | 226 | 107 | 119 | 30 | 0.55 |
| 30 | 225 | 71 | 154 | 40 | 0.60 |
| 30 | 221 | 34 | 187 | 50 | 0.62 |
| | | The permeator was post-treated twice | | | |
| 25 | 223 | 113 | 110 | 35 | 1.24 |
| 25 | 222 | 96 | 126 | 40 | 1.29 |
| 25 | 219 | 63 | 156 | 50 | 1.31 |
| 30 | 224 | 99 | 125 | 35 | 1.20 |
| 30 | 223 | 80 | 143 | 40 | 1.25 |
| 30 | 223 | 46 | 177 | 50 | 1.28 |
| | | Distilled water as feed solution | | | |

# CONCLUSIONS

The performances of B-9 and B-10 hollow fibre membrane modules including the measurements of the closed end bore pressures were investigated for two feeds, pure water and sodium chloride solutions. The experimental results were analysed using a computer program. The experimental and theoretical results were compared. The measured values of fibre bore pressures were used to predict the effective fibre bore diameters by using a computer program.

As seen from the results of B-9 and B-10 modules performances, the permeate flow rates increased with increasing temperature and pressure, and in both cases were proportional to the net driving pressures.

As would be expected, the water permeability constant, $k_1$, of B-9 module was found to be higher than the values obtained from the B-10 modules. Considering the water permeability constants, both membrane modules showed similar characteristics that the $k_1$ values obtained at 20°C and 25°C did not show much variation with pressure. Those for 30°C showed a tendency to decrease with increasing pressure.

In the experiments with B-9 module, the $k_1$ values obtained from pure water and salt solution experiments were similar. However, in the experiments with B-10 module, the $k_1$ values obtained from pure water experiments were higher than the values obtained from salt solution experiments.

The salt rejection of the B-10 module was found to be highly dependent upon post-treatment history, which made it difficult to detect any consistent effect of pressure or temperature on the salt permeability constat, $k_2$. However, in continuous operation with B-10 module, a decrease in salt permeability with increasing pressure was reported by Murayama et al (36). This effect is opposite for the B-9 module in that the salt permeability constant, $k_2$ was found to increase with increasing pressure. This was also reported by Ohya et al (38) who suggested that this phenomenon was due to some imperfections on the surface of the B-9 membranes.

Fibre bore pressure measurements were made at the closed ends of the fibre bundles. However, these measured values were found to be significantly higher than the theoretically determined values assuming fixed geometries of 95/45μ OD/ID for B-10 and 85/42μ OD/ID for B-9 membrane modules. These measured bore pressures were about two times as high in the case of the B-9 module and four times as high in the case of the B-10 membrane module.

Sensitivity analyses were made using the computer program to investigate possible reasons for the higher bore pressures measured (see Appendix 6). The effect of possible errors in the measurement of the following parameters were investigated:- the fibre packing density, the active and buried fibre lengths, the pressure drop across the bundle, the feed and permeate flow rates and the fibre diameters. The theoretical model used in these analyses assumed that the fibres in the bundle were straight and parallel to the bundle axis and were axially and radially uniform in diameters. The variations introduced in the sensitivity analysis were also assumed to be uniform for the bundle.

However, the results of this sensitivity analysis, with the exception of those for the variation of the fibre bore diameters, indicated that unreasonably large variations in these parameters would have to take place in order to explain the large discrepancy between the measured and predicted values of the bore pressure losses. In the theoretical analysis, the solution to the problem is sensitive to the assumptions concerning the fibre bore diameter, as can be seen from fact that it occurs to the fourth power in the expression for the characteristic length of a fibre;

$$G^2 = Di^4 \rho/(128 \mu k_1 D_o)$$

As seen from the sensitivity analyses, fig. 6.30, decreasing the assumed bore diameter from 45μ to 33μ increases the fibre bore pressure from 5 atm. to 16 atm. The theoretically predicted fibre bore pressure losses, based on the fixed fibre geometry, were compared with the measured bore pressure losses and this may suggest that the fibre bores may be considerably constricted under operational conditions.

Studies on the capability of hollow fibre membranes to withstand high pressures by Orofino (39) suggested that the maximum compaction occurs at the inner surface. Ohya et al (38) also suggested that the fibre bores become constricted under pressure, thus supporting the concept of bore shrinkage.

In the analysis of the experimental results, the measured values of bore pressure losses are used to estimate the effective bore diameters by using the computer program. The results indicate that if this analysis is correct, the fibres are considerably compressed under normal operating conditions. The nominal B-9 bore diameter of 42μ would appear to be reduced to 37μ and the bore diameter of B-10 from 45μ to something in the range from 31 to 35μ.

However, in this analysis, a uniform bore shrinkage was assumed and also the buried length in the open end tube plate was assumed to shrink in the same manner as the active length. In reality, the fibres buried in the open end tube plate are not under such compressions, and therefore the fibre bores here would not be expected to contract. If the analysis were to take this fact into account then the estimated degree of bore shrinkage would be even greater. In this respect the present analysis is expected to underestimate the magnitude of the bore shrinkage.

In reality, the variation of the pressure difference across the fibre wall along the fibre might become significant when the axial bore pressure drop is taken into account. In this case, the fibres towards the open end tube plate would be exposed to the highest net pressure difference and hence would be expected to undergo the greatest bore shrinkage. Thus the fibres may become non-uniform axially or slightly conical in shape. This would tend to distort the pressure distribution along the fibre bore and could also cause a higher pressure at the closed end of the fibre.

Other possible explanations of the high bore pressures measured might include:- possible constriction of the fibres within the open end resin tube plate (this is thought to be unlikely because the bore diameters measured on the open end tube plate surface agreed well with those measured on broken free fibres), it is possible that there is significant variation in the bore diameters throughout the bundle and that all the pressure tappings were made into the ends of particularly narrow bored fibres (this is not felt to be likely).

The fibre bore pressures, in pure water experiments, were higher than salt solution experiments. As seen on figure 6.29, the apparent fibre bore shrinkage was higher in pure water experiments than salt solution experiments. The bore shrinkage, in pure water experiments, was expected to be smaller but the opposite effect was observed here. However, the theory does not explain this phenomenon and this aspect does require further investigation.

Finally, if the water permeability constants are determined allowing for the fibre bore shrinkage, the modified effective water permeability constants, $k_{1eff}$, would be higher than the values neglecting the bore shrinkage effect.

In the analysis of the whole fibre bundle, the axial variation of brine concentration became more significant when the fibre bore shrinkage was taken into account. The fibres towards the open end tube plate were exposed to the highest net driving pressure and hence increasing the productivity and the brine concentration locally. Thus, this phenomenon may lead to a local concentration polarisation type effect especially at higher recoveries.

Future Work.

In this work, the performance of B-9 and B-10 hollow fibre membrane modules with fibre bore pressure measurements were investigated under normal operating conditions. The measured values of fibre bore pressures were found to be significantly higher than theoretically predicted values. It is suggested that a likely explanation of this discrepancy is that the bore diameters are considerably constricted under the high operating pressure differences normally used.These measured values of bore pressures were used to predict effective bore diameters using a computer program. This investigation suggests that the constriction of the bores of hollow fibre membranes under normal operating conditions offers the most likely explanation of the high bore pressures measured.

If the fibre bore is constricted under the influence of external pressure, obviously there must also be a compressive effect on the outside skin of the fibre. As a future work, this point may be investigated by measuring the fibre outside diameter under pressure. This work may be done by using a single fibre in a pressure apparatus with a transparent part so that the fibre outside diameter can be measured by optical means.

This investigation was carried out under normal operating conditions, e.g. applied pressures 35 to 50 atm. for B-10 and 14 to 25 atm. for B-9 with 20 to 30$^{o}$C feed temperatures. Fibre bore pressure measurements may be made at lower applied pressures using pure water as feed to investigate the initial compressive effect. If in such experiments the effective bore diameters are found to approach the nominal or measured values as the operating pressure is reduced to very low values, then this would provide further support for the fibre bore shrinkage theory. Pressures higher than the above values with different feed temperature may also be investigated, possibly to the point of fibre collapse.

# REFERENCES

# REFERENCES


1. A.M.S. Al-Adsani, A.B. Hasan and A.A. Malik.
Testing of three different types of R.O. membranes.
Desalination, 22 (1977) 271

2. J.J. Allard, J.M. Rovel and P. Treille
Potable water supply of Riyadh by R.O. desalting plants.
Desalination, 22 (1977) 227

3. A.E. Allegrezza, R.D. Burchesky, G. Gotz, R.B. Davis and M.S. Coplan
Hollow fibre composite R.O. membrane.
Desalination, 20 (1977) 87

4. W. Banks and A. Sharples
Studies on desalination by R.O.
J. Appl. Chem., 16 (1966) 153

5. J.K. Beasley
The evaluation and selection of polymeric materials for R.O. membranes
Desalination, 22 (1977) 181

6. J.K. Beasley
The future of R.O. in water desalination
Desalination, 30 (1979) 69

7. G.M. Berlyne and M. Morag
Metabolic effect of drinking brackish water
Desalination, 10 (1972) 215

8. G.M. Berlyne and R. Yagil
Chemical drinking water standards
Desalination, 13 (1973) 217

9. F. Besik
R.O. in treatment of domestic and municipal waters
Ref. 47, Chapter 24

10. P. Blais
Polyamide membranes
Ref. 47, Chapter 9

11. D.C. Brandt
Seawater R.O. Three case histories using Du Pont "Permasep" B-10 permeators.
N.W.S.I.A. Journal, 6 (1979) 25

12. V.P. Caracciolo, N.W. Rosenblatt and V.J. Tomsic
Du Pont hollow fibre membranes
Ref. 47, Chapter 16

13. K.C. Channabasappa.
Status of R.O. desalination technology
Desalination, 17 (1975) 31

14. C. Chen and C.A. Petty
Flow characteristics of semipermeable hollow fibres undergoing R.O.
Desalination, 12 (1973) 281

15. M.S. Dandavati, R.D. Mahendra and W.N. Gill
Hollow fibre R.O. Experiments and analysis of radial flow systems.
Chem. Eng. Science, 30 (1975) 877

16. R.B. Davis, R.D. Burchesky and M.J. Coplan
Hollow fibre composite membrane modules for R.O.
Desalination, 22 (1977) 221

17. B.M. Fabuss
Principles of Desalination by K.S. Speigler (Ed)
Academic Press, New York, 1966. Second Ed. pp 766

18. E. Gabbrielli and J.P Gerofi
Appropriate mineral content of desalination water
Desalination, 49 (1984) 95

19. H.E.A. Ghulaigah and B. Ericsson
Riyadh's R.O. water treatment plants.
Desalination, 30 (1979) 301

20. W.N. Gill and B. Bansal
Hollow fibre R.O. systems analysis and design
A.I. Ch. E. Journal, 19 (No. 4) (1973) 823

21. W.S. Gilliam and H.E. Podall
Recent developments of the R.O. process for desalination
Desalination, 9 (1971) 201

22. F. Guanghu, A. Baoquan, C. Jiayan and Z. Lingying
The mechanism of the formation of aromatic polyamide type asymmetric R.O. membranes
Desalination, 46 (1983) 321

23. W.T. Hanbury, A. Yuceer, M. Tzimopoulos and C. Byabagambi
Pressure drops along the bores of hollow fibre membranes - their measurement, prediction and effect on fibre bundle performance.
Desalination, 38 (1981) 301

24. J.J. Hermans
Physical aspects governing the design of hollow fibre modules.
Desalination, 26 (1978) 45

25. T.D. Hodgson
Selective properties of C.A. membranes towards ions in aqueous solutions.
Desalination, 8 (1970) 99

26. O. Kedem
Water and salt transport in hyperfiltration
Ed. by Lonsdale and Podall (See ref. 29)

27. Y. Kunisada, Y. Murayama and M. Hirai
The development of seawater desalination by R.O. process in Japan
Desalination, 22 (1977) 243

28. T.J. Larson and G. Leitner
Desalting seawater and brackish water
Desalination, 30 (1979) 525

29. H.K. Lonsdale
Recent advances in R.O. membranes
Desalination, 13 (1973) 317

30. H.K. Lonsdale and H.E. Podall
R.O. membrane research
Plenum Press London 1972

31. H.K. Lonsdale, U. Merten and R.L. Riley
Transport properties of cellulose acetate osmotic membranes.
J. Appl. Poly. Sci., 9 (1965) 1341

32. U. Merten
Desalination by R.O.
M.I.T. Press, 1966

33. C.H. McClain
Fluid flow in pipes
The Industrial Press, 1952

34. M.L. McGlashan
Chemical Thermodynamics
Academic Press Inc. (London) Limited, 1979

35. M.S. Massey
Mechanics of fluids
Butler and Tanner Limited, 1968

36. Y. Murayama, T. Kasamatsu and J.G. Gaydos
Live seawater experience in Japan with hollow fibre permeators.
Desalination, 19 (1978) 439

37. H. Ohya
An expression method of compaction effects on R.O. membranes at high pressure operation.
Desalination, 26 (1978) 163

38. H. Ohya, H. Nakajima, K. Takagi and Y. Negishi
An analysis of R.O. characteristics of B-9 hollow fibre module
Desalination, 21 (1977) 257

39. T.A. Orofino
Technology of hollow fibre R.O. systems
Ref. 47 Chapter 15

40. M. Panar, H.H. Hoehn and R.R. Hebert
The nature of asymmetry in R.O. membranes
Macromolecules, 6 (1973) 777

41. D. Pepper, A.I. Rogan and C. Tanner
R.O. desalination of high sulphate water in Corfu
4th Int. Symnp. on fresh water from the sea, 4 (1973) 297

42. Permasep Engineering Manual
E.I. Du Pont de Nemours and Co., 1982

43. H.W. Pohland
Seawater desalination and R.O. plant design
Desalination, 32 (1980) 157

44. C.E. Reid
Principles of Reverse Osmosis, Ed. by U. Merten
M.I.T. Press, 1966

45. C.P. Shields
Five year's experience with R.O. systems using Du Pont "Permasep" permeators
Desalination, 28 (1979) 157

46. M. Soltanieh and W.N. Gill
An experimental study of the complete mixing model for radial flow hollow fibre R.O. systems.
Desalination, 49 (1984) 57

47. S. Sourirajan
Chapter 1, 3 Reverse Osmosis and synthetic membranes
Nat. Res. Council of Canada Publication, Canada 1977

48. S. Sourirajan
Reverse Osmosis
Logos Press, 1970

49. R.R. Sullivan and K.L. Hertel
The flow of air through porous media
J. Appl. Physics, 11 (1970) 761

50. H. Strathmann and K. Kock
The formation mechanism of phase inversion membranes
Desalination, 21 (1977) 241

51. R.M. Terril and P.W. Thomas
On laminar flow through a uniformly porous pipe
Appl. Sci. Res., 21 (1969) 37

52. F.T. Wall
Chemical Thermodynamics
Freeman and Company, 1965 (U.S.A.)

53. H.L. Weissberg
Laminar flow in the entrance region of a porous pipe
The physics of fluids, 2 (No. 5) (1959) 510

54. H. Winters, I.R. Isquith, W. Mahan, W. Arthur and A.B. Mindler
Non-acid pretreatment and control of microogranisms in seawater R.O.
W.S.I.A. 10th Annual Conf. (and Trade Fare) Technical Proceedings, Volume 2, Honolulu, Hawaii 1982

# APPENDIX

# APPENDIX I

## Post treatments (PT-A and PI-B) "Permasep" permeators.

Every B-9 permeator is post treated with PT-A (polyvinyl methyl ether) duing the manufacturing process. PT-A increases the salt rejection by reducing salt flow through membrane or fibre imperfections (coupled flow).

New B-10 permeators usually must be treated with PT-B before placing on-stream after the initial flushing. Also, B-10 permeators must be retreated with PT-B after any cleaning operation. The PT-B absorbs on the membrane surface, which enhances the salt rejection. Thus, diffusive salt flow rather than coupled flow is reduced.

Procedure for PT-B post treatment

1) Flush the permeator with chloring-free product or good quality water prior to post treatment. Use a once through (brine and product to drain) of 38 litres of water. (In this case, distilled water was used here).

2) Prepare a solution containing 1 wt percent citric acid plus 80 mg/litre of PT-B (tannic acid). The solution was prepared with 80 litre distilled water.

3) Recirculate the PT-B solution through the permeator. A brine flow of about 7 L/m with pressure of 6.8 to 10.2 atm. is recommended.

4) After one hour, stop recirculating and drain the solution to waste.

5) Flush the residual PT-B solution from the permeator with clean water at 3.4 to 5.1 atm and a brine rate of 17 L/m for five minutes.

6) After the system operation has stabilised, check the performance to determine the effectiveness of PT-B treatment.

# APPENDIX II

## "Biz" cleaning procedure

The need for cleaning is based on the change in productivity, salt rejection, and bundle pressure drop. However, salt rejection and brine bundle pressure drop are usually the more sensitive indicators. If either the salt passage or the brine bundle pressure drop increases by 1.5 times, cleaning is recommended.

This assumes that the changes in the reverse osmosis performance are caused by fouling rather than other causes. Cleaning with "Biz" detergent is effective in removing colloidal fouling.

Biz cleaning procedure.

1) Flush permeators with product water prior to cleaning using a once through flush of 38L per permeator. The brine pH must be 6.0 or above.

2) In the mix tank, prepare a 0.5 wt. percent "Biz" detergent (with 17.6% phosphorus) solution. Alternate detergents to Biz are given in PEM ( ). (In this cleaning here, the solution was prepared with Ariel detergent and distilled water).

3) Add with agitation sufficient NaOH solution to increase the pH to 11.0.

4) Circulate the cleaning solution through the permeator. Take the first 20% of the solution to drain via the brine return valve, and then recycle the cleaning solution through the mix tank. A brine flow of about 17 L/m is recommended at a pressure of 3.4 - 10.2 atm.

5) The effect of the "Biz" cleaking can be monitored by observing the effluent. If the effluent is darker than the feed, colloidal material is being removed. The flushing operation should be conducted for at least 2 hours/or as dictated by the amount of foulants.

6) When cleaning is complete, stop recirculation. Drain mix tank solution to waste. Flush residual cleaning solution from permeator with product water (pure water) by operating at 3.4 - 5.1 atm. and 17 L/m brine rate in the normal feed direction. During this flush, brine and product go to drain. The unit may then be flushed with brine and product to drain using regular feed water at reduced pressure of less than 13.6 atm. until no foaming occurs.

7) After post treatment (PI-B), return permeator to normal operation and check the performance to determine cleaning and post treatment effectiveness.

# Appendix 3.

Aqueous sodium chloride solutions electrical conductivity vs. concentration.

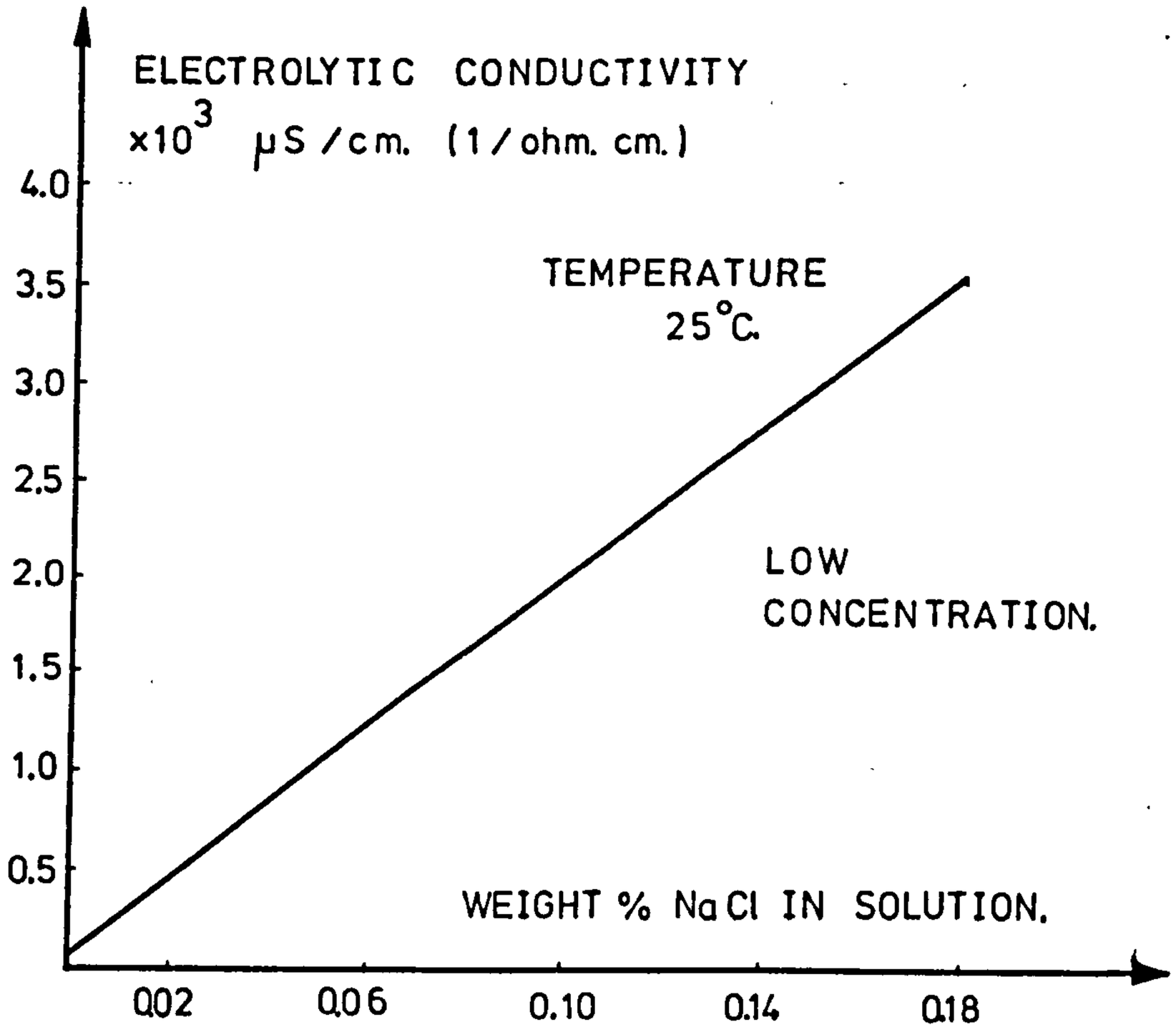


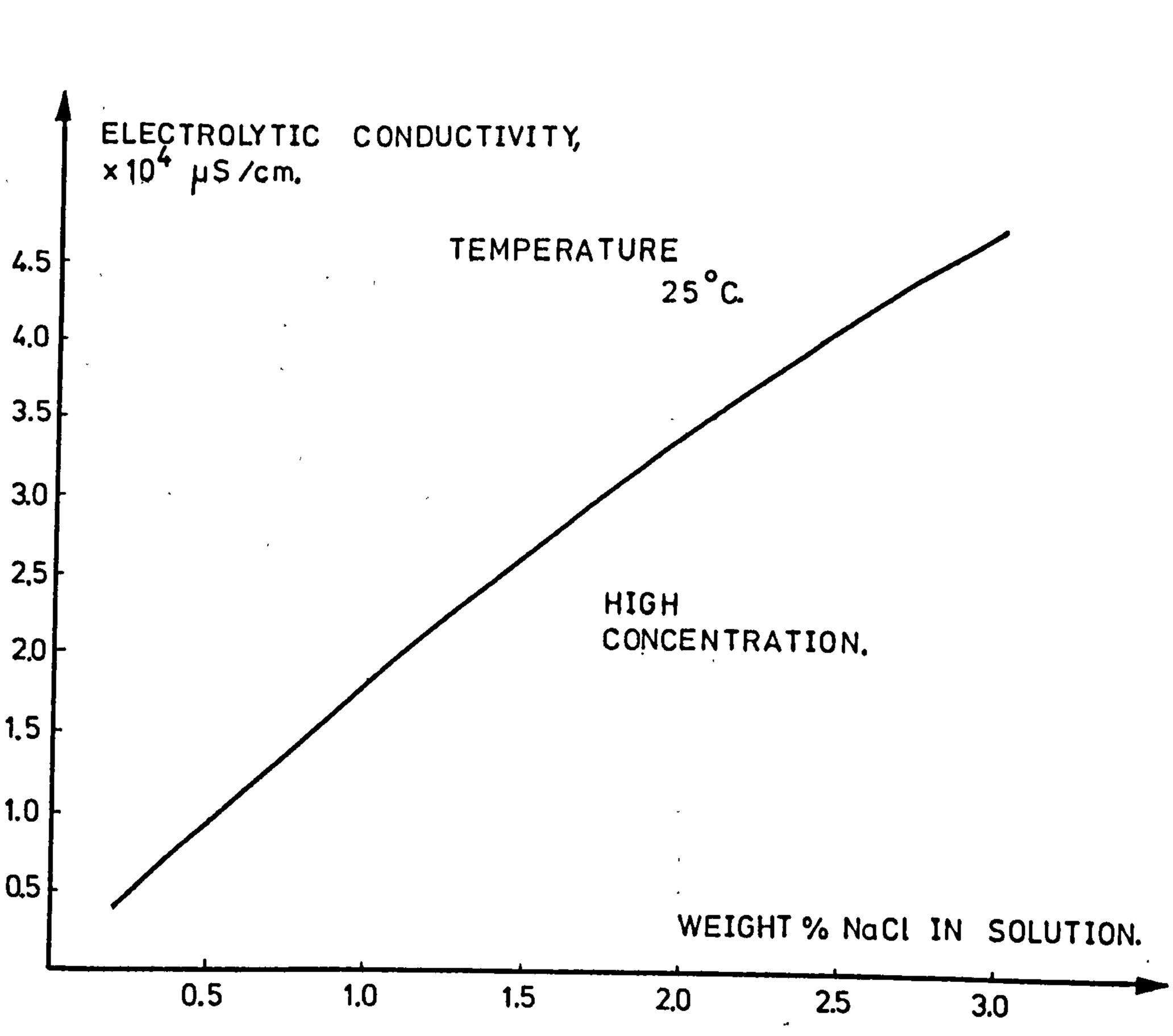

# APPENDIX 4.

## COMPUTER PROGRAM, INPUT AND OUTPUT

The computer programs used in the analysis of experimental results employ a numerical iterative solution to the problem of predicting detailed bundle performance based on the analytical solutions in Chapter 5.

The steps below were followed in running the program. First, the fibre and bundle dimensions were fed into the computer as constants. After that, the measured values from the bundle performance were fed into the computer, e.g. temperature, pressure, flow rate and concentration of feed and, flow rate and concentration of permeate. Initial estimates of the membrane permeability constants, $k_1$ and $k_2$, are guessed and fed into the computer.

The initially guessed values of $k_1$ and $k_2$ are readjusted by the computer until the computer output of the product flow rate and concentration are equal to the measured values or the discrepancy is less than one percent. After this, the computer can print out the variation of water flux, brine concentration and product concentration distribution axially and radially within the bundle. The fibre bore pressures at the closed ends and the permeate velocities at the open end are also predicted.

Modifications were made to the computer program to investigate the effects of variations in the other parameters. For example, in the computer program (VID) the measured values of fibre bore pressures are input and the bore diameter is adjusted until the predicted and measured bore pressure drops match. The value of the bore diameter at which the match occurs is taken to be the effective bore diameter. Samples of the computer program outputs can be found in Appendix 4A and B.

# APPENDIX 4.A

## Sample Hollow Fibre Program Output for the fixed diameter, (FD)

INPUT

TEMPERATURE = 25°C
BRINE DP = 1.49 ATM
K2 X $10^6$ = 0.81 CM/S
FEED in cc/s = 347
FEED CONCENTRATION in ppm = 20,000
WRKNG PRESS = 45 ATM
K1 X $10^6$ = 1.68 GM/SQCM/S/ATM
MD in cc/s = 69
FBR BORE cm = 0.0045

OUTPUT MODULE OUTPUT IS 68.9 CC/S. PERMEATE CONCENTRATION,CD IS 446 PPM.

### WATER FLUX DISTRIBUTION,J1 X 100,000, IN CM/S,

| AXIAL POSITION, X = | 0.0 | 17.5 | 35.0 | 52.5 | 70.0 in cm. | |
|---|---|---|---|---|---|---|
| RADIAL POSITION, R in cm. | | | | | | |
| 5.3 | 3.59 | 3.62 | 3.68 | 3.78 | 3.92 | |
| 4.5 | 3.78 | 3.81 | 3.88 | 3.99 | 4.16 | |
| (closed end) 3.7 | 3.94 | 3.96 | 4.04 | 4.17 | 4.35 | (open end) |
| 2.8 | 4.07 | 4.10 | 4.18 | 4.32 | 4.51 | |
| 2.0 | 4.19 | 4.22 | 4.31 | 4.45 | 4.66 | |
| 1.2 | 4.31 | 4.34 | 4.43 | 4.58 | 4.79 | |

### BRINE CONCENTRATION DISTRIBUTION, CB,IN PERCENT

| AXIAL POSITION, X = | 0.0 | 17.5 | 35.0 | 52.5 | 70.0 in cm. | |
|---|---|---|---|---|---|---|
| RADIAL POSITION, R in cm. | | | | | | |
| 5.3 | 2.45 | 2.46 | 2.47 | 2.49 | 2.51 | |
| 4.5 | 2.31 | 2.31 | 2.32 | 2.33 | 2.34 | |
| (closed end) 3.7 | 2.19 | 2.19 | 2.20 | 2.20 | 2.21 | (open end) |
| 2.8 | 2.10 | 2.10 | 2.11 | 2.11 | 2.12 | |
| 2.0 | 2.04 | 2.04 | 2.04 | 2.04 | 2.05 | |
| 1.2 | 2.00 | 2.00 | 2.00 | 2.00 | 2.00 | |

### PERMEATE VELOCITY AT FIBRE END AND BORE PRESSURE LOSS

| RADIAL POSITION, R | U CM/S | PL ATM. |
|---|---|---|
| 5.3 | 4.85 | 3.28 |
| 4.5 | 5.12 | 3.46 |
| 3.7 | 5.34 | 3.60 |
| 2.8 | 5.53 | 3.73 |
| 2.0 | 5.69 | 3.84 |
| 1.2 | 5.86 | 3.95 |

### PRODUCT CONCENTRATION DISTRIBUTION. CD,IN PPM

| AXIAL POSITION, X = | 0.0 | 17.5 | 35.0 | 52.5 | 70.0 | in cm. | |
|---|---|---|---|---|---|---|---|
| RADIAL POSITION, R in cm. | | | | | | | |
| 5.3 | 553.3 | 550.6 | 543.7 | 533.0 | 519.1 | | |
| 4.5 | 494.1 | 491.2 | 483.7 | 472.0 | 456.7 | | |
| (closed end) 3.7 | 450.8 | 447.8 | 440.0 | 427.8 | 412.0 | (open) | |
| 2.8 | 418.7 | 415.6 | 407.8 | 395.5 | 379.5 | (end) | |
| 2.0 | 394.7 | 391.7 | 383.9 | 371.6 | 355.8 | | |
| 1.2 | 376.2 | 373.3 | 365.5 | 353.5 | 337.9 | | |

# APPENDIX 4.B

## Sample Hollow Fibre Program Output for variable internal diameter, (VID)

INPUT

TEMPERATURE = 25°C
BRINE DP = 1.49 ATM
K2 X $10^6$ = 0.83 CM/S
FEED in cc/s = 347
FEED CONCENTRATION in ppm = 20,000
WRKNG PRESS = 45 ATM
K1 X $10^6$ = 2.25 CM/SQCM/S/ATM
MD in cc/s = 69
FBR BORE cm = 0.00331

OUTPUT MODULE OUTPUT IS 68.9 CC/S. PERMEATE CONCENTRATION,CD IS 456 PPM.

### WATER FLUX DISTRIBUTION,J1 X 100,000, IN CM/S,

| AXIAL POSITION, X = | 0.0 | 17.5 | 35.0 | 52.5 | 70.0 in cm. | |
|---|---|---|---|---|---|---|
| RADIAL POSITION, R in cm. | | | | | | |
| 5.3 | 3.27 | 3.36 | 3.61 | 4.02 | 4.61 | |
| 4.5 | 3.40 | 3.51 | 3.80 | 4.29 | 4.99 | |
| 3.7 (closed end) | 3.52 | 3.64 | 3.96 | 4.50 | 5.30 | (open end) |
| 2.8 | 3.62 | 3.75 | 4.09 | 4.68 | 5.55 | |
| 2.0 | 3.71 | 3.85 | 4.21 | 4.84 | 5.76 | |
| 1.2 | 3.81 | 3.95 | 4.33 | 4.99 | 5.95 | |

### BRINE CONCENTRATION DISTRIBUTION, CB,IN PERCENT

| AXIAL POSITION, X = | 0.0 | 17.5 | 35.0 | 52.5 | 70.0 in cm. | |
|---|---|---|---|---|---|---|
| RADIAL POSITION, R in cm. | | | | | | |
| 5.3 | 2.40 | 2.41 | 2.46 | 2.53 | 2.66 | |
| 4.5 | 2.27 | 2.28 | 2.31 | 2.36 | 2.44 | |
| 3.7 (closed end) | 2.17 | 2.17 | 2.19 | 2.22 | 2.27 | (open end) |
| 2.8 | 2.09 | 2.09 | 2.10 | 2.12 | 2.14 | |
| 2.0 | 2.04 | 2.04 | 2.04 | 2.05 | 2.06 | |
| 1.2 | 2.00 | 2.00 | 2.00 | 2.00 | 2.00 | |

### PERMEATE VELOCITY AT FIBRE END AND BORE PRESSURE LOSS

| RADIAL POSITION, R | U CM/S | PL ATM. |
|---|---|---|
| 5.3 | 8.95 | 10.86 |
| 4.5 | 9.45 | 11.42 |
| 3.7 | 9.87 | 11.89 |
| 2.8 | 10.22 | 12.28 |
| 2.0 | 10.53 | 12.63 |
| 1.2 | 10.83 | 12.99 |

### PRODUCT CONCENTRATION DISTRIBUTION, CD,IN PPM

| AXIAL POSITION, X = | 0.0 | 17.5 | 35.0 | 52.5 | 70.0 | in cm. | |
|---|---|---|---|---|---|---|---|
| RADIAL POSITION, R in cm. | | | | | | | |
| 5.3 | 606.5 | 593.7 | 562.8 | 521.1 | 477.0 | | |
| 4.5 | 551.2 | 536.9 | 502.2 | 455.0 | 403.7 | | |
| 3.7 (closed end) | 509.6 | 494.4 | 457.9 | 408.1 | 353.9 | (open) | |
| 2.8 | 478.0 | 462.5 | 425.1 | 374.4 | 319.4 | (end) | |
| 2.0 | 453.8 | 438.2 | 400.6 | 349.9 | 295.2 | | |
| 1.2 | 434.4 | 419.0 | 381.8 | 331.7 | 277.9 | | |

APPENDIX 5

```
(*HOLLOW FIBRE REVERSE OSMOSIS PROGRAM*)
(**************************************)

PROGRAM HOLLOWFIBRE;
USES TRANSCEND,SCREENDATE;
CONST TPI2=19.74;X2=20;W=1E5;
      R2=20;
TYPE  BZ = ARRAY 0..X2,0..R2  OF REAL;
      BQ = ARRAY 0..R2  OF REAL;
      DATAA = ARRAY 0..7  OF REAL;
      DATAF = FILE OF DATAA;

VAR   PQ:INTERACTIVE;CD,J1,C:BZ;DSM,U1,DMD,PL:BQ;
      E,G,K3,NF,DO,DI,RO,R1,CF,MF,P1,L,DR,LIM,
      ERROR1,DPFF,DX2,DX1,PHI,PF,PFO,K1,K2,DU,U,
      FPL,ERROR,PF3,P11,DPB,DPF,PF1,RR,DR1,MD,ZZ,MFL,DX,X,
      MD1,CDO1,T,MU,K,PDB,A1,B1,SL,DPF1,DR2,PF2,DA,DMS,MS,MSF,SM,CDO  :REAL;
      FR,I,R,N,RA,NA :INTEGER;
      NP14,NP13,
      A,NPO,ZP,NP,NP1,NP2,NP3,NP4,NP5,NP6,NP7,NP8,NP9,NP10,NP11,NP12:STRING;
      B:CHAR;

SEGMENT PROCEDURE SIX;
BEGIN
   DR1:= (RO-R1)/R2;MFL:= MF/L;DX:= L/X2;
 DR2:=4.93*DI*DI*NF*DR1;DR:= 19.7*NF*DO*DR1/CF/MFL;
 LIM:= (P1-PHI*CF)/100;
 DX2:= -32*MU*DX/DI/DI;DX1:= 4*DX*DO/DI/DI;
 DA:= K2*3.14*DO*DX;K3:=K2;
 FOR N:= 0 TO X2 DO  C N,0 := CF;
 SM:=6.283*NF*DR1;
 K:=PDB/LN(RO/R1);
 G:=DI*DI/SQRT(128*MU*DO*K1); E:=2/(EXP(L/G) + EXP(-L/G));
END;

SEGMENT PROCEDURE TWO;

PROCEDURE TRACE;
VAR SP:CHAR;
BEGIN SP:=' ';
      WRITELN(PQ,A1,SP,B1,SP,J1 N,R ,SP,U,SP,DPF,SP,PF);
END;

PROCEDURE OG;
BEGIN
 MS:=(DSM 0 +DSM R2 )/2;
 MD:=(DMD 0 +DMD R2 )/2;
 FOR R:=1 TO R2-1 DO
      BEGIN
         MS:= MS+DSM R ;
         MD:= MD+DMD R
      END;
  CDO:= 1E6* MS/MD
END;
```

```
BEGIN
 FOR R:= 0 TO R2  DO
  BEGIN RR:= R1+R*DR1;DPB:=K*LN(RR/R1);P1:= P11-DPB;
    PF:=(P1-PHI*C 0,R )*(1-E);PF2:=PF;PF3:=PF2;MSF:=0;
    REPEAT U:=0;  FOR N := 0 TO X2 DO
      BEGIN
        A1 := K1*(P1-PF-PHI*C N,R )-K3;
        B1 := K1*K3*(P1-PF);
        J1 N,R  := (A1+SQRT(A1*A1+4*B1))/2;
        DU := DX1*J1 N,R ;
        U := U+DU;
        DPF := DX2*U;
        PF := PF+DPF;
      END;
        DPF1:=-32*MU*SL*U/DI/DI;PF:=PF+DPF1;
        PF3:=PF2; PF1 := PF-DPF;
        PF:=PF2-PF1*E;PF2:=PF;WRITELN(PF1:2:3)
    UNTIL ABS(PF1)<0.01;
    RR := R1+R*DR1;U1 R  := U-DU;
    DMD R :=DR2*RR*U1 R ;PL R :=PF3;
    IF R<R2 THEN FOR N:=0 TO X2 DO
       C N,R+1 :=C N,R +DR*SQR(C N,R )*
       J1 N,R *RR;
       FOR N:=0 TO X2 DO
    BEGIN
        CD N,R :=K2*C N,R /J1 N,R ;
        DMS := DA*C N,R ;MSF := MSF+DMS
     END;
    MSF:=MSF-DMS;DSM R :=SM*RR*MSF;
        WRITELN('           R = ',R);;WRITELN(PF3)
  END;
  OG;
END;
```

```
SEGMENT PROCEDURE FOUR;
BEGIN
  PAGE(OUTPUT);
  WRITELN(PQ,'WATER FLUX DISTRIBUTION,J1 X 100,000,');
   WRITELN(PQ,'     IN CM/S, VS. X AND R ');WRITELN(PQ);
  WRITE(PQ,'X=    ');
  FOR NA:=0 TO 4 DO  BEGIN N:= 5*NA;X:=N*DX;
                        WRITE(PQ,X:2:1,'  ')
                  END;
  WRITELN(PQ);
  WRITE(PQ,' R');
  WRITELN(PQ);
  WRITELN(PQ);
 FOR RA:= 10 DOWNTO 0 DO
  BEGIN R:= 2*RA; RR:= R1+R*DR1;
        WRITE(PQ,RR:1:1);
        FOR NA:=0 TO 4 DO
        BEGIN N:= 5*NA;X:= W*J1 N,R ;
              WRITE(PQ,X:1:2,'  ')
        END;
        WRITELN(PQ)
  END;

  WRITELN(PQ);

WRITELN(PQ,'BRINE CONC.CB,IN PERCENT, VS. X AND R ');
WRITELN(PQ);
WRITE(PQ,'X=    ');
FOR NA:=0 TO 4 DO  BEGIN N:= 5*NA;X:=N*DX;
                      WRITE(PQ,X:2:1,'  ')
                END;
WRITELN(PQ);
WRITE(PQ,' R');
WRITELN(PQ);
WRITELN(PQ);
FOR RA:= 10 DOWNTO 0 DO
 BEGIN R:= 2*RA; RR:= R1+R*DR1;
       WRITE(PQ,RR:2:1);
       FOR NA:=0 TO 4 DO
       BEGIN N:= 5*NA;X:= 100*C N,R ;
             WRITE(PQ,X:1:2,'  ')
       END;
       WRITELN(PQ)
 END;

 WRITELN(PQ);
```

```
WRITELN(PQ,'PERMEATE VELOCITY AT FIBRE END AND PRESSURE LOSS VS.  R ');
WRITELN(PQ);
WRITELN(PQ);
WRITE(PQ,' R      U CM/S          PF ATM.');
WRITELN(PQ);
WRITELN(PQ);
FOR RA:= 10 DOWNTO 0 DO
 BEGIN R:= 2*RA; RR:= R1+R*DR1;
       WRITE(PQ,RR:1:1,'  ');
       X:= U1 R ;
            WRITE(PQ,X:2:2,'          ');X:=PL R ;WRITE(PQ,X:2:2);
       WRITELN(PQ)
 END
END;

SEGMENT PROCEDURE FIVE;
BEGIN

   WRITELN(PQ);

  WRITELN(PQ,'PRODUCT CONC.CD,IN PPM, VS. X AND R ');
  WRITELN(PQ);
  WRITE(PQ,'X=    ');
  FOR NA:=0 TO 4 DO  BEGIN N:= 5*NA;X:=N*DX;
                       WRITE(PQ,X:2:1,'     ')
                END;
  WRITELN(PQ);
  WRITE(PQ,' R');
  WRITELN(PQ);
  WRITELN(PQ);
  FOR RA:= 10 DOWNTO 0 DO
   BEGIN R:= 2*RA; RR:= R1+R*DR1;
         WRITE(PQ,RR:2:1);
         FOR NA:=0 TO 4 DO
         BEGIN N:= 5*NA;
               WRITE(PQ,' ',CD N,R *1E6:6:1,'  ').
         END;
         WRITELN(PQ)
   END;

   WRITELN(PQ);

END;

PROCEDURE TEN;
 BEGIN
      WRITELN(PQ);WRITELN(PQ);WRITELN(PQ,'MODULE OUTPUT IS ',MD:1:1,' CC/S.');
      WRITELN(PQ);WRITELN(PQ,'PERMEATE CONCENTRATION,CD IS ',TRUNC(CDO):4,' PPM.
      WRITELN(PQ);WRITELN('PRESS  SPACE½ FOR NEXT CASE');
      WRITELN(PQ,'PRESS  E½ TO EXIT');
      READ(B)
END;
```

```
PROCEDURE NEW;
BEGIN
   PROMPTAT(0,'TEMPERATURE ? = ');INR(T);
   PROMPTAT(1,'WRKNG PRESS ? = ');INR(P11);
   PROMPTAT(2,'BRINE DP    ? = ');INR(PDB);
   PROMPTAT(3,'K1 X 10**6   ? = ');INR(K1);K1:=K1*1E-6;
   PROMPTAT(4,'K2 X 10**6   ? = ');INR(K2);K2:=K2*1E-6;
   PROMPTAT(5,'MD in cc/s  ? = ');INR(MD1);
   PROMPTAT(6,'CD in ppm   ? = ');INR(CDO1);
   PROMPTAT(7,'FEED in cc/s? = ');INR(MF);
   PROMPTAT(8,'FEED in g/g ? = ');INR(CF);
   PROMPTAT(9,'FIBRE PRESS ? = ');INR(DPFF);
   PROMPTAT(10,'FBR BORE cm ? = ');INR(DI);
   WRITELN(PQ,'TEMPERATURE  = ',T);
   WRITELN(PQ,'WRKNG PRESS  = ',P11);
   WRITELN(PQ,'BRINE DP     = ',PDB);
   WRITELN(PQ,'K1 X 10**6    = ',K1);
   WRITELN(PQ,'K2 X 10**6    = ',K2);
   WRITELN(PQ,'MD in cc/s   = ',MD1);
   WRITELN(PQ,'CD in ppm    = ',CDO1);
   WRITELN(PQ,'FEED in cc/s = ',MF);
   WRITELN(PQ,'FEED in g/g  = ',CF);
   WRITELN(PQ,'FBR BORE cm  = ',DI);
   PHI:=785.5*(T+273)/298;
   MU:=1.002*EXP((20-T)/(T+109)*(3.1559+1.9157E-3*(T-20)))/1.01325E8;
   NF:=10000;DO:=0.0095;RO:=5.25;R1:=1.25;
   L:=70;SL:=11.8;
   CRT(ERASEOS);
END;

BEGIN
     RESET(PQ,'PRINTER:');A:=' = ';
BEGIN NEW;
   REPEAT SIX;TWO;
          WRITELN(PQ,'MD',A,MD:6:4);
          WRITELN(PQ,'MD1',A,MD1:6:4);
          WRITELN(PQ,'CDO',A,CDO:6:4);
          WRITELN(PQ,'K2',A,K2*1E6:6:4);
          K1:=K1*MD1/MD;K2:=K2*MD1*CDO1/MD/CDO;
          WRITELN(PQ,'K1',A,K1*1E6:4:2);
          WRITELN(PQ,'K2',A,K2*1E6:6:4);
          WRITELN(PQ);
          ERROR:=ABS(MD1-MD)/MD1+ABS(CDO1-CDO)/CDO1;
          WRITELN('ERROR = ',ERROR:4:4);
   UNTIL ERROR < 0.01;
           FOR FR :=0 TO 20 DO
      BEGIN FPL:=PL FR ;
            WRITELN(PQ,'FPL at ',FR,' = ',FPL:6:2);
      END;
           WRITELN(PQ);WRITELN(PQ,'MD',A,MD:4:2);
           WRITELN(PQ,'CDO',A,CDO:3:0);
           WRITELN(PQ,'K1',A,K1*1E6:4:2);
           WRITELN(PQ,'K2',A,K2*1E6:6:4);
           WRITELN(PQ,'DI',A,DI:7:5);
           FOUR;FIVE;TEN;
 END;CLOSE(PQ);
END.
```

# APPENDIX 6.

Sensitivity analyses were made using the computer program to investigate possible reasons, other than bore shrinkage, for the discrepancy between the high bore pressures measured and the lower values predicted.

## 1. Error in Packing Density Measurement.

Variation in the assumed (counted) fibre packing density has little effect; e.g. variation in the fibre packing density from 9000 to 10000/ $cm^2$ makes about 1μ decrease in the effective bore diameter which increases the bore pressure about 1 atm., fig. 6.30 and 31.

## 2. Errors in the Active Fibre Length Measurement.

Some variation of the fibre active and buried length has also small effect on the variation of fibre bore pressure. Measurement of fibre active and buried length were made on the outside of the fibre bundle. The active length of some fibres may vary differentially with the buried length due to the bundle construction, e.g. decrease in the active length increases the length of fibres buried in epoxy resin. However, the variation is not thought to be large and it may be ± 5 cm, at most, for 70 cm active length with average 11 cm buried length. Such a variation makes less than half atm. difference in the bore loss predictions; Figures A.6. a and c.

## 3. Possible Effects due to Errors in Flow Measurements

The measured fibre bore pressure variation in the repeated experiments was generally less than 1 atm. Variation of permeate flow rate was less than 5% in the repeated experiments. However the effect is small, Figure A.6.d.

## 4. Possible Effects due to Membrane Fouling.

Membrane fouling was suspected due to the build up of the brine pressure drop across the fibre bundle. The membrane was occasionally cleaned which reduced the brine pressure drop. However, each of the experiments were repeated at least twice with different degrees of fouling and the permeate flow rates and bore pressure drops were almost the same. Therefore it was concluded that membrane fouling practically had very small effect.

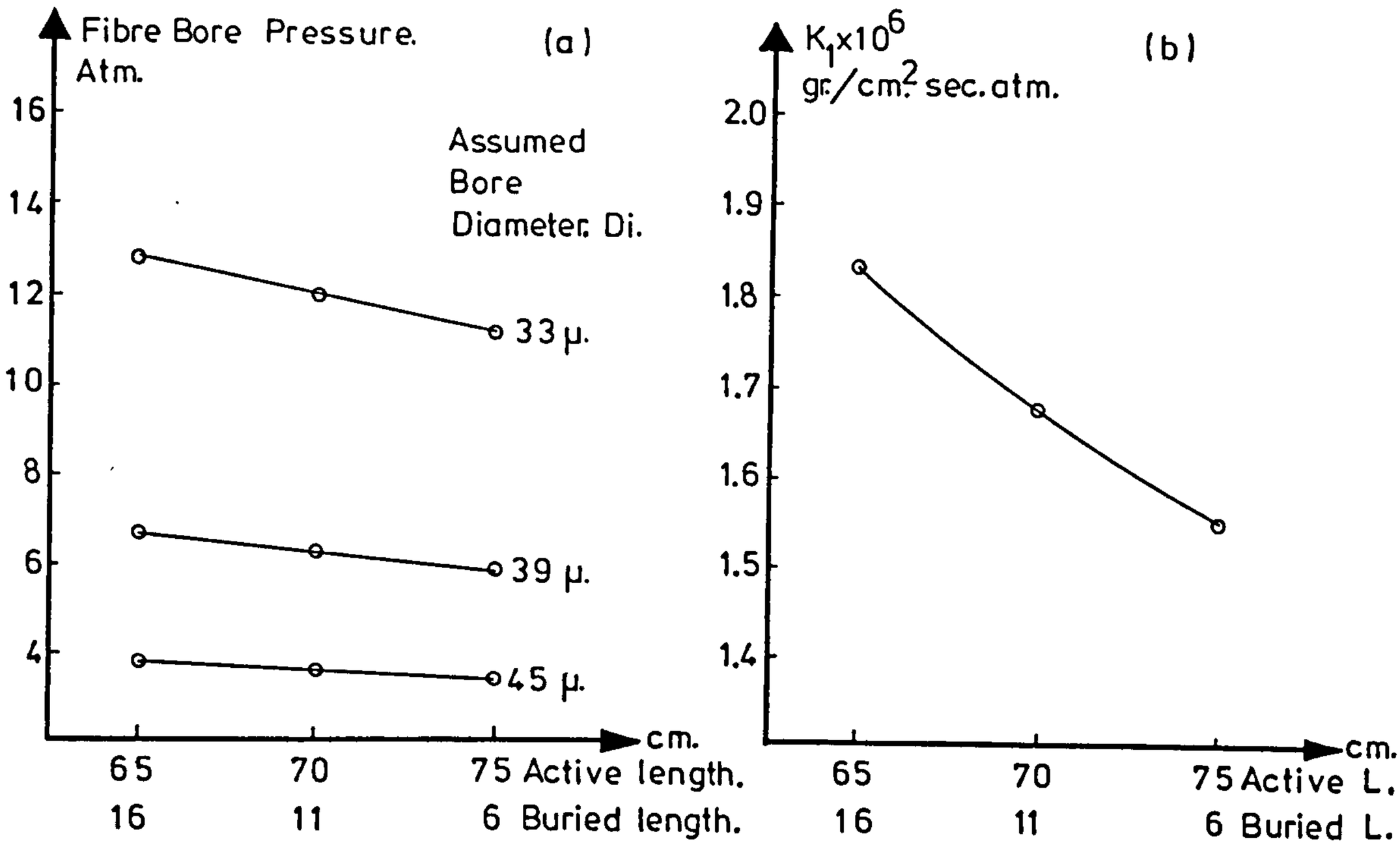


Figure A6.

Sensitivity of numerical solutions, for the bore pressure loss and $k_1$ values, due to the effects of variations in the active and buried fibre lengths, with differing assumed bore diameters and permeate flow rates.